

# Rational design of carbon-based materials for purification and storage of energy carrier gases of methane and hydrogen

Shohreh Mirzaei<sup>1,2</sup>, Ali Ahmadpour<sup>1,2,\*</sup>, Zongping Shao<sup>3</sup>, Arash Arami-Niya<sup>3,\*\*</sup>

<sup>1</sup> Department of Chemical Engineering, Faculty of Engineering, Ferdowsi University of Mashhad (FUM), P.O. Box 91779-48944, Mashhad, Iran.

<sup>2</sup> Industrial Catalysts and Adsorbents and Environment Research Lab., Oil and Gas Research Institute, FUM, Iran.

<sup>3</sup> Discipline of Chemical Engineering, Western Australian School of Mines: Minerals, Energy and Chemical Engineering, Curtin University, GPO Box U1987, Perth, WA 6845, Australia.

## Abstract

Today, fast-growing energy demands and fuel resource depletion are among the hottest concerning issues that treating our world. So, a huge need is felt to find efficient, affordable and eco-friendly energy storage and production systems. Much current research effort proved that gaseous energy carriers such as CH<sub>4</sub> and H<sub>2</sub> seem to be the right choice for alternative fuel resources. However, the most important challenge with this new-faced resource is the comparatively low volumetric energy storage density. Fortunately, the high-pressure gas storage technique inside the porous media of solid adsorbent is considered as one best way to tackle the energy density problem. Famous family of porous carbon materials, with a suitable pore size distribution centred in the micropore range and a large number of adsorption sites per volume of solid, open up a great scope for gas storing applications. This review article represents the state-of-the-art with a precise focus on what has and can be done to improve/enhance the gas/energy storage capacity of traditional and novel structures of low-cost carbon-based adsorbents. We review a wide variety of design strategies to synthesis carbonaceous adsorbents, with a strong focus on creating the connection between structural properties and gas adsorption performance. In this regard, various synthesis techniques have been studied with emphasis on the more interesting recent progress that allows better control and optimisation of porosity of porous carbons for maxing gas storage capacity. We will also show

---

\* Corresponding author. Tel: +98-51-38805006. Email: [Ahmadpour@um.ac.ir](mailto:Ahmadpour@um.ac.ir)

\*\* Corresponding author. Tel: +61-8-9266-5482. Email: [Arash.araminiya@curtin.edu.au](mailto:Arash.araminiya@curtin.edu.au)

that carbon-based adsorbents, particularly activated carbons, have been extensively studied and remain a powerful candidate in the search for an energy carrier economy. In the end, a perspective is provided to forecast the future development of carbon-based materials.

## Contents

Abstract .....	1
1. Introduction.....	3
2. Activated carbons.....	11
2.1 Physically activated carbons .....	13
2.2 Chemically activated carbons .....	16
2.2.1 Chemical agent.....	16
2.2.2 Raw materials.....	19
2.3 Surface-modified activated carbons.....	26
2.4 Hydrothermal carbons.....	29
2.5 Templated carbons .....	32
2.6 Carbide-derived carbons .....	36
2.7 Ordered (structured) adsorbent .....	39
2.7.1 Dense carbons .....	39
2.7.2 Foam-like carbons.....	43
2.7.3 Carbon fibres.....	46
3. Carbon Nano-allotropes .....	49
3.1 0D Carbon fullerenes.....	50
3.2 1D Carbon nanotube .....	57
3.3 2D Graphene .....	66
3.4 3D Graphene .....	70
4. Summary and outlook .....	72

## 1. Introduction

The energy crisis and environmental effects are interconnected concerning issues the world is dealing with today. For years, the nations have been alarmed by the possible climate changes due to an increasing level of carbon dioxide in the atmosphere. Moreover, according to the worldwide energy consumption statistics, oil and coal as the primary available energy resources will deplete in the next few decades (Figure 1) [1, 2]. Therefore, a significant challenge is to find efficient potential energy sources to replace conventional fossil fuels. Gasses such as methane ( $\text{CH}_4$ ) and hydrogen ( $\text{H}_2$ ) are the best alternative green energy carriers. The combustion of these gases generates a significant amount of energy (Methane  $50\text{-}55 \text{ MJ.Kg}^{-1}$  and hydrogen  $120\text{-}142 \text{ MJ.Kg}^{-1}$ ) and, at the same time, produces a clean residue [3, 4]. It has been estimated that these energy carriers can supply 80% of the energy demands [5].

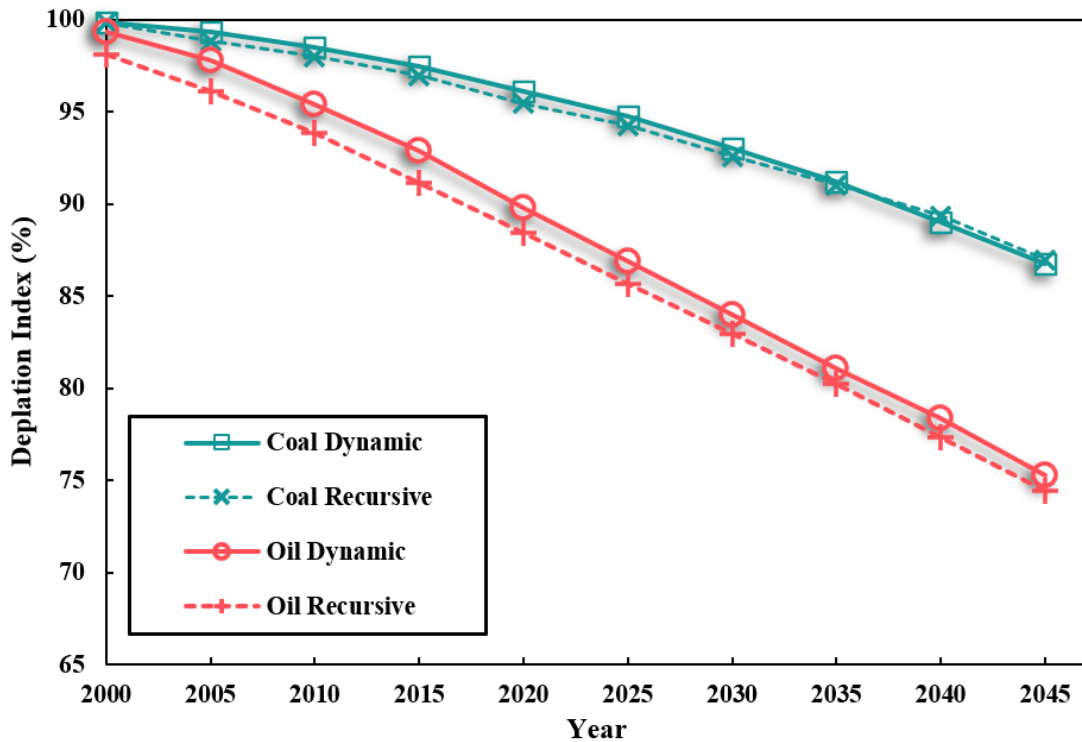


**Figure 1.** Global depletion of coal and oil as the primary resources of fossil fuel predicted by recursive-dynamic MIT Emissions model [6].

Methane, the main constituent of natural gas (NG), is known as an alternative energy source due to its accessibility and clean-burning properties over conventional fuels. Among all hydrocarbons, methane emits the least amount of pollutants during the combustion [5]. The U.S. Energy Information Administration (EIA) revealed that “natural gas expected to remain most-consumed fuel in U.S. industrial sector up to 2050” [7]. Also, EIA projects that natural gas consumption in Asia will continue to outpace supply (see Figure 2) [8]. The agency reported that natural gas production will continue growing through 2050 amid rising global energy consumption, especially in power generation and transportation [7]. A vehicle running on CH<sub>4</sub> would produce 70% less CO, 87% less non-methane organic gas, 87% less nitrogen oxide, and 20% less CO<sub>2</sub> compared with those running on gasoline [9]. However, the low energy yield of each litre of natural gas (0.033 MJ) at the standard condition in contrast with the gasoline (34.2 MJ) is one of the main drawbacks in the NG application as a source of energy.

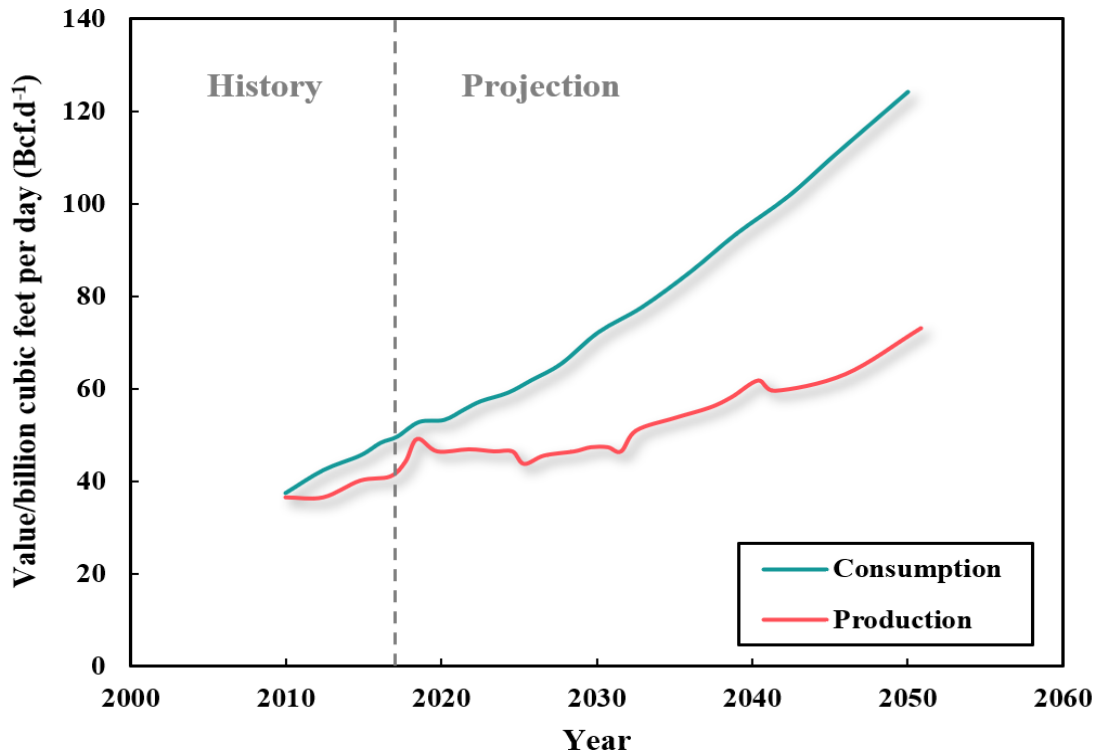


**Figure 2.** Asia natural gas consumption and natural gas production were specified from 2010 and predicted up to 2050 [8].

Natural gas storage has predominately been conducted through compressed natural gas (CNG) or liquefied natural gas (LNG) systems. However, these methods have been considered expensive<sup>1</sup> due to the high compression and liquefaction prices and the costly storage tanks that should withstand high pressures (200-250 bar) or low temperatures (-162 °C). Adsorbed natural gas (ANG) systems have been proposed to increase natural gas's energy density at low pressures (35-65 bar) and room temperature. To be economically equivalent to the other NG storage techniques, the US Department of Energy (DOE) initiated the CH<sub>4</sub> storage targets; in 1993, the DOE defined the storage target 150 cm<sup>3</sup>.cm<sup>-3</sup>, volume of CH<sub>4</sub> at standard condition per volume adsorbent (V.V<sup>-1</sup>), at 25 °C and 35 bar pressure. The DOE target was raised up to 180 cm<sup>3</sup>.cm<sup>-3</sup> after a few years and then recently to 350 cm<sup>3</sup>.cm<sup>-3</sup> (for volumetric measurements) and 0.5 kg.kg<sup>-1</sup> (for gravimetric capacity)[12, 13].

Besides CH<sub>4</sub>, the use of H<sub>2</sub>, as a clean source of energy with zero carbon foot print, attracted considerable interest in recent years due to its fascinating characteristics; H<sub>2</sub> as the light element (second lightest element after helium), produces the largest amount of energy on a gravimetric basis in comparison with other fuels as shown in Figure 3 [5]. On a mass basis, the energy content of H<sub>2</sub> (120 MJ.kg<sup>-1</sup>) is nearly three times larger than gasoline (44 MJ.kg<sup>-1</sup>). Besides, as a fuel, H<sub>2</sub> produces water after the combustion reaction. However, H<sub>2</sub> has a low volumetric energy density

---

<sup>1</sup> **A)** The study on the economic feasibility associated with compressed natural gas vehicle fueling provide estimated cost range of \$250000-\$600000 for instalation of medium CNG station with capacity of 500-800 gasoline gallon equivalent per day.

[10] M. Smith, J. Gonzales, Costs associated with compressed natural gas vehicle fueling infrastructure, National Renewable Energy Lab.(NREL), Golden, CO (United States), 2014..

**B)** The expenses of diffrent phase related to the LNG opeation are generally included exploration & production (\$0.60–1.2 per one million British thermal units, or MMBtu), liquefaction (\$0.90–1.30/MMBtu), shipping (\$0.50–1.80/MMBtu), storage & regasification (\$0.40–0.60/MMBtu).

[11] J. Cho, G.J. Lim, S.J. Kim, T. Biobaku, Liquefied natural gas inventory routing problem under uncertain weather conditions, International Journal of Production Economics 204 (2018) 18-29.

at the ambient temperature and atmospheric pressure. Liquefied H<sub>2</sub> has a relatively higher energy density of 8 MJ.l<sup>-1</sup>, but still is lower than the conventional fuels such as gasoline (32 MJ.l<sup>-1</sup>).

Developments in H<sub>2</sub> storage technologies, such as metal hydrides, spillover, physisorption and chemisorption, might improve the H<sub>2</sub> low volumetric energy density. However, most of these strategies are still far from commercialization due to economic and/or technical challenges. Among the current technics, physisorption of H<sub>2</sub> on porous materials seems to be promising due to its fast kinetics and the reversibility of the storage process [14]. To make the adsorptive storage of H<sub>2</sub> comparable to liquefied H<sub>2</sub>, in 2020, the US Department of Energy (DOE) specified a target adsorbed H<sub>2</sub> value of 0.040 kg H<sub>2</sub>.l<sup>-1</sup> and 0.055 kg H<sub>2</sub>.kg<sup>-1</sup> system on a volumetric and gravimetric basis (See Figure 3).

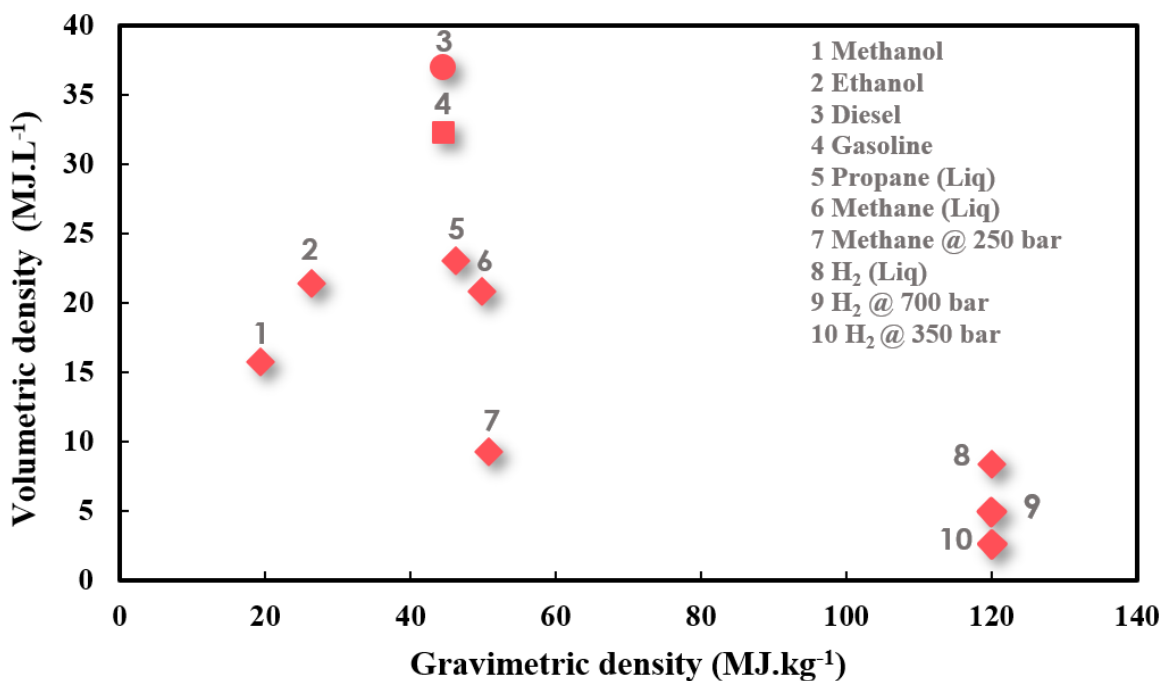


**Figure 3.** Comparison of energy density for different types of fuels on gravimetric and volumetric scales [5].

Several types of adsorbents have been investigated in the literature for gas storage applications, including porous carbons [15], zeolites [16], metallic organic frameworks (MOFs) [17], porous

aromatic frameworks (PAFs) [12, 18] and metal oxides [19, 20]. Based on what has been reported, to maximise the gas storage capacity, adsorbents should meet the following requirements:

- (1) micropore size distribution with predominant pores around 0.8 -1.1 nm width for methane and 0.6 nm for hydrogen storage (should be noted that with such an optimum PSD, two CH<sub>4</sub> and H<sub>2</sub> molecules can be adsorbed easily inside the micropores)[21-23],
- (2) high packing density to guarantee that volumetric storage capacity will be high [24-27],
- (3) appropriate thermal properties (i.e. high specific heat capacity and low heat of adsorption) to minimize the thermal fluctuations inside the adsorbent bed [28, 29],
- (4) better to be extremely hydrophobic [23, 30],
- (5) preferably inexpensive and potential for mass production [31, 32].

The advantages and disadvantages of some groups of adsorbents are listed in Table 1. As can be seen, although some of the novel adsorbents such as MOFs or PAFs can be designed to possess optimum pore size distribution and an exceptional gas adsorption capacity (near the latest DOE target), their costly and complex synthesis methods hinders their practical application.

Carbon-derived adsorbents are one of the main studied classes of adsorbents for gas storage and energy-related applications due to their particular characteristics such as high porosity, and chemical/thermal/mechanical stability. More importantly, compared to other porous materials that require the use of expensive precursors and time-consuming synthesis, production of carbon derived adsorbents is affordable. As shown in Figure 4, there is a wide range of carbon-derived products, including activated carbons, carbon fibres, carbon foams, carbon molecular sieves and carbon nano-allotropes (i.e. fullerene, carbon nanotube, graphene sheets and carbon graphitic structures).

**Table 1.** Some critical features of well-known groups of adsorbents.

Adsorbent's type	Feature	
	Advantage	Disadvantage
<b>Carbons</b> [15]	<ul style="list-style-type: none"> <li>+ Large surface area (up to 3000 m<sup>2</sup>.g<sup>-1</sup>), +</li> <li>Tunable pore size distribution,</li> <li>+ Light weight</li> <li>+ High adsorptive characteristics (CH<sub>4</sub> uptake &gt; 190 V.V<sup>-1</sup> &amp; H<sub>2</sub> uptake ~ 11.5 wt.%)</li> <li>+ Abundant and eco-friendly precursors</li> <li>+ Simple production methods</li> <li>+ Possibility structural modifications</li> <li>+ Excellent stability in extreme conditions of temperature and humidity</li> <li>+ Generally hydrophobic surfaces</li> <li>+ High heat and electrical conductivities</li> <li>+ Acceptable cost, the capacity of large production</li> <li>+ Excellent mechanical properties</li> </ul>	<ul style="list-style-type: none"> <li>- Low adsorption capacity and selectivity in comparison with novel adsorbents such as MOFs.</li> <li>- Challenging to prepare different batches of a carbonaceous adsorbent with a uniform structure (As zeolites or MOFs).</li> </ul>
<b>Zeolites</b> [16]	<ul style="list-style-type: none"> <li>+ Medium gas storage capacity</li> <li>+ Large portion of micro/mesopores</li> <li>+ Low cost</li> <li>+ Good mechanical properties</li> </ul>	<ul style="list-style-type: none"> <li>- Relatively low surface area in comparison with ACs and some novel adsorbents</li> <li>- High affinity to water</li> <li>- Difficult synthesis process</li> <li>- Regeneration needs more effort in comparison with other classes of the adsorbents</li> </ul>
<b>Metallic organic frameworks (MOFs)</b> [17]	<ul style="list-style-type: none"> <li>+ High surface area (area up to 7000 m<sup>2</sup>.g<sup>-1</sup>)</li> <li>+ Tunable pore volume/size distribution</li> <li>+ Higher gas storage capacity usually more than carbon materials<sup>[33]</sup> (CH<sub>4</sub> uptake &gt; 250 V.V<sup>-1</sup> &amp; H<sub>2</sub> uptake ~ 11 wt.%)</li> <li>+ High gas selectivity</li> </ul>	<ul style="list-style-type: none"> <li>- Expensive raw material and production methods</li> <li>- Difficult synthesizing processes</li> <li>- Low thermal stability</li> <li>- Poor mechanical strength</li> <li>- Unstable in the presence of moisture</li> </ul>
<b>Porous aromatic frameworks (PAFs)</b> [12, 18]	<ul style="list-style-type: none"> <li>+ Very high surface area (up to 7500 m<sup>2</sup>.g<sup>-1</sup>)</li> <li>+ Very high gas storage/separation capacity (CH<sub>4</sub> uptake &gt; 250 V.V<sup>-1</sup> &amp; H<sub>2</sub> uptake ~ 64 wt.%)</li> <li>+ Exceptional thermal and chemical stability</li> <li>+ Synthesised via various coupling reactions</li> <li>+ Chemically resistant to harshly acidic, alkaline and humid environments</li> </ul>	<ul style="list-style-type: none"> <li>- Current coupling reactions for PAF syntheses are expensive</li> <li>- Organometallic catalysts which are used in PAFs preparation method hardly can be removed from the framework</li> <li>- Difficulties in morphologies engineering and shapes for specific applications</li> </ul>
<b>Metal Oxides</b> [19, 20]	<ul style="list-style-type: none"> <li>+ Good electrical and ionic conductivity properties</li> <li>+ Ability of reversible capacity</li> <li>+ High mechanical stability</li> <li>+ Relatively high gravimetric H<sub>2</sub> storage capacity</li> </ul>	<ul style="list-style-type: none"> <li>- Expensive materials</li> <li>- Slow reaction Kinetics</li> <li>- High dissociation temperatures</li> <li>- Unpublished data for CH<sub>4</sub> uptake over last years</li> </ul>



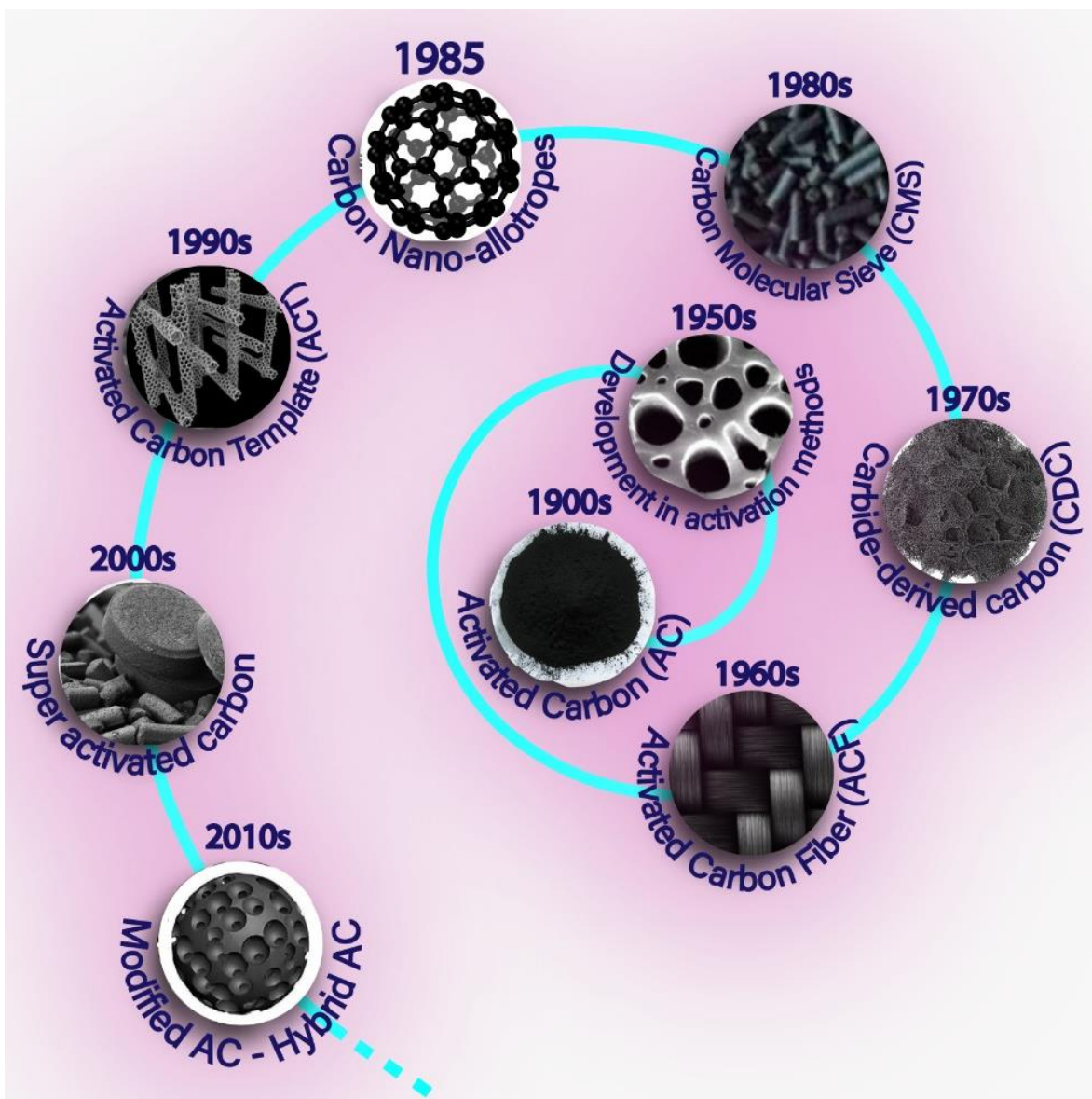


**Figure 4.** A road map sketch over the developmental history of the porous carbons

The gas adsorption capacity of solids strongly depends on their porosity and surface properties. Careful fabrication of carbonaceous matters can significantly improve their properties for specific applications. For instance, some new-reported activated carbons possess a significant porosity and surface area of more than  $3000 \text{ m}^2 \cdot \text{g}^{-1}$ . However, it needs to be considered that the porosity of adsorbents does not necessarily guarantee their high gas storage capacity. Numerous investigations are still going on to optimise production methods for the cost-effective microporous carbons that

satisfy the latest value of the DOE target. The linear relationship between methane adsorption capacity and micro/meso porosity of adsorbents has been discussed by Rodríguez-Reinoso et al. and Monge et. al [31, 34]. They found out that the sample with the highest BET surface area (Brunauer, Emmett and Teller,  $S_{\text{BET}}$ ) shows the largest gravimetric  $\text{CH}_4$  uptake at any desired pressure. However, the low packing density of this sample directly affects its volumetric storage capacity, which results in its relatively low volumetric  $\text{CH}_4$  uptake. On the other hand, the sample with a medium level of microporosity and packing density shows the highest value of volumetric  $\text{CH}_4$  capacity among all the prepared ACs. It can be concluded that the best sample for ANG purposes is the one with the best balance among micro porosity and the packing density[13, 34].

The majority of available research outcomes on carbon preparation rely on a trial and error approach with relatively considerable uncertainty and poor reproducibility of the results. One best way to maximise carbon-based materials' gas storage performance is to design them with a precise and predictable synthesis approach. Such an approach provides a specific large-scale synthesis pathway which is a complete departure from conventional methods. This review aims to concentrate on five topics of; **(1)** theoretical and experimental design of different classes of carbon-based adsorbents for gas storage/separation applications with deep emphasis on  $\text{H}_2$  and  $\text{CH}_4$ , **(2)** conventional carbon-based adsorbents **(3)** novel structured microporous carbons, **(4)** carbon nano allotropes, **(5)** the future for carbon-based gas adsorbents.

In the present review study, we mostly presented more recent research articles though the previous related literature were also monitored, and used if it was necessary. According to statistics, up to January 2022, about 5,214 and 13,701 publications were respectively matched with search topics of “carbon+methane adsorption/storage/separation” and “carbon+hydrogen dsorption/storage/separation” [35]. Within the last 10 years, the number of publications in this

particular field has increased and this is reflecting the rapid expansion of this research topic [35]. Therefore, we believe it is an appropriate time to provide a comprehensive guide to the developments in this field over the past decade.

## **2. Activated carbons**

Activated carbons (ACs) is one the main members of porous carbon materials which have been extensively investigated in different fields of application. Their tunable micro/mesoporosity has been instrumental in achieving their best performances, especially for fuel gas storage and separation requests. A variety of synthesis approaches have been developed to control the pore size distributions in these materials - some of these were undoubtedly succeeded in theoretical and experimental assessment [23, 24, 30, 32, 36-42]. In this work, some of the efficient practices reported in the literature were reviewed.

ACs are prepared through the decomposition of organic substances with high carbon content (which is called carbonization process) followed by the activation of the carbonized materials to improve the porosity, as presented in Figure 5. The starting materials for AC production could be classified into two main groups of non-renewable materials and renewable biomass resources. As shown in Table 2, various fossil-based precursors such as coal [24, 43], petrol coke [44, 45], pitch [42, 46] as well as synthetic polymers [47, 48] are categorised as non-renewable precursors. Renewable sources with inherent advantages like cost-effectiveness and availability are classified into three main groups including (i) polysaccharides (e.g. starch [49] and chitosan [50]) (ii) raw or waste biomass (e.g. date seed [51] and Mandarin peels [52]) and (iii) microorganisms, (e.g. microalgae [53] and fungi [14]) (see Table (3)).

According to the literature, the precursors with a high carbon content are promising candidates for the gas storage/separation application [26, 32, 39]. However, it is possible to enhance the fixed carbon content of the starting materials by prewashing them in two different media of water and/or mild acid [54]. The unwanted organic attachments/contaminations like sands and loose ash can be eliminated by water washing. The chemically bonded compound including ash elements can be effectively removed from the solid structure by the acid washing process. Suppose the washed-precursors still possess a low amount of carbon, it is essential to raise it by removing light volatiles through an initial heat treatment (i.e. pre-carbonisation) before the production procedure[54].

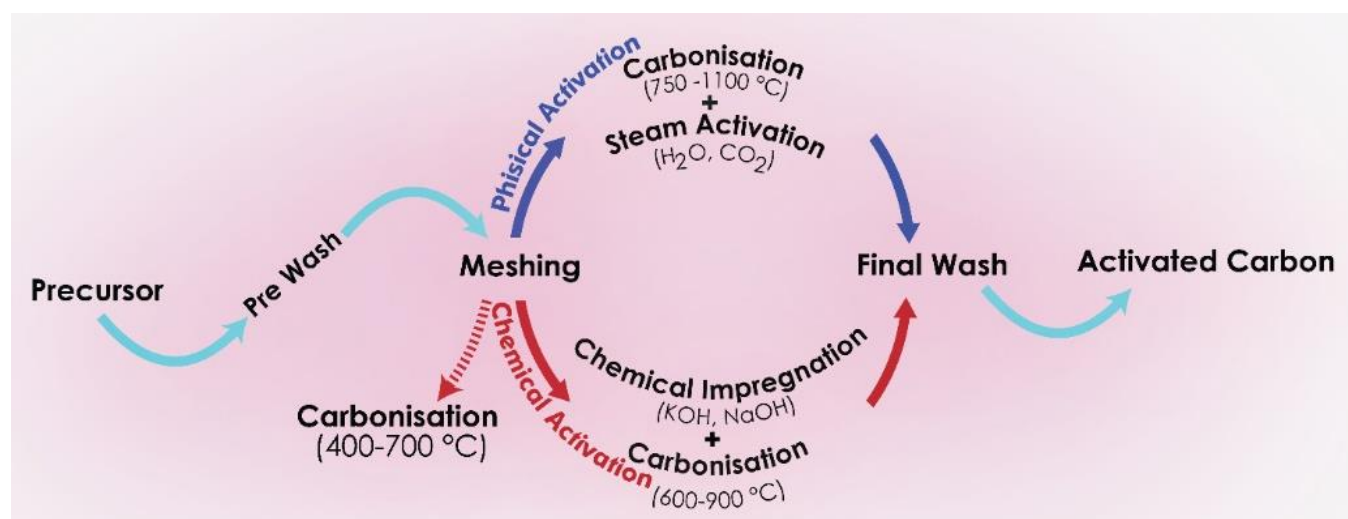


**Figure 5.** Schematic diagram introducing the preparation process of AC adsorbent

A high temperature of up to 650-700 °C is applied during carbonisation to evaporate and remove volatile components from the precursor under an oxygen-free environment. In other words, non-carbon ingredients are volatilized under inert gasses such as N<sub>2</sub> and Ar, which causes an increase in the carbon content of the carbonized samples [42]. In the next step, The carbonised product with a carbon content of higher than 85%, called char or biochar, will be activated to form fine solid cavities (i.e. porosity) inside their structure [55, 56]. Activation is involved with consecutive

reactions inside the precursor's framework under the thermal condition [54]. The presence of some functional groups (e.g. alkyl species ( $=CH_2$ ), C–C, C–O–C, and C–O–H), which can serve as active sites, is inevitably essential for the activation reactions to develop the micro/mesoporosity. The lack of these functional groups in the matrix structure of the carbonized precursors harms the formation of appropriate micropore distributions and consequently the gas storage capacity of the final AC [13, 23, 24, 30, 32, 36-42].

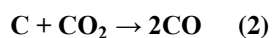
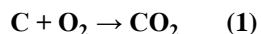
Here, we reviewed several conventional and novel production approaches for ACs comprising physical activation, chemical activation, combined physico-chemical activation, hydrothermal carbonization, templating method together with practical techniques for assembly of ordered/structured adsorbents. The synthesis principles, type of carbon starting materials (precursors), pore structure formation, as well as the  $CH_4/H_2$  storage and separation performance of the prepared ACs were analyzed under each preparation approach.

## **2.1 Physically activated carbons**

Physical activation, also known as “thermal oxidation”, is considered an inexpensive approach for producing activated carbon without applying any chemical. This method can produce ACs with well-developed porosity in the solid structure favourable for gas adsorption requests. The primary purpose of such activation is to extend and open the incipient porosity developed during the carbonization [57]. This method mainly involves partial gasification of the carbon framework under controlled atmospheres of oxygen [5]/ air [5]/ carbon dioxide [58]/ steam [59] or their mixtures [60] at a high-temperatures of (700-1400 °C).

Among many preparation parameters, activation temperature and gas flow rate can effectively impress the final textural features of activated carbon [5, 54]. The activation temperature generally

depends on the reactivity between the raw carbon materials and oxidant agents. However, it is recommended to hold the temperature at a medium point to assure a diffuse regime control of the reaction and prevent the fast gasification of the external surfaces [5]. In the case of gas flow rate, adjusted entering gas speed is required. With high gas flow rates, the physical agent does not deeply penetrate inside the precursor's structure, and the burn-off (i.e. amount of the carbons which react with oxygen and leave the solid structure as a CO or CO<sub>2</sub> gases) issue becomes more important than developing the porosity. On the other hand, a slow gas flow rate (below 10 ml/min) favours creating more uniform microporosity due to more even gasification of the whole carbon particle network [37]. The following reactions happen during the activation of the carbon materials under an oxidant environment of oxygen/ air (reaction 1), carbon dioxide (reaction 2) and steam (reaction 3), which result in the formation of highly porous structures [13]:



Among many of the reported physically prepared ACs for gas storage requests [57, 61-63], spherical porous carbons (SPCs), shown in Figure 6, have been attracted great interest because of their high surface-to-volume ratio, good structural features and ample void space for encapsulating plenty of guest molecules [62, 64]. Generally, the SPCs are derived from renewable resources (e.g. starch, nutshells, glucose) via the CO<sub>2</sub> activation technique [62, 65-67]. Li *et al.* prepared starch-derived porous carbons with spherical morphology via an environmental-friendly and straightforward CO<sub>2</sub> activation without using any template [62]. The physical activation process of starch-based carbon spheres (CSs) was involved with two stages of (i) carbonisation, where the CSs were heated up to 500 °C in a tube furnace under flowing N<sub>2</sub> (60 ml. min<sup>-1</sup>, 99.9% purity) for 180 min, afterwards (ii) the temperature raised to 1000 °C under CO<sub>2</sub> atmosphere (100 ml.min<sup>-1</sup>,

99.9% purity) to activate the carbonized CSs for 150 min. Based on the SEM results depicted in Figure 6, the high-temperature-activated CSs were thermally and morphologically stable - the spherical morphology was maintained fixed with no significant changes after the high-temperature activation. They also reported an exceptionally high surface area of  $3350 \text{ m}^2 \cdot \text{g}^{-1}$  and a high pore volume of  $1.75 \text{ cm}^3 \cdot \text{g}^{-1}$  for the activated CS. Moreover, high uptakes values for  $\text{CH}_4$  ( $16.7 \text{ mmol} \cdot \text{g}^{-1}$ , at 20 bar and  $25 \text{ }^\circ\text{C}$ ) and  $\text{H}_2$  (6.4 wt.%, 22 bar and  $-196 \text{ }^\circ\text{C}$ ) made these adsorbents a promising candidate for gas storage application.

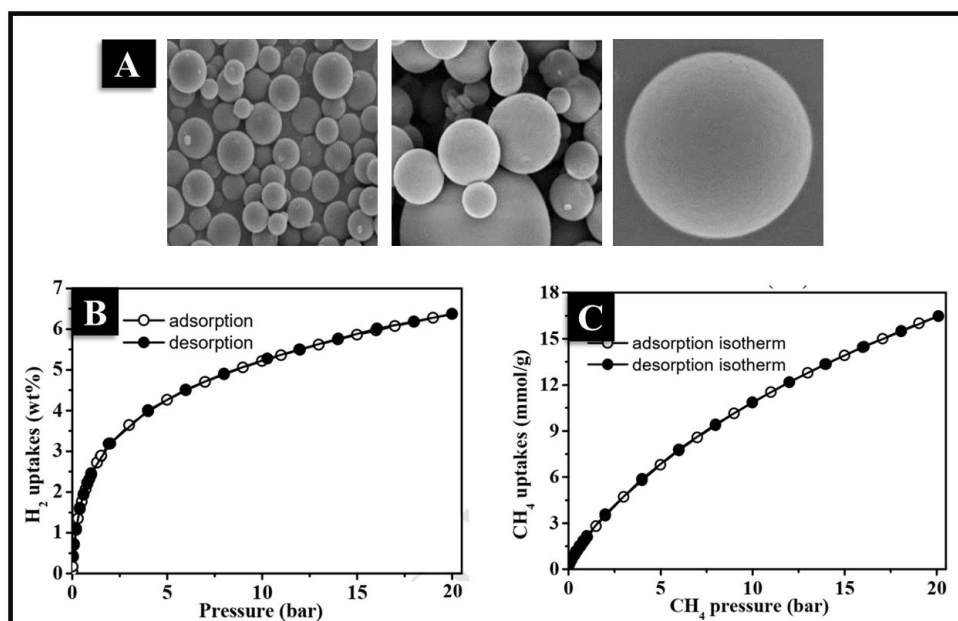


**Figure 6.** (A) SEM images for carbon spheres at different magnifications (from left to right 7000, 10000 and 40000 respectively), (B) Gravimetric  $\text{H}_2$  adsorption isotherm at  $30 \text{ }^\circ\text{C}$ , (C) gravimetric  $\text{CH}_4$  adsorption reversibility at  $30 \text{ }^\circ\text{C}$ . Reproduced from ref [62]. Copyright 2016, Elsevier Ltd.

The physical activation can be considered as an inexpensive green (chemical-free) approach to produce ACs with narrow pore size distribution and good physical stability. However, the gas storage capacity of the physically activated adsorbents, especially on a volumetric scale, is usually lower than those prepared with other methods [23, 68-70]. This might be related to the relatively low packing density of the ACs produced by this method. Therefore, a balance between the

microporosity and bulk/packing density should be kept for gas storage purposes, especially for onboard vehicles.

## **2.2 Chemically activated carbons**

Chemical activation is believed to be one of the favourite approaches capable of developing low-cost and efficient micro/mesoporous carbonaceous adsorbents for gas storage requests. Chemical activation, which is also known as “wet oxidation”, includes a series of chemical reactions between a solid precursor and a chemical activating agent during the heating process under an inert environment. The precursor + chemical agent complex is simultaneously thermalized and activated at the targeted temperature (400 to 800 °C) under nitrogen or argon atmosphere. The chemical activation is considered economical for preparing ACs due to the relatively lower activation temperature and shorter retained time than the physical activation. Moreover, the resultant ACs show to have a higher specific surface area, uniform pore size distribution (PSD), and relatively higher packing density; these advantages positively affect the volumetric adsorption capacity of the products. The last item is especially essential for onboard gas storage applications.

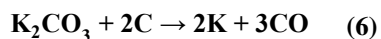
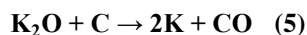
### **2.2.1 Chemical agent**

A detailed study on the mechanism of different chemical activation reactions in the precursor + chemical agent complex can be found in Rodriguez et al. efforts [60, 71]. They reported that although all kinds of chemical agents react with the precursor, some apparent differences are observed at the end of the impregnation step in the resulting materials. The most common chemical agents can also be divided into three species; (i) the strong chemicals, including KOH and NaOH [57, 68, 72-74], (ii) the middle range activating agents include  $K_2CO_3$  and  $Na_2CO_3$  [75-77], and (iii) the weak alkaline activating agents, also known as salts of strong alkalis



and weak acids, comprising  $\text{ZnCl}_2$  and  $\text{H}_3\text{PO}_4$  [57, 78-82]. KOH is the most effective activating chemical for synthesising ACs with an extremely high specific surface area among these alkaline activating agents. Potassium hydroxide can suppress the generation of tar, allow a lower activation temperature during the activating reaction, accelerate the removal of noncarbon components and enhance the reaction rate of pyrolysis [83]. Besides, reaction with KOH as a chemical agent widens the micropore,  $\text{ZnCl}_2$  increases small mesoporosity and  $\text{H}_3\text{PO}_4$  forms a more heterogeneous pore size distribution in the matrix structure of the final adsorbent [71].

The likely reactions that might be happening between KOH and carbon raw materials are presented in the following equations:



The initial mixing of the precursor and the chemical agent, also called the “mass-transfer” step, is critical to reaching well-developed porous carbons for gas storage uses. The raw carbon materials can be mixed with the agent in an aqueous solution (impregnation method) or just directly by grinding in the solid phase (dry method). Depending on the application of interest, either of these mixing methods is efficient. As a general rule, activated carbon produced via the dry mixing of precursor + alkaline agents has a higher and more well-developed porosity than those made by the impregnation method [23, 68]. In a study by Byamba-Ochir et al. [55], they investigated the impact of dry and wet initial mixing of NaOH as the activating agent on the porous texture of anthracite-based carbons. It was shown that the activation of the dry mixed sample resulted in a higher BET surface area of 1375-2063  $\text{m}^2\cdot\text{g}^{-1}$  than those prepared by the impregnation method (816-1763  $\text{m}^2\cdot\text{g}^{-1}$ ). Moreover, since the dry process requires less time and energy consumption than the

impregnation method, physical or dry mixing is preferable to produce activated carbons on an industrial scale.

Finding optimum synthesis conditions to achieve a high gas capacity is challenging since many different preparation parameters were involved in the chemical activation process. Moreover, a multivariate study including an empirical investigation and laboratory analysis is quite expensive and time-consuming. Practising soft computations and using their nonlinear mapping capability and lack of necessity for detailed mechanical knowledge seems to be an excellent choice to attain ACs with high stored gas capacity. Several well-known empirical models are used for similar material designs to maximize the corresponding adsorbent's gas storage characteristics [24, 82, 84, 85]. We investigated the effect of different preparation variables (activation agent ratio, activation temperature and retention time) on the specifications of the coal-based ACs. The CH<sub>4</sub> adsorption capacity of the ACs was examined experimentally, and the results were analyzed systematically through empirical models (see Figure 7) [24]. Mathematical optimization tools (i.e. response surface methodology and genetic algorithm) were used to find the best preparation condition where the highest gas adsorption capacity can be achieved.

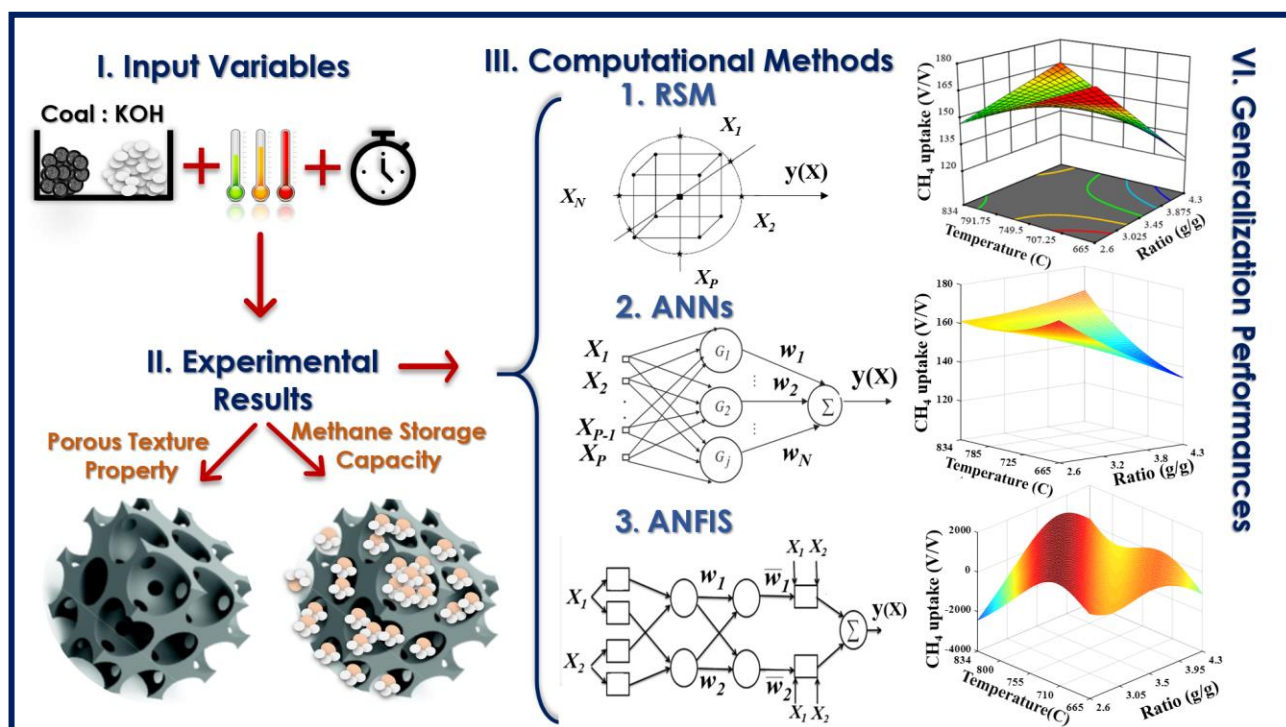


**Figure 7.** A schematic illustration of experimental and theoretical pathways. Reproduced from ref [24]. Copyright 2020, American Chemical Society.

In a similar study, Ahmadpour et al. applied the models of artificial neural networks and adaptive neuro-fuzzy interference systems to predict ACs porosity characterization (i.e. BET surface areas;  $S_{\text{BET}}$ , and micropore volumes;  $V_{\text{micro}}$ ) [84]. They found that the models were able to predict the experimental data reasonably.

### 2.2.2 Raw materials

The pore structure and consequently gas adsorption capacity of ACs profoundly is affected by many parameters such as type of precursors, type and amount of chemical agents, carbonization temperature, and activation parameters (e.g. thermal condition and retention time) [69, 84]. Here, the effect of the preparation parameters of precursors and activation agents on the gas storage capacity of the prepared ACs are discussed.

Sawant *et al.* used raw and calcined petroleum cokes as a carbon precursor to prepare activated carbons on medium and pilot-scale by chemical activation method [45]. Results showed that raw petroleum coke was a favourable choice as a precursor, whereas the enhanced graphitic arrangement limits the applicability of the calcined petroleum coke. The prepared activated carbon exhibited a high specific surface area of  $3578 \text{ m}^2.\text{g}^{-1}$  and high  $\text{CH}_4$  storage capacity of  $10.87 \text{ mmol.g}^{-1}$  at  $30 \text{ }^\circ\text{C}$  and  $37 \text{ bar}$ , and  $\text{H}_2$  capacity of  $26.67 \text{ mmol.g}^{-1}$  at  $-196 \text{ }^\circ\text{C}$  and  $3 \text{ bar}$ . Based on the equilibrium adsorption data of  $\text{CO}_2$ ,  $\text{CH}_4$ ,  $\text{CO}$ , and  $\text{N}_2$  measured on the prepared powder ACs at different temperatures, it was concluded that the adsorbents are promising applicants for gas separation. In another study [42], we prepared a series of ACs from carbonized coal tar pitch (CTP) using  $\text{KOH}$  as the activating agent to investigate the effect of two-stage treatment (acidification and carbonization) of the CTPs on the structural properties and  $\text{CH}_4$  adsorption capacity of the prepared adsorbents. Depending on the thermal condition in the pre-carbonization step, the post-activated samples showed different  $\text{CH}_4$  storage capacities. Among all ACs, a sample with  $S_{\text{BET}}$  of  $2261 \text{ m}^2.\text{g}^{-1}$  which carbonized at  $600 \text{ }^\circ\text{C}$  for  $2 \text{ h}$  and later activated at  $900 \text{ }^\circ\text{C}$  for  $3 \text{ h}$ , showed the maximum  $\text{CH}_4$  uptake.

Past decades have witnessed a rapid development of synthetic polymers and related materials, including poly(vinylidene chloride)[86], phenyl-trimethylsilane [47], Polypyrrole [87], terephthalaldehyde [88], benzimidazole-linked polymers [48], polythiophene [89], porous coordination polymers [90], as potential precursors for the preparation of ACs for gas storage and purification applications. Cai *et al.* synthesized poly(vinylidene chloride)-based carbon (PC) with ultrahigh microporosity by simple carbonization and moderate  $\text{KOH}$  activation [86]. The obtained samples possessed a high surface area (up to  $2150 \text{ m}^2.\text{g}^{-1}$ ) and pore volume (up to  $0.9 \text{ cm}^3.\text{g}^{-1}$ ). The  $\text{CH}_4$  uptake value for the activated PC was reported up to  $10.25 \text{ mmol.g}^{-1}$  (16.4 wt.% or 147

V.V<sup>-1</sup>) at 25 °C and 20 bar. Moreover, they measured a large H<sub>2</sub> adsorption capacity of 4.8 wt.% at -196 °C and 20 bar for the activated PC. The sample was shown to have a moderate selectivity for CO<sub>2</sub>/CH<sub>4</sub> and CH<sub>4</sub>/N<sub>2</sub>. Attia and colleagues [87] developed a flexible AC by chemical activation of commercial viscose rayon cloth fibre. The final adsorbent showed a high surface area of 2000 m<sup>2</sup>.g<sup>-1</sup> and superior storage capacity for CH<sub>4</sub> (7.5 mmol.g<sup>-1</sup>, at 20 bar and 25 °C) and H<sub>2</sub> (4 wt.%, at 20 bar and -196 °C). They also reported a high separation selectivity of 15.9 for CO<sub>2</sub>/CH<sub>4</sub> based on the ideal adsorbed solution theory (IAST) model.

Shirazani and co-worker's synthesized nanoporous carbon spheres by KOH activation of starch as the starting carbon source to reach the high CH<sub>4</sub> uptake [49]. The best nanoporous sample with a carbon: KOH ratio of 1:4 showed a high specific surface area of 2222.3 m<sup>2</sup>.g<sup>-1</sup>, pore volume up to 1.72 cm<sup>3</sup>.g<sup>-1</sup> and CH<sub>4</sub> storage capacity of 12.8 mmol.g<sup>-1</sup> (at 25 °C and 35 bar). In another study, Jung *et al.* prepared a set of porous carbons by KOH activation of fruit by-products (i.e. Mandarin peels) [52]. A scalable synthesis approach was designed for recycling and converting these economically bio-wastes to valuable products, wherein the impact of carbonization and activation temperatures and activating agents was thoroughly investigated. As-made nanoporous carbons demonstrated good textural properties such as a high surface area of ~2500 m<sup>2</sup>.g<sup>-1</sup> and pore volume of 1.04 cm<sup>3</sup>.g<sup>-1</sup>. Experimental measurements proved that these nanoporous materials possessed a promising sorption capacity for H<sub>2</sub> (6.1 wt.% at -196 °C and 25 bar) and CH<sub>4</sub> (9.65 mmol.g<sup>-1</sup> at 25 °C and 25 bar) together with an excellent gas separation performance for binary mixtures of (CO<sub>2</sub> + CH<sub>4</sub>), (CH<sub>4</sub> + N<sub>2</sub>) and CO<sub>2</sub> + N<sub>2</sub>).

An almost new term of “Physio-chemical” methodology generally represents a combination of two conventional physical and chemical activation approaches, involving chemical impregnation of carbon precursors with an activating agent, followed by a physical activation step under an

oxidizing gas atmosphere (mainly CO<sub>2</sub>). Well-regulated porous textural properties and surface modification ability are considered the advantages of this mixed-method [91]. In this method, the chemical agent generates small micropores while the physical activation makes the pores' size homogenous and narrows pore size distribution around an optimum diameter/width. Up to date, several valuable studies have been reported for the synthesis of physio-chemically activated carbons for gas storage/separation uses [91-93]. Preacher and coworkers prepared several ACs in powder, granule, and monolith form using a both chemical and physical activation approaches to improve the gas adsorption capacity of solids [91]. They used H<sub>3</sub>PO<sub>4</sub> and ZnCl<sub>2</sub> as the chemical agents, and CO<sub>2</sub> was used as a physical activator. The H<sub>3</sub>PO<sub>4</sub> and ZnCl<sub>2</sub>-activated samples respectively showed acceptable CH<sub>4</sub> adsorption values of 155 V.V<sup>-1</sup> and 165 V.V<sup>-1</sup> (25 °C and 35 bar). Based on the experimental observations, the maximum gas storage values were verified for the series prepared with ZnCl<sub>2</sub> rather than the prepared sample using H<sub>3</sub>PO<sub>4</sub>. These results were justified by the formation of narrower pore width distribution centered around 0.8 nm by ZnCl<sub>2</sub> activation, such PSD is about twice the dimension of the methane molecule and provides a fine space for optimizing the methane storage capacity [93].

Although the combined activation approach enjoys the advantages of both originated physical and chemical activation methods, it is a complex and energy-consuming technique. As a result, there is a considerable gap between laboratory studies and large-scale production for industry application [83].

**Table 2.** Non-renewable porous carbons prepared by activation for gas storage.

Precursor + Activator	Porosity			$\rho$ packed (g.cm <sup>-3</sup> )	H <sub>2</sub> uptake (wt.%)	CH <sub>4</sub> Storage Capacity (V.V <sup>-1</sup> )	Selective Separation Capacity (SSC)		Measurement Condition	Reference
	S <sub>BET</sub> (m <sup>2</sup> .g <sup>-1</sup> )	V <sub>t</sub> / V <sub>p</sub> (cm <sup>3</sup> .g <sup>-1</sup> )	d <sub>ave</sub> (nm)				CO <sub>2</sub> /CH <sub>4</sub>	CH <sub>4</sub> /N <sub>2</sub>		
DOE targets	-	-	-	-	5.5	350	-	-	H <sub>2</sub> @ -196 °C, 20 bar CH <sub>4</sub> @ 25 °C, 35 bar	[94, 95]
1,3 bis(cynomethyl imidazolium) chloride + KOH	1317	0.64 / 0.43	0.59	-	2.96	-	-	-	H <sub>2</sub> @ -196 °C, 1 bar	Sethia et al.[96] (2016)
Poly (vinylidene chloride) (PVDC) + KOH	2151	0.90 / 0.85	1.44	0.64	5	147	-	-	H <sub>2</sub> @ -196 °C, 20 bar CH <sub>4</sub> @ 25 °C, 20 bar	Cai et al.[86] (2014)
Polypyrrole + ZnCl <sub>2</sub> /NH <sub>4</sub> Cl	1911	0.85 / 0.60	0.85	-	4	7.5 mmol. g <sup>-1</sup>	3.4	-	H <sub>2</sub> @ -196 °C, 20 bar CH <sub>4</sub> @ 25 °C, 20 bar SSC @ 25 °C, 20 bar	Attia et al.[87] (2020)
Ethylene tar + KOH	2465	1.12 / 0.89	0.80	0.60	-	150	-	-	CH <sub>4</sub> @ 25 °C, 35 bar	Casco et al.[32] (2015)
Decanted oil + KOH	2700	1.23 / 0.93	0.80	0.62	-	160	-	-	CH <sub>4</sub> @ 25 °C, 35 bar	Casco et al.[32] (2015)
Mesophase pitches + KOH	3290	2.25 / 1.10	-	0.53	-	156	-	-	CH <sub>4</sub> @ 25 °C, 35 bar	Casco et al.[39] (2015)
Benzimidazole- linked polymers (BILP) + KOH	1630	0.66 / 0.59	0.70	-	-	1.7 mmol. g <sup>-1</sup>	13	-	CH <sub>4</sub> @ 25 °C, 1 bar SSC @ 0 °C, 1 bar	Ashourirad et al.[48] (2015)
Nitrogen-rich BILP + KOH	2059	0.89/ 0.74	0.90	-	-	1.5 mmol. g <sup>-1</sup>	10	-	CH <sub>4</sub> @ 25 °C, 1 bar SSC @ 0 °C, 1 bar	Ashourirad et al.[48] (2015)
Petroleum tar pitch and powdered coal + KOH	1044	0.5 / 0.46	0.98	0.42	-	5.05 mmol. g <sup>-1</sup>	-	2.23	CH <sub>4</sub> @ 25 °C, 40 bar SSC @ 25 °C, 1 bar	Arami-Niya et al.[46] (2016)
Nitrogen-rich polymer + KOH	2146	1.96 / 0.91	3.20	-	-	2.12 mmol. g <sup>-1</sup>	47.1 (C <sub>2</sub> H <sub>2</sub> /CH <sub>4</sub> )		CH <sub>4</sub> @ 0°C, 1.13 bar SSC @ 25 °C, 1.13 bar	Wang et al.[88] (2016)
Hyper crosslinked porous polymers + KOH	3101	184 / 1.40	1.40	-	3.25	2.76 mmol. g <sup>-1</sup>	-	-	H <sub>2</sub> @ -196°C, 1.13 bar CH <sub>4</sub> @ 0 °C, 1.13 bar	Zhang et al.[47] (2017)
Calcined petroleum cokes + KOH	3575	191 / 1.26	2.10	-	-	1.96 mmol. g <sup>-1</sup>	2.1	2.8	CH <sub>4</sub> @ 24°C, 1.13 bar SSC @ 15 °C, 1.13 bar	Sawant et al.[45] (2017)
Carbon black + KOH	1639	1.25 / 0.66	0.82	-	234.71 cm <sup>3</sup> .g <sup>-1</sup>	-	-	-	H <sub>2</sub> @ -196 °C, 1 bar	Heo et al.[3] (2019)
Anthracite + KOH	2160	0.75	0.98	0.53	-	175	-	-	CH <sub>4</sub> @ 25 °C, 40 bar	Mirzaei et al.[24] (2020)

Coal tar pitch + KOH	2261	0.74	2.17	0.70	-	184	-	-	CH <sub>4</sub> @ 25 °C, 40 bar	Mirzaei et al.[42] (2020)
Anthracite + KOH/urea treatment	1965	0.56	2.07	0.63	0.26 mmol. g <sup>-1</sup>	190	-	-	H <sub>2</sub> @ 25 °C, 20 bar CH <sub>4</sub> @ 25 °C, 40 bar	Mirzaei et al.[25] (2020)
Viscose rayon fabric + ZnCl <sub>2</sub> /NH <sub>4</sub> Cl + CO <sub>2</sub>	1205	- / 0.46	0.78	-	1.68	0.72 mmol. g <sup>-1</sup>	4.5	-	H <sub>2</sub> @ -196 °C, 1 bar CH <sub>4</sub> @ 25 °C, 1 bar SSC @ 25 °C, 1 bar	Kostoglou et al.[92] (2017)
Polypyrrole + KOH	3225	2.43 / -	1.3	-	6.5	-	-	-	H <sub>2</sub> @ -196 °C, 20 bar	Adeniran et al.[97] (2015)



**Table 3.** Renewable porous carbons prepared by activation for gas storage.

Precursor + Activator	Porosity			$\rho_{\text{packed}}$ (g.cm <sup>-3</sup> )	H <sub>2</sub> Uptake (wt. %)	CH <sub>4</sub> Storage Capacity (V.V <sup>-1</sup> )	Selective Separation Capacity (SSC)		Measurement Condition	Reference
	S <sub>BET</sub> (m <sup>2</sup> .g <sup>-1</sup> )	V <sub>t</sub> / V <sub>p</sub> (cm <sup>3</sup> .g <sup>-1</sup> )	d <sub>ave</sub> (nm)				CO <sub>2</sub> /CH <sub>4</sub>	CH <sub>4</sub> /N <sub>2</sub>		
Oil-tea seed shell + NaNH <sub>2</sub>	774	0.32 / 0.27	0.54	-	-	0.94 mmol. g <sup>-1</sup>	12.48	4.9	CH <sub>4</sub> @ 25 °C, 1 bar SSC @ 25 °C, 1 bar	Zhang et al.[98] (2019)
Starch + KOH	2222	1.73 / -	3.08	-	-	12.81 mmol.g <sup>-1</sup>	-	-	CH <sub>4</sub> @ 25 °C, 35 bar	Shirazani et al.[49] (2020)
Date seed + KOH	2609	- / 0.70	0.63	0.69	-	13.2 mmol. g <sup>-1</sup>	-	-	CH <sub>4</sub> @ 25 °C, 35 bar	Altwala et al.[51] (2020)
Dry algae + KOH	1247.2	0.69 / -	0.51	-	-	1.3 mmol. g <sup>-1</sup>	10.1	4.1	CH <sub>4</sub> @ 25 °C, 1 bar SSC @ 25 °C, 1 bar	Wang et al.[53] (2018)
Chitosan + KOH	2513	1.08 / 0.97	1.25	-	2.88	-	-	-	H <sub>2</sub> @ -196 °C, 1 bar	Wrobel et al.[50] (2015)
Mandarin peels + KOH	2426	1.04 / 0.96	0.78	-	6.10	6.07 mmol. g <sup>-1</sup>	13.6	-	H <sub>2</sub> @ -196 °C, 25 bar CH <sub>4</sub> @ 25 °C, 25 bar SSC @ 25 °C, 25 bar	Jung et al.[52] (2020)
Coconut shells + KOH	1932	1.39 / 0.85	0.17	-	11.16	-	-	-	H <sub>2</sub> @ -196 °C, 60 bar	Park et al.[99] (2019)
Neolamarckia cadamba + KOH	3246	1.33 / 1.08	1.59	-	2.81	-	-	-	H <sub>2</sub> @ -196 °C, 1 bar	Hu et al.[100] (2019)
Starch + CO <sub>2</sub>	3350	1.75 / 1.67	1.19	-	6.4	10.7 mmol. g <sup>-1</sup>	-	-	H <sub>2</sub> @ -196 °C, 20 bar CH <sub>4</sub> @ 25 °C, 20 bar	Li et ai. [62] (2016)
Agricultural waste + N <sub>2</sub>	790	0.32 / 0.25	0.70	-	1.29	1.38 mmol. g <sup>-1</sup>	15	-	H <sub>2</sub> @ -196 °C, 20 bar CH <sub>4</sub> @ 40 °C, 1 bar SSC @ 40 °C, 1 bar	Park et al.[61] (2018)
Crab shell + CO <sub>2</sub>	1708	- / 0.89	0.55	-	-	1.74 mmol. g <sup>-1</sup>	-	6.8	CH <sub>4</sub> @ 25 °C, 1 bar SSC @ 25 °C, 1 bar	Kim et al.[58] (2018)
Phenolic resin + CO <sub>2</sub>	1107	0.46 / 0.39	0.70	-	2.48	-	-	-	H <sub>2</sub> @ -196 °C, 20 bar	Tian et al.[101] (2020)
Poly (furfuryl alcohol) + CO <sub>2</sub>	1530	0.67 / 0.42	3.6	-	1 mmol. g <sup>-1</sup>	-	-	-	H <sub>2</sub> @ 25 °C, 20 bar	He et al.[102] (2014)
Coconut shells + ZnCl <sub>2</sub> + CO <sub>2</sub>	1599	0.77 / 0.70	-	0.44	-	199 cm <sup>3</sup> .g <sup>-1</sup>	-	-	CH <sub>4</sub> @ 25 °C, 35 bar	Prauchner et al.[91] (2016)
Coconut shells + H <sub>3</sub> PO <sub>4</sub> + CO <sub>2</sub>	2191	1.12 / 0.78	-	0.36	-	220 cm <sup>3</sup> .g <sup>-1</sup>	-	-	CH <sub>4</sub> @ 25 °C, 35 bar	Prauchner et al.[91] (2016)

### 2.3 Surface-modified activated carbons

Besides the direct effect of carbon's microporosity on gas storage capacity, modifying the solid's surface chemistry (surface functionalization) can improve the adsorbent-adsorbate interaction and gas adsorption capacity. Nitrogen (N), and fluorine (F) containing contents, as well as other cations, are some of the functional groups which can be introduced (doped) into the carbon skeleton to create some momentary polarisation in the gas molecules [25, 103-107]. However, the impact of these heteroatom-dopings on the storage efficiency of gases, especially CH<sub>4</sub> and H<sub>2</sub>, is rarely studied and is often controversial. Herein, we briefly summarised the recent investigations to clarify the influences of surface chemistry on the gas uptake of carbons.

Nitrogen/oxygen doping is a common modification method to introduce basic sites into the carbon framework and enhance the polarity of the carbon surface [25, 106]. The high electronegativity of nitrogen/oxygen-containing surface groups might affect the non-polar gas molecules near carbon pores, which results in a higher uptake of H<sub>2</sub> and especially CH<sub>4</sub> molecules [25, 104]. The regular tetrahedron structure of a CH<sub>4</sub> molecule, the central C atom exhibits high electronegativity restricted by four electropositive H atoms [38]. The electronegative N and O atoms of the surface functional groups contribute their electrons to the H atoms of CH<sub>4</sub> and promote the adsorption of CH<sub>4</sub>. On the other hand, a repulsive force is evident between the C atom of the CH<sub>4</sub> molecule and the electronegative atoms of the functional groups, resulting in a reduction in the amount of CH<sub>4</sub> uptake [38]. Therefore, the introduction of functional groups on the surface of ACs has a two-fold impact (attractive and repulsive interactions) on the CH<sub>4</sub> adsorption characteristics of the corresponding adsorbents (Figure 8) [38, 108].

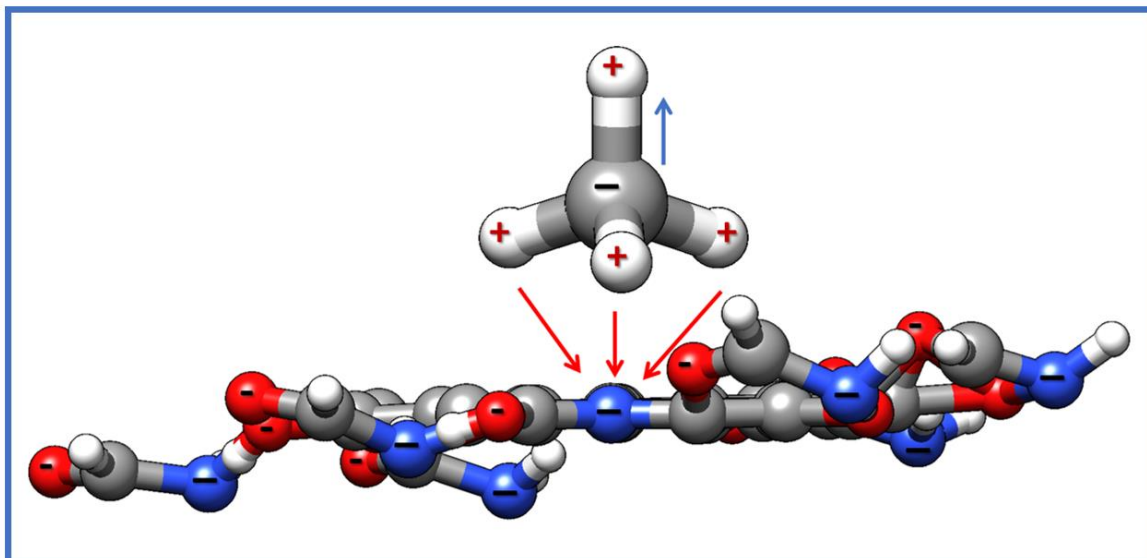


**Figure 8.** Schematic display of the interaction between the adsorbate ( $\text{CH}_4$ ) and charged atoms in the functional group of the AC-OX-U adsorbent. The visualized colors of gray, white, red and blue represent the atoms of carbon, hydrogen, oxygen, and nitrogen, respectively.

Introducing different functional groups on the surface of the ACs may have either electron-withdrawing or -donating effects. This issue influences the  $\text{H}_2$  adsorption capacity of adsorbents [109]. In other words,  $\text{H}_2$  has a weak bipole, so the adsorption of this molecule toward the solid structure of the modified ACs is profoundly affected by the electronegativity of the surface functional groups. The N- (3.04) and O-containing (3.44) functional groups exhibit strong electronegativity, but C atoms (2.55) in the matrix structure of ACs show an ultra-strong electropositivity [38, 110]. Therefore, the nitrogen and oxygen-containing group introduce negative-charge characteristics on the surface, while the carbon exhibits relatively positive-charged characteristics. As a result, this electronegativity gap will electrically attract the  $\text{H}_2$  molecule into the modified carbonaceous adsorbents [110].

We have previously studied the effect of oxygen/urea (as a source of nitrogen-containing components) on the gas storage capacity of porous carbons [25]. After functionalization of the carbon surface, the volumetric  $\text{CH}_4$  adsorption capacity of the corresponding sample was increased

by 11 % to  $190 \text{ cm}^3 \cdot \text{cm}^{-3}$  at  $25 \text{ }^\circ\text{C}$  and 40 bar. However, it was concluded that larger micropore volume is preferable to increase the  $\text{H}_2$  storage capacity of ACs, which shows the inductive effect of surface chemistry as a secondary role in  $\text{H}_2$  uptake. Similar results were reported by other authors [104, 111]. Li et al. developed cost-efficient ACs for gas storage and separation purposes via KOH activation of anthracite followed by urea treatment as a surface modification step [106]. The as-prepared carbon samples maintained developed microporosity of  $0.20\text{-}0.32 \text{ cm}^3 \cdot \text{g}^{-1}$  and a good BET surface area of  $912\text{-}1615 \text{ m}^2 \cdot \text{g}^{-1}$ . The gas adsorption measurements showed that although nitrogen doping contributes significantly to the selectivity of  $\text{CO}_2/\text{CH}_4$ , 8.09 based on IAST calculation, it almost harms the  $\text{CH}_4$  uptake of the N-dope carbons ( $1.46 \text{ mmol} \cdot \text{g}^{-1}$  at  $25 \text{ }^\circ\text{C}$  and 1 bar) compared to those simple counterpart samples ( $1.59 \text{ mmol} \cdot \text{g}^{-1}$  at  $25 \text{ }^\circ\text{C}$  and 1 bar). This observation might be interpreted by the fact that methane molecule possesses relatively low polarizability and heteroatom doping does not facilitate  $\text{CH}_4$  storing [106].

Blankenship II et al. experimentally optimized the fabrication of ACs to generate a set of porous carbons that simultaneously enjoyed a high surface area and high level of microporosity along with a high oxygen-rich nature [104]. They observed a positive effect of having extra oxygen functional groups at low pressure, where interaction between the hydrogen and surface becomes more important than at higher pressure where hydrogen uptake is more likely to occur via space-filling mechanisms. Such AC samples exhibited enhanced gravimetric hydrogen storage capacity of up to 8.9 wt% (total uptake) and 7.2 wt.% (excess uptake) at  $-196 \text{ }^\circ\text{C}$  and 30 bar. The result of hydrogen storage value is among the highest ever reported for porous carbons; the best previous reports have been in the range of 4–7.5 wt% [21, 112-114]. Table 4 summarizes some of the best activated carbons modified with functional groups or heteroatoms.

**Table 4.** Surface-modified porous carbons prepared for gas storage.

Precursor + Activator	Porosity		Functional groups/ Heteroatom	H <sub>2</sub> Uptake (wt.%)	CH <sub>4</sub> Storage Capacity (V.V <sup>-1</sup> )	Measurement Condition	Reference
	S <sub>BET</sub> (m <sup>2</sup> .g <sup>-1</sup> )	V <sub>t</sub> / d <sub>ave</sub> (cm <sup>3</sup> .g <sup>-1</sup> / nm)					
Activated carbon fibers	1053	0.50 / -	Fluorine	1.32	-	H <sub>2</sub> @ 30 °C, 100 bar	Lee et al. [115] (2007)
Activated carbon fibers	1468	0.70 / -	Ni	1.63	-	H <sub>2</sub> @ 30 °C, 100 bar	Lee et al. [115] (2007)
Poly Acrylonitrile + KOH	2500	0.75 / 1.60	Fluorine	-	150	CH <sub>4</sub> @ 25 °C, 35 bar	Im et al.[116] (2009)
Anthracite + KOH	1320	0.62 / -	Urea (CO(NH <sub>2</sub> ) <sub>2</sub> )	-	1.5 mmol.g <sup>-1</sup>	CH <sub>4</sub> @ 25 °C, 1 bar	Li et al.[106] (2013)
Nanoporous carbons*	3184	1.43 / -	-OH	-	10.30 mmol.g <sup>-1</sup>	CH <sub>4</sub> @ 25 °C, 60 bar	Lu et al. [38] (2014)
Nanoporous carbons*	3598	1.35 / -	-NH <sub>2</sub>	-	9.85 mmol.g <sup>-1</sup>	CH <sub>4</sub> @ 25 °C, 60 bar	Lu et al. [38] (2014)
Nanoporous carbons*	3548	1.36 / -	-COOH	-	9.50 mmol.g <sup>-1</sup>	CH <sub>4</sub> @ 25 °C, 60 bar	Lu et al. [38] (2014)
Hydrochar + KOH	3771	1.75 / 1.20	O	8.90	-	H <sub>2</sub> @ -196 °C, 30 bar	Scott et al. [104](2017)
Glucose + NaHCO <sub>3</sub>	1002	0.90 / 3.16	MgO nanoparticles	-	12 mmol.g <sup>-1</sup>	CH <sub>4</sub> @ 25 °C, 30 bar	Ghosh et al. [107] (2018)
Commercial AC	825	0.24 / -	Nitric acid + Ni	0.26 mmol.g <sup>-1</sup>	3.14 mmol.g <sup>-1</sup>	H <sub>2</sub> @ 30 °C, 10 bar CH <sub>4</sub> @ 30 °C, 9 bar	Rezvani et al. [117](2019)
Waste Wool + KOH	862	0.50 / -	N	-	1.70 mmol.g <sup>-1</sup>	CH <sub>4</sub> @ 0 °C, 1 bar	Li et al.[118] (2019)
Anthracite + KOH	1878	1.14 / 1.91	-OH	0.44 mmol.g <sup>-1</sup>	124.39	H <sub>2</sub> @ 25 °C, 20 bar CH <sub>4</sub> @ 25 °C, 40 bar	Mirzaei et al. [25] (2020)
Anthracite + KOH	1924	0.92 / 1.89	-NH <sub>2</sub>	0.39 mmol.g <sup>-1</sup>	178.75	H <sub>2</sub> @ 25 °C, 20 bar CH <sub>4</sub> @ 25 °C, 40 bar	Mirzaei et al. [25] (2020)
Anthracite + KOH	1695	0.88 / 2.07	-C(O)NH	0.26 mmol.g <sup>-1</sup>	190	H <sub>2</sub> @ 25 °C, 20 bar CH <sub>4</sub> @ 25 °C, 40 bar	Mirzaei et al. [25] (2020)
Coal + KOH	3037	1.30 / -	Ammonia + Boron	4.14	-	H <sub>2</sub> @ -196 °C, 1 bar	Kopac et al. [119](2020)
Lignite + KOH	500	0.046 / -	N	0.50	-	H <sub>2</sub> @ 30 °C, 30 bar	Han et al. [120](2021)

\* This symbol represents theoretical study.

## 2.4 Hydrothermal carbons

Hydrothermal Carbonization (HTC) is a well-established thermochemical synthesis approach for making functional carbon materials with high surface area and controlled porosity from wet or dry carbohydrates or lignocellulosic biomass [121]. During hydrothermal carbonization, water media acts as both solvent and catalyst, helping hydrolysis reactions and decomposition of the biomass into smaller fragments, which results in the formation of coal-like solid materials. Over the past decade, HTC considered a powerful technique for synthesising carbons from biomass [121, 122].

Preparation parameters such as the nature of the precursor and its thermal stability, temperature, residence time, and operation pressure should be optimised to reach the maximum efficiency in the HTC method [123]. As a general rule, increasing the temperature and pressure of the hydrothermal conditions increases the conversion of the biomass feedstock into carbon particles [76].

One of the main restrictions associated with the HTC technique is the relatively poor textural characteristics of the products (i.e. low surface area and undeveloped porosity). Thus the prepared adsorbents can not efficiently be applied for gas storage and separation. Post-activation of the hydrochars might be considered as a solution for producing ACs with high surface area [124]. Yuan et al. synthesized a series of nitrogen-doped porous carbons from a mixture of algae and glucose via hydrothermal carbonization and post-chemical activation [122]. They observed that post-KOH activation leads to a significant increase in the BET surface area of the ACs from 284 to 1538 m<sup>2</sup>.g<sup>-1</sup>. It was concluded that the products' CH<sub>4</sub> (2.5 mmol.g<sup>-1</sup> at 0 °C and 1 bar) and H<sub>2</sub> (0.1 mmol.g<sup>-1</sup> at 0 °C and 1 bar) storage capacity were primarily governed by narrow micropore volume and BET surface area. This study further supports the standpoint that post-synthesis activation is an efficient way to develop the porosity of carbon frameworks.

The HTC's temperature strongly influences the porosity of the post-activated carbons [124]. When the HTC is conducted in the temperature range of 200 to 250 °C, two factors of a higher density of carbonyl components and the low degree of aromatization facilitate the development of porosity during KOH activation. Falco and colleagues evaluated the impact of different HTC temperatures on porosity and gas adsorption properties of biomass-derived ACs [121]. They prepared HTC carbons, modified with an additional KOH activation step, from a pure monosaccharide (i.e. glucose), its polymer (i.e. cellulose) and lignocellulosic biomass (i.e. rye straw) under different

thermal conditions. Results showed the HTC temperature is a highly influential parameter affecting the development of the ACs porosity and PSDs. It was reported that the samples prepared at medium HTC temperature (180–240°C) possessed higher total/micropore volume (in the range of 0.94–1.21 cm<sup>3</sup>.g<sup>-1</sup>), whilst those obtained under higher HTC temperature (upper that 280 °C) exhibited lower microporosity development (lower than 0.95 cm<sup>3</sup>.g<sup>-1</sup>) after the KOH activation.

Blankenship and Mokaya studied the preparation of HTC porous carbons from cigarette filters/butts for H<sub>2</sub> storage [125]. They showed that ACs produced via sequential processes of HTC and KOH-activation owned an ultra-high surface area of 4300 m<sup>2</sup>.g<sup>-1</sup> and pore volume of 2.09 cm<sup>3</sup>.g<sup>-1</sup> arising almost entirely (49%) from micropores. Due to the combined effects of super-high microporosity and an oxygen-rich nature of the ACs surface, the adsorbent exhibited unprecedentedly high H<sub>2</sub> storage capacity of 9.4 wt.% at -196 °C and 20 bar, rising to total uptake of 11.2 wt.% at 40 bar.

According to what has been reviewed in this section, hydrothermal carbonization is almost a new-conversion technique, ultimately converting waste materials to value-added products for practical uses, especially in the gas storage field. Table 5 summarizes some of the best samples fabricated by the HTC method.

**Table 5.** Porous carbons prepared by the HTC method for gas storage.

Precursor + Activator	Porosity			$\rho_{\text{packed}}$ (g.cm <sup>-3</sup> )	H <sub>2</sub> Uptake (wt.%)	CH <sub>4</sub> Storage Capacity (V.V <sup>-1</sup> )	Measurement Condition	Reference
	S <sub>BET</sub> (m <sup>2</sup> .g <sup>-1</sup> )	V <sub>t</sub> / V <sub>p</sub> (cm <sup>3</sup> .g <sup>-1</sup> )	d <sub>ave</sub> (nm)					
D-glucose + KOH	2210	1.21 / 0.90	1.22	0.38	-	86	CH <sub>4</sub> @ 25 °C, 40 bar	Falco et al.[121] (2013)
Cellulose + KOH	2250	1.26 / 0.90	0.55	0.39	-	86	CH <sub>4</sub> @ 25 °C, 40 bar	Falco et al.[121] (2013)
Rye straw + KOH	2200	1.11 / 0.92	0.52	0.43	-	105	CH <sub>4</sub> @ 25 °C, 40 bar	Falco et al.[121] (2013)
Sucrose + K <sub>2</sub> CO <sub>3</sub>	1375	0.63 / 0.58	0.70	0.76	-	90	CH <sub>4</sub> @ 25 °C, 10 bar	Mestre et al.[76] (2014)
Sucrose + KOH	2431	1.14 / 0.90	0.77	0.36	-	40	CH <sub>4</sub> @ 25 °C, 10 bar	Mestre et al.[76] (2014)
Mixture of algae/ glucose + KOH	1192	0.54 / 0.48	1.2	-	0.08 mmol.g <sup>-1</sup>	2.68 mmol.g <sup>-1</sup>	H <sub>2</sub> @ -196 °C, 1 bar CH <sub>4</sub> @ 0 °C, 1 bar	Yuan et al. [122] (2016)
Mixture of algae/ glucose + KOH	1534	0.69 / 0.57	1.41	-	0.11 mmol.g <sup>-1</sup>	2.15 mmol.g <sup>-1</sup>	H <sub>2</sub> @ -196 °C, 1 bar CH <sub>4</sub> @ 0 °C, 10 bar	Yuan et al. [122] (2016)
Fresh cigarette Filter + KOH	4113	1.87 / 0.79	0.60	-	3	-	H <sub>2</sub> @ -196 °C, 1 bar	Blankenship et al.[125] (2017)
Smoked cigarette filters+ KOH	4310	2.09 / 1.71	0.64	-	4	-	H <sub>2</sub> @ -196 °C, 1 bar	Blankenship et al.[125] (2017)
Sucrose + KOH	2240	- / 1	0.65	-	0.18	-	H <sub>2</sub> @ 25 °C, 20 bar	Schaefer et al.[126] (2016)
Wood sawdust + KOH	2797	1.74 / -	0.80	-	6.1	-	H <sub>2</sub> @ -196°C, 20 bar	Adeniran et al.[97] (2015)
Potato starch + KOH	3220	2.27 / 1.21	0.85	-	6.4	-	H <sub>2</sub> @ -196°C, 20 bar	Sevilla et al.[127] (2016)
Mixtures of polypyrrole/r aw sawdust + KOH	3815	2.18 / 0.66	1.2	-	12.6	-	H <sub>2</sub> @ -196°C,100 bar	Balahmar et al. [128](2019)
Lignin waste + KOH	1924	0.95 / 0.87	0.70	-	4.7	-	H <sub>2</sub> @ -196°C, 20 bar	Sangchoom et al.[129] (2015)
Starch + CO <sub>2</sub>	3350	1.75 / 1.67	1.52	-	6.4	10.7 mmol.g <sup>-1</sup>	H <sub>2</sub> @ -196°C, 20 bar CH <sub>4</sub> @ 25 °C, 20 bar	Li et al.[62] (2016)

## 2.5 Templated carbons

Recently, many research attempts have been devoted to fabricating new carbon-based adsorbents with controlled and well-defined porosity inside the adsorbent's skeleton [130-132]. Traditional activation methods are associated with difficulties such as harsh reaction/operation conditions,



disordered/ununiform/broad pore size distribution and relatively low carbon yield of final adsorbents. Templating approach is considered one of the effective strategies to produce porous carbons due to its ability for tailoring well-organized porous morphologies purposefully and precisely. This method makes it possible to adjust the pore structure and PSD of porous carbons precisely, facilitate the preparation conditions (i.e. reducing operating temperature and energy consumption), and improve the carbon yield, resulting from a low corrosion rate in the skeleton of carbon [131]. The advantages mentioned above make the templated carbons one of the most appropriate candidates for gas storage/separation in recent years [131-133].

Generally speaking, the templating approach involves several steps: (1) carbon raw materials and templating agents need to be mixed, where carbon is assembled with the templating agent (soft templating) or set inside the porosity of the agent (hard templating); (2) the resultant should be exposed to thermal treatment (i.e. carbonization) to remove the agent from the mixture [131]. Two main approaches of soft and hard templating are common to develop the porosity inside the carbon framework. Soft templating or endo-templating denotes the preparation of porous materials mainly using self-assembled organic molecules/supramolecules (e.g. surfactants in a particular solution and in the presence of a polymerizable carbon precursor [131]). They will be decomposed and removed from the media during the thermal condition. Consequently, the porous carbon materials can be directly obtained after the carbonization process (see Figure 9). The hard templating or exo-templating approach includes the following steps; (1) carbon precursor is introduced into the appropriate porous template agents (e.g. zeolites, and silica) through the methods of wet impregnation and chemical vapour deposition (CVD) or a combination of both of them, (2) the two phases appear to be polymerized and crosslinked and finally (3) suitable solutions such as HF or NaOH is used to decompose the inorganic template so that the well-ordered porous carbons will

be obtained (see Figure 9) [134]. Between two templating techniques, hard templating is more economical and can provide higher specific surface area and ordered microporous architectures [13, 131].

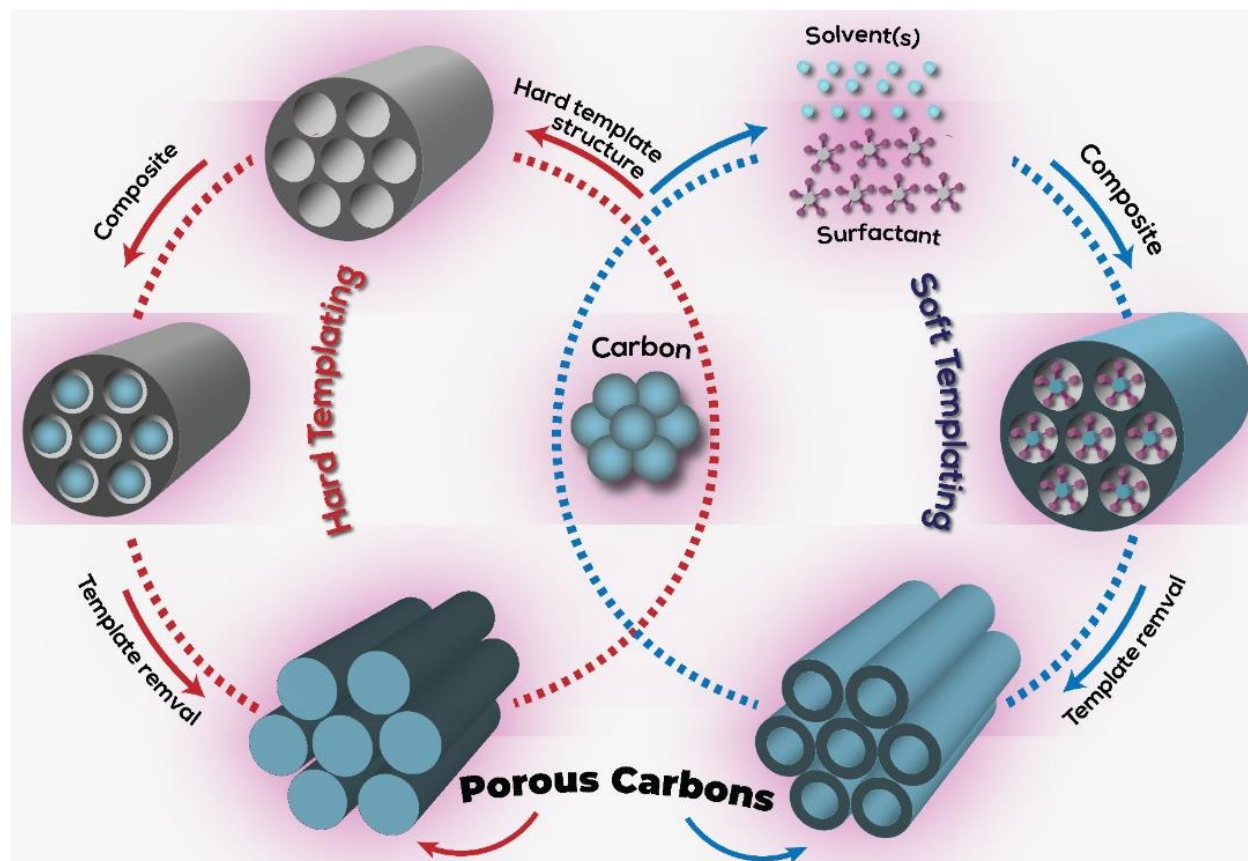


**Figure 9.** Schematic illustration of the synthesis process of soft and hard templating.

From a practical point of view, zeolite-templated carbons (ZTCs) are believed to be one of the critical subclasses of hard templating carbons, especially for gas storage uses. These microporous carbons represent high surface areas (up to  $3500 \text{ m}^2 \cdot \text{g}^{-1}$ ) and a periodic array of pores complementary to the zeolite structure used in the template carbonization [133]. Due to the significant gas sorption capacity of ZTCs at room temperature, several researchers focused on the practical application of these adsorbents in the vehicle industry. For example, Stadie and co-

workers successfully synthesized high template fidelity ZTCs to enhance CH<sub>4</sub> and hydrogen uptake at room temperature [133, 135]. The remarkably high gas storage capacity of ZTCs (CH<sub>4</sub>: ~12 mmol.g<sup>-1</sup> at 25 °C and 35 bar & H<sub>2</sub>: 8.27 mmol.g<sup>-1</sup> at 25 °C and 30 bar) was reported. An extensive surface area of 3591 m<sup>2</sup>.g<sup>-1</sup> and, more importantly, the presence of narrow micropores (~1.2 nm) in the ZTCs structure was reported as the main reasons behind their significant storage capacity. Such a narrow pore width inside the materials' framework is nearly close to the optimal value of 1.14 nm, which is recommended for maximum gas uptake [7, 65].

The uniform crystal morphology of ZTCs is their other important characteristic, which provides the opportunity to have adsorbents with homogenous particle size distributions and higher packing density compared with the conventional activated carbons [136]. In recent research on CH<sub>4</sub> adsorption, Beta (BEA)<sup>2</sup> and faujasite (FAU)<sup>3</sup> zeolite structures were used as a solid template to prepare the ZTCs [136]. It has been demonstrated that the micropore size distribution of ZTCs was systematically controlled by post-synthesis thermal treatment. As a result, the unique feature of thermal contraction was observed for ZTC-types, which was not reported for former ACs. The final adsorbent with tailored micropore size distribution (in the range of 1.1-1.5 nm) indicated one of the most promising volumetric CH<sub>4</sub> storage values of 210 cm<sup>3</sup>.cm<sup>-3</sup> within the pressure range of 0-65 bar. In a relevant study, an ordered carbon was synthesized via a soft-template approach as a potential adsorbent for H<sub>2</sub> adsorption [137]. The final adsorbent showed uniform pore size distribution with an average pore diameter of 6.26 nm and pore volume of 0.87 cm<sup>3</sup>.g<sup>-1</sup>. Hydrogen storage capacity was recorded in a volumetric apparatus at three different temperatures (-196, -

---

<sup>2</sup> BEA zeolite is among the most widely used zeolites. It exhibits a three-dimensional pore system formed by 12-membered ring channels with a diameter of 0.76 × 0.64 and 0.55 × 0.55 nm, which ensures good accessibility of acid sites, high thermal stability and high acidity.

<sup>3</sup> The faujasite framework has been attributed the code FAU by the International Zeolite Association. It consists of sodalite cages which are connected through hexagonal prisms.

78.5, and 25 °C), maximum gas uptake value of 1.27 wt.% was found to be reached at -196 °C and 1.05 bar pressure. Some of the ACs prepared by templated method were listed in Table 6.

**Table 6.** Porous carbons prepared by template method for gas storage.

Precursor + Template	Porosity			H <sub>2</sub> Uptake (wt.%)	CH <sub>4</sub> Storage Capacity (V.V <sup>-1</sup> )	Measurement Condition	Reference
	S <sub>BET</sub> (m <sup>2</sup> .g <sup>-1</sup> )	V <sub>t</sub> / V <sub>p</sub> (cm <sup>3</sup> .g <sup>-1</sup> )	d <sub>ave</sub> (nm)				
Furfuryl alcohol + Zeolite NH <sub>4</sub> Y	2135	1.4 / 0.57	1.50	2.24	10.98 mmol.g <sup>-1</sup>	H <sub>2</sub> @ -196°C, 1 bar CH <sub>4</sub> @ 25 °C, 35 bar	Guana et al.[138] (2015)
Acetylene + Zeolite beta	1073	0.75 / 0.29	0.90	-	80	CH <sub>4</sub> @ 25 °C, 35 bar	Antoniou et al.[139] (2014)
Furfuryl alcohol + Zeolum zeolite molecular sieve	3591	-	1.25	28.6 mmol.g <sup>-1</sup>	12.32 mmol.g <sup>-1</sup>	H <sub>2</sub> @ -196 °C, 1 bar CH <sub>4</sub> @ 25 °C, 35 bar	Stadie et al.[133, 135] (2012 & 2013)
Zeolite structure BEA + CVD	2447	1.07 / 0.99	1.33	-	210	CH <sub>4</sub> @ 25 °C, 65 bar	Choi et al.[136] (2018)
Zeolite structure FAU + CVD	2145	0.95 / 0.88	1.33	-	185	CH <sub>4</sub> @ 25 °C, 65 bar	Choi et al.[136] (2018)
Furfuryl alcohol + mesoporous ZnO/Zn(OH) <sub>2</sub>	1013	3.39 / -	0.67	1.14	-	H <sub>2</sub> @ -196°C, 1.01 bar	Kim et al.[140] (2020)
Phloroglucinol + mesoporous ZnO/Zn(OH) <sub>2</sub>	1075	3.01 / -	0.74	1.19	-	H <sub>2</sub> @ -196°C, 1.01 bar	Kim et al.[140] (2020)
Furfural alcohol + zeolite 13X	3332	1.66 / 1.18	1.2	7.3	-	H <sub>2</sub> @ -196 °C, 20 bar	Masika et al.[114] (2013)
Glucose + NaY zeolite	1600	-	1.35	-	7 mmol.g <sup>-1</sup>	CH <sub>4</sub> @ 295 °C, 40 bar	Shi et al.[41] (2015)

## 2.6 Carbide-derived carbons

Carbide-derived carbons (CDCs), or “mineral carbons”, are attractive candidates for gas storage mainly due to their tunable pore size distribution (PSD) with sub-Angstrom accuracy [141, 142]. In some ways, many similarities exist between the synthesis of CDCs and the templating approach. The rigid metal carbide lattice acts as a template in the CDCs preparation, with the metal atoms extracted layer-by-layer. Thus, the as-prepared carbon structure is ‘templated’ by the carbide structure (see Figure 10). In this way, there is a significant chance of adjusting the porosity at the

atomic level by controlling the chlorination condition (e.g. temperature) or selection of metal carbides (precursors) such as  $B_4C$ ,  $ZrC$ ,  $Ti_3SiC_2$ ,  $Ti_2AlC$  [143].

Structural properties of the initial carbides (precursors) and CDCs preparation method significantly impact the tunable PSD characteristics of these materials. CDCs can be produced by selective etching of metals from crystalline metal carbides [13]. Several approaches have been recommended for selective removal of metal or metalloid atoms from carbides, including hydrothermal leaching, thermal decomposition, etching at high temperatures in molten salts, halogenation and electrochemical etching at room temperature. Among them, halogenation is considered to be the most efficient route to prepare nanoporous carbons. Chlorine ( $Cl_2$ ) is known as the most commonly used agent for halogens etching.

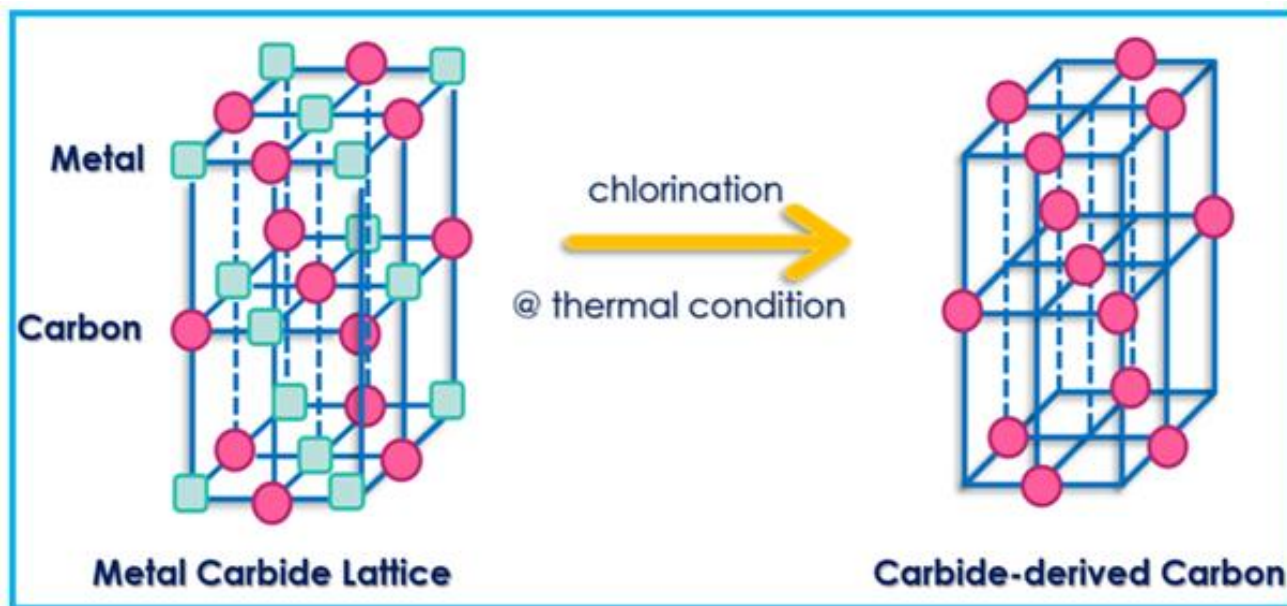


**Figure 10.** Schematic diagram of Carbide-derived carbons fabrication

As an example, titanium tin carbides ( $Ti_2SnC$ )-based CDCs were synthesized via chlorination at 400–1100 °C to study their gas adsorption properties [144]. The as-prepared CDCs under low

chlorination temperature (400–500 °C) mainly showed an amorphous carbon structure contained with the chlorides. Increasing the temperature up to 600°C resulted in the disappearance of the chlorides; hence the main composition of CDCs was amorphous carbon. At higher chlorination temperatures (near 1100 °C), an apparent trend of graphitization was detected. The CDC chlorinated at 1100°C showed a  $S_{\text{BET}}$  of 1580  $\text{m}^2\cdot\text{g}^{-1}$  and a gas adsorption capacity of 206  $\text{cm}^3\cdot\text{g}^{-1}$  (at 60 bar 25 °C) for  $\text{CH}_4$  and 442  $\text{cm}^3\cdot\text{g}^{-1}$  (at 35 bar -196 °C) for  $\text{H}_2$ .

As mentioned earlier, the pore size of CDCs can be fine-tuned by optimizing the preparation condition. However, there is a limitation in applying such materials, especially for gas storage or as electrochemical capacitors, where larger specific surface areas are required - the highest values of  $S_{\text{BET}}$  reported for CDCs are in the range of 2000-2500  $\text{m}^2\cdot\text{g}^{-1}$  [143]. Gogotsi and co-workers activated TiC based CDCs physically and chemically using air + carbon dioxide and KOH, respectively, under different thermal conditions. They investigated the influence of the activation on hydrogen and  $\text{CH}_4$  storage capacity of the final products [145-147]. These early studies on post-synthesis activation of CDCs demonstrated the possibility of enhancing and adjusting the porosity of CDCs through the use of chemical or physical activation and the importance of the activation temperature and duration. After the activation, surface area and pore volume increased to 3360  $\text{m}^2\cdot\text{g}^{-1}$  and 1.4  $\text{cm}^3\cdot\text{g}^{-1}$ , respectively, two times the raw CDCs. The increase in total pore volume might be accompanied by the widening of small micropores and the formation of an additional mesopore volume contribution, which is not desirable for hydrogen storage. However, Gogotsi and co-workers found an enhancement in hydrogen uptake, reaching a value of 4.7 wt.% at -196 °C and 60 bar, up to 52% higher than the raw CDCs [147]. The point that should be remarked here is the benefit of higher porosity of the obtained carbons after activation for  $\text{CH}_4$  uptake. Indeed, they observed 50 % enhancement in  $\text{CH}_4$  uptake of activated CDCs (18 wt.%) compared to the

raw samples (12 wt.%) [146]. Likewise, later work by Sevilla and Mokaya represented a comprehensive study on the possibility of improving the porous textural properties of CDCs via further post-synthesis treatments and the ramifications of such modifications on the hydrogen storage capacity of the adsorbents [143]. They found that post-synthesis chemical activation improves the CDCs' surface area and pore volume around 47% and 58%, respectively. Consequently, the hydrogen storage capacity was promoted up to 63%.

## **2.7 Ordered (structured) adsorbent**

Traditional carbon-based adsorbents are fabricated in beads or granules, which are associated with some disadvantages in operational conditions such as mass transfer limitations and loss of the space between the particles, affecting the bed's volumetric capacity [148]. It is possible to tackle the problem by reducing the particle size to less than 0.5 mm or using the powder form of the adsorbent. However, applying smaller particle size adsorbents causes a higher pressure drop and bed's temperature (due to higher heat of adsorption) [149]. With advantages such as a low bed's pressure drop, good thermal properties, fair mass transfer kinetics and sufficient working capacity, structured adsorbents were reported as promising alternatives for conventional adsorbents in the form of beads or granules [148, 149]. Ordered/structured porous adsorbents can mainly be categorised into dense structures (e.g. monoliths and pellets), foams, and fibres, which will be investigated in this section.

### **2.7.1 Dense carbons**

Mobile adsorptive gas storage/separation requests need to consider the volumetric adsorption capacity of microporous carbon materials besides their gravimetric capacity. The gravimetric

storage capacity of adsorbents is strongly affected by their microporosity; however, the volumetric capacity depends on both porosity and packing density of the as-made adsorbents. Although ACs in powder form show a large specific surface area ( $>3500 \text{ m}^2 \cdot \text{g}^{-1}$ ), their low bulk density might question their ability for energy storage. Reshaping the low-dense ACs powder into dense/bulked structures such as pellets or monoliths makes it possible to compensate for the limiting factor [150]. The rational design of monoliths to carbon-based adsorbents can simultaneously achieve optimal bulk density and microporosity, which is genuinely convenient for practical applications.

Activated carbons can be compacted into monoliths or pellets with or without the use of a binder simply by the selection of appropriate carbon precursors. The synthesis procedures to prepare bulked ACs with/without binder are represented in Figure 11 [21]. It needs to be remarked that besides the templated and carbide-derived carbons, dense ACs are also promising candidates for gas storage. With relatively high volumetric storage capacity, these materials enjoy simple, well-established and low-cost production methods [112].



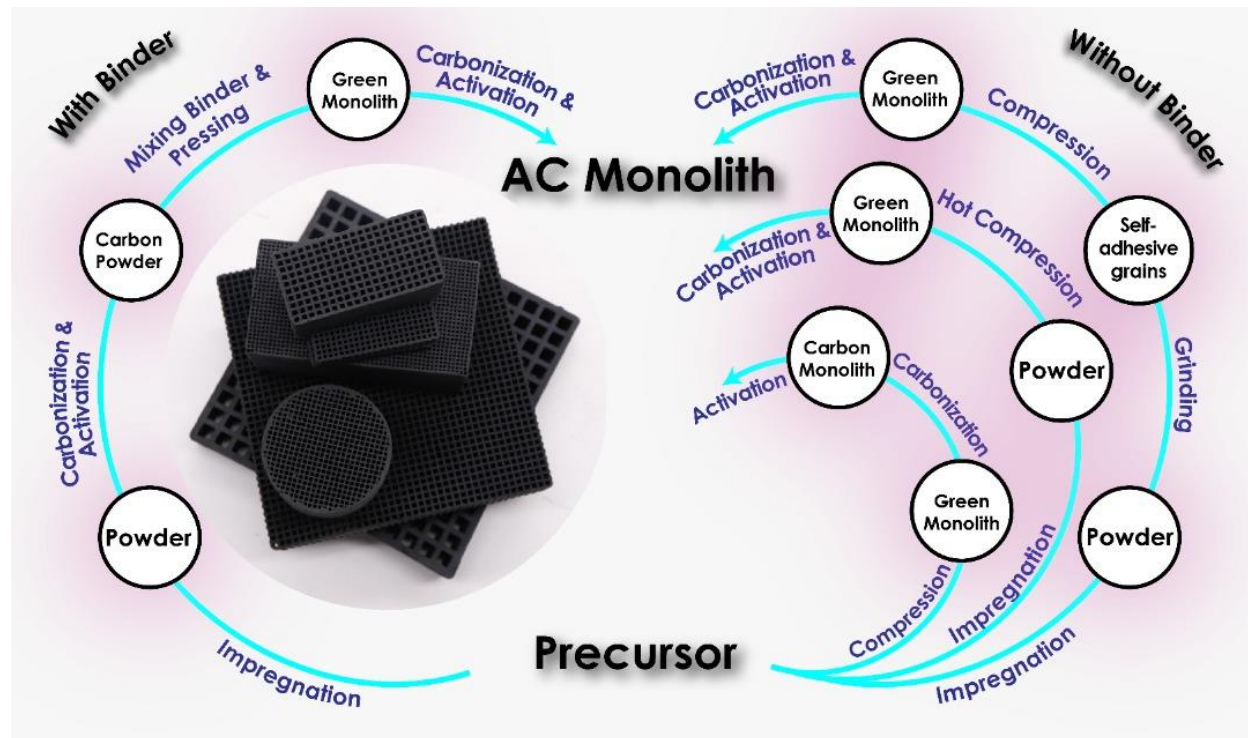


**Figure 11.** Synthesis procedures of dense adsorbent with/without binder

One effective way to prepare dense ACs is the compactification approach that includes a pressing step before thermochemical activation [97]. Adeniran and Mokaya represented a method wherein powdered KOH and carbon precursor mixtures were mechanically compressed under 7400 bar pressure into pellets/disks. Afterward, the compressed mixture was activated at two different temperatures, 600 °C (low levels of activation) and 800 °C (high levels of activation). As-made bulked ACs possessed higher porosity than analogous conventionally activated carbons. The designed method showed good efficiency under either low or high activation temperatures. Highly compressed-activated carbons treated at 800 °C showed a surface area of around 4000 m<sup>2</sup>.g<sup>-1</sup> and pore volume up to 3.0 cm<sup>3</sup>.g<sup>-1</sup> along with superior hydrogen uptake (9.6 wt.% or 38 g.l<sup>-1</sup> at -196 °C and 40 bar). In a similar study, the effect of densification was studied on the porosity and gas storage properties of the corresponding ACs [97]. The results indicated that the produced carbons held a

significant proportion of their porosity ( $3500 \text{ m}^2.\text{g}^{-1}$  and  $2.7 \text{ cm}^3.\text{g}^{-1}$ ) whilst attaining exceptional volumetric hydrogen storage ( $49 \text{ g.l}^{-1}$  at  $-196 \text{ }^\circ\text{C}$  and 40 bar).

Chen and colleagues recently reported the development of high-performance dense carbon nanoflower pellets (Figure 12), via a facile method of free radical polymerization of acrylonitrile, for on-board  $\text{CH}_4$  storage applications [150]. Old-style efforts have been conducted by hydraulic pressing the AC powders into dense pellets with an almost 10% binder. In this way, fragile pellets with low mechanical stability were hardly made. In a particular way designed by Chen et al., freestanding polymer pellets can be readily made via controlling the packing of AC nanoflowers monodispersed particles, which significantly improves the bulk density. Freestanding polymer pellets can be readily obtained by reducing the solvent concentration (from 2:1 to 1:2 acetone/acrylonitrile) before the polymerization step and drying the formed polyacrylonitrile particles at  $70 \text{ }^\circ\text{C}$  under vacuum. As-made adsorbents showed a record-setting bulk density ( $0.96 \text{ g.cm}^{-3}$ ) with interconnected micro/meso/macropores and a surface area of  $1077 \text{ m}^2.\text{g}^{-1}$ . This simple production method could record high  $\text{CH}_4$  storage capacities of 165 and  $196 \text{ cm}^3.\text{cm}^{-3}$  at 35 and 65 bar, respectively.

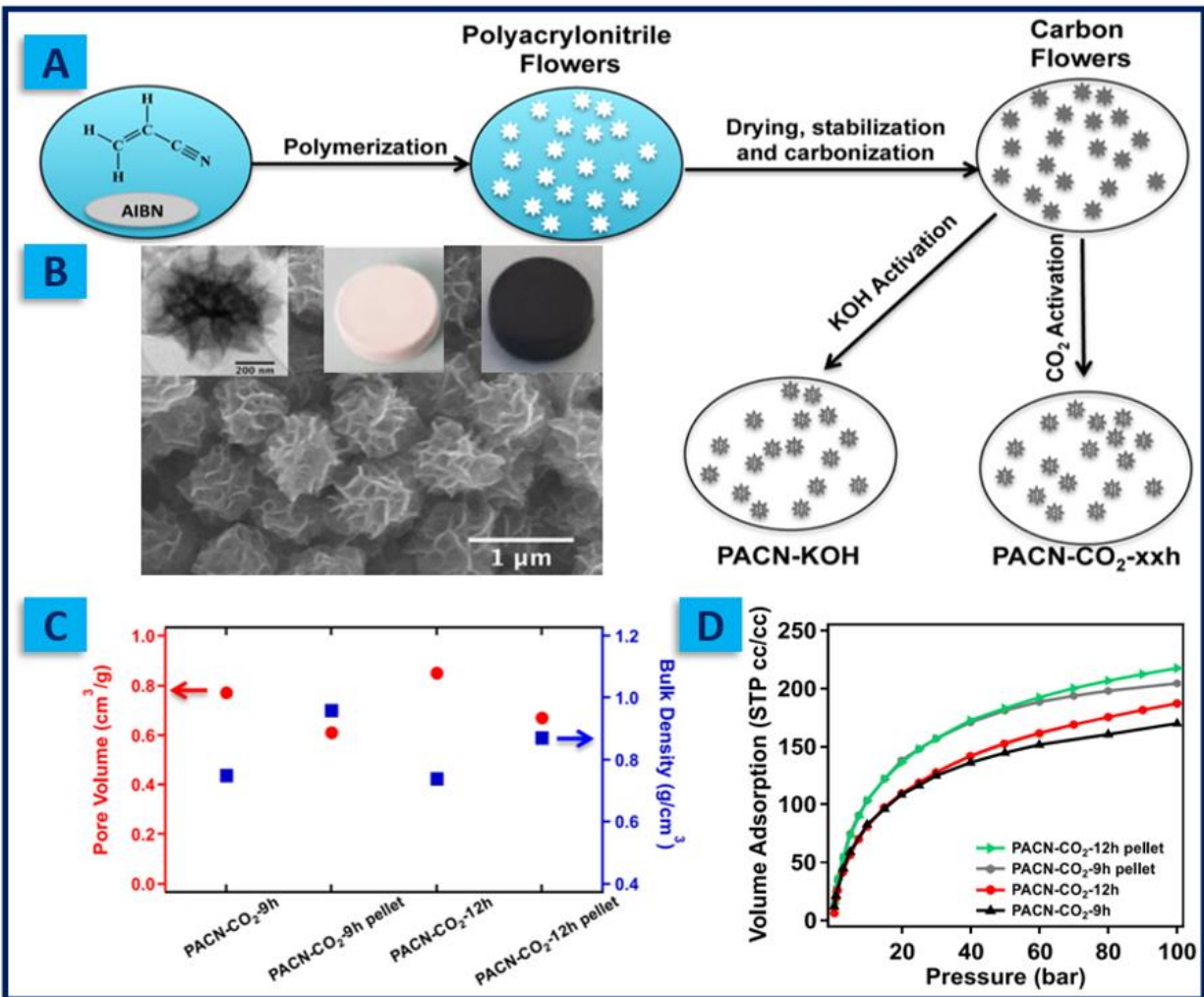


**Figure 12.** (A) Synthetic scheme of porous carbon nanoflowers powders with different activation methods, (B) SEM image of the samples, (C) Summary of porosity and bulk density for activated carbon nanoflower pellets vs powders, (D) Volumetric CH<sub>4</sub> uptakes at 25 °C for activated carbon nanoflower pellets vs powders. Reproduced from ref [150]. Copyright 2020, American Chemical Society.

### 2.7.2 Foam-like carbons

Carbon foams are spongy carbonaceous materials with cellular microstructures and hierarchical pore arrangements that attracted significant interest because of their unique structure and extraordinary performance in adsorption, energy storage, catalyst support, sensors and electromagnetic interference shielding applications [151]. Carbon foams possess adjustable 3D porous architecture with high strength, good thermal stability, high electrical conductivity, and

large specific surface area. As illustrated in Figure 13, carbon foams hold two kinds of pore structures; (i) open-cell structures and (ii) closed-cell cellular structures. The first one includes ligaments and joints inside a unit cell (Figure 13 (A)), while the other type is composed of the cell walls, ligaments and joints. The ligament denotes the edge of the cell which connects the two neighbouring cells; more information about carbon foam structures was reported elsewhere [151].

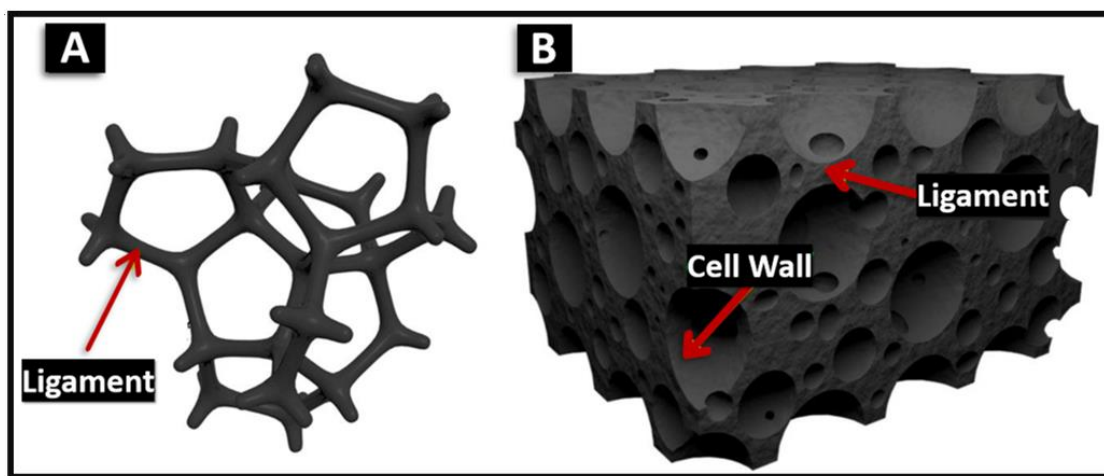


**Figure 13.** Modelling of the typical microstructure of carbon foam: (A) open-cell, (B) closed-cell. Reproduced from ref [151]. Copyright 2020, Royal Society of Chemistry.

Carbon foams can be produced using different carbonaceous precursors such as polymers [152, 153], pitches [46, 154], and biomass materials [155, 156]. Generally speaking, for carbon foam fabrication, regardless of the precursors, carbonization step at 750-1400 °C is needed to remove impurities and un-wanted atoms (i.e. H, S, N, and O) and provide the final product with a better structure and morphology of carbon matrix [151].

A comprehensive study on the adsorption of a series of gasses, N<sub>2</sub>, CH<sub>4</sub>, and CO<sub>2</sub>, on carbon foams, was reported by Arami-Niya et al. [156]. They produced nitrogen-doped AC foams from banana peels using a self-template method with zinc nitrate, 2-aminophenol-and furfural and investigated

the effect of carbonization temperature and post-carbonization, CO<sub>2</sub> activation on the pore structure and gas uptake of the final adsorbent. The carbon foams demonstrated a nitrogen content of about 6.0 wt.% and featured cellular macroporous structures with BET-specific surface areas up to 1426 m<sup>2</sup>.g<sup>-1</sup>. The potential of the carbon foams for CO<sub>2</sub>/N<sub>2</sub>, CO<sub>2</sub>/CH<sub>4</sub> and CH<sub>4</sub>/N<sub>2</sub> separations was assessed using adsorption isotherm at 40 bar and 298 K. The results showed gas uptake values of 3.29, 5.29 and 9.21 mmol.g<sup>-1</sup> for N<sub>2</sub>, CH<sub>4</sub> and CO<sub>2</sub> respectively.

Pitches are considered a customary carbonaceous precursor used to produce carbon foams due to their low cost and ease of accessibility [46, 157]. Typically, the synthesis process of pitch-based materials involves several steps of foaming, carbonization, graphitization and finally activation. Foaming strategies include blowing, and spontaneous foaming, wherein pitch releases light components and small molecules (volatilization). Afterwards, as-made foam materials experience carbonization (750-1400 °C) and graphitization (usually higher than 2100 °C), to form the final carbon foam structures [151]. In similar research by Arami-Niya and coworkers, AC monoliths were fabricated with foam-like features from petroleum tar pitch at ambient pressure using coal powder to stabilize the liquified pitch [46]. They studied the impact of coal to pitch ratio on foam morphology and micropore development. The carbon-foam sample with 50 wt.% coal to pitch featured an open-cell structure with cell widths of around 2 mm and a well-developed microporosity that presented a BET specific surface area of 1044 m<sup>2</sup>.g<sup>-1</sup>. Moreover, this sample showed adsorption capacities of 7.398 mmol.g<sup>-1</sup> CO<sub>2</sub>, 5.049 mmol.g<sup>-1</sup> CH<sub>4</sub> and 3.516 mmol.g<sup>-1</sup> N<sub>2</sub> at 25 °C and pressures close to 35 bar.

### 2.7.3 Carbon fibres

Over the past few decades, activated carbon fibres (ACFs) attracted lots of interest due to their unique characteristics comprising fibrous structure[158], well-developed porosity[159, 160], high volumetric gas adsorption capacity[160], excellent packing density[161], fast adsorption kinetics and simplicity of handling[158, 160, 162]. These materials can be synthesized using different raw materials (like phenolic resins, mesophase pitch, pitch fiber, polyacrylonitrile, or biomass). However, due to the extra processing steps, e.g. converting the initial materials into the fibrous form, production of these materials is relatively expensive [160]. The main challenge behind the fabrication of ACFs is to obtain homogeneous pore size structures which can improve their gas adsorption properties.

ACFs can be produced through carbon fibres' physical or chemical activation [158]. No matter of the precursors, e.g. polymers, pitches or biomass, the production method of ACFs includes the steps of spinning, stabilization, pre-treatment (acid impregnation before carbonization), carbonization and activation [158, 160]. During the spinning process, the first step of the ACF production, the carbon-based precursors in the shape of granular or powder, will be converted into a continuous fibre. Diverse techniques have been reported for the spinning process, such as melt spinning [158, 163, 164], wet spinning [165] and dry spinning [166]; depending on the nature of the precursor, each of these methods can be chosen. Melt spinning involves three steps of (1) melting the precursor, (2) extruding through a spinneret containing numerous small capillaries, and finally (3) drawing of the fibres. During the wet spinning, fibres are produced from the precipitation of a concentrated solution, extruded inside a coagulation fluid. In the dry spinning method, the fibres are formed by evaporating the solvent in a drying vessel.

Oxidative or thermal stabilization is considered a crucial phase to reach high-quality ACFs. The treatment temperature in the range of 150-400 °C, precursor diameter, and raw fibre characteristics are the critical thermal treatment parameters [167]. The primary purpose of stabilization is to produce a fibre structure that can withstand the rigours of high-temperature processing. Carbonization comprises several complex physiochemical changes such as dehydrogenative condensation, polymerization, aromatization and removal of almost every impurities (e.g. O, N, CO, H<sub>2</sub> and H<sub>2</sub>O) from the as-prepared fibre resulting in up to 90% improvement in carbon content [167]. Activation was detailed described earlier in section 2.

Conte and co-workers synthesized a series of ACFs via CO<sub>2</sub> activation of poly p-phenylene terephthalamide, commercially known as Kevlar<sup>4</sup> [160]. They assessed the porosity and the gas adsorption properties of the as-prepared samples in various activation conditions, including time (in the range of 60-240 min), temperature (in the range of 750-850 °C) and CO<sub>2</sub>-flow rate (0.3, 0.9 and 1.2 l.min<sup>-1</sup>). Under the optimum activation condition, the ACFs illustrated a high micropore fraction up to 94% of the total pore volume with a specific surface area of 1109 m<sup>2</sup>.g<sup>-1</sup> and a CH<sub>4</sub> uptake of 5 mmol.g<sup>-1</sup> at 40 bar and 25 °C. In a similar study, Hwang et al. developed a new strategy to control the surface porosity of activated carbon fibres and maximise hydrogen storage capacity [168]. They prepared KOH-activated carbon fibres from polyvinyl alcohol/polyacrylonitrile (PVA/PAN) bi-component, as a precursor, using the wet spinning method. As- prepared ACFs showed a highly porous structure with a surface area of 3058 m<sup>2</sup>.g<sup>-1</sup> and micropore volume of 1.18 cm<sup>3</sup>.g<sup>-1</sup>. AFCs were measured to have a superior hydrogen storage capacity of 5.14 wt.% at -196 °C and 100 bar,

---

<sup>4</sup> Poly p-phenylene terephthalamide (PPTA) namely Kevlar® is an aramidic synthetic fiber with a high content of carbon and, typically, high mechanical properties as resistance to traction, cut, heat and flames. The chemical formula of Kevlar® monomer is [-CO-C<sub>6</sub>H<sub>4</sub>-CO-NH-C<sub>6</sub>H<sub>4</sub>-NH-]<sub>n</sub>

[160] G. Conte, S. Stelitano, A. Policicchio, F.D. Minuto, V. Lazzaroli, F. Galiano, R.G. Agostino, Assessment of activated carbon fibers from commercial Kevlar® as nanostructured material for gas storage: Effect of activation procedure and adsorption of CO<sub>2</sub> and CH<sub>4</sub>, Journal of Analytical and Applied Pyrolysis 152 (2020) 104974.

much higher than the previously reported ACFs. In another study, Kostoglou et al. developed a mechanically stable and flexible nanoporous carbon from almost new attractive starting materials of raw viscose rayon fabric [92]. The rayon fabric was first impregnated in an aqueous solution of 4.0 wt.% ammonium chloride and 4.0 wt.% zinc chloride. After drying, the sample was introduced into a tubular furnace to be activated by heating at 930 °C under the CO<sub>2</sub> atmosphere (see Figure 14). The values of S<sub>BET</sub> and V<sub>micro</sub> of the prepared ACs were estimated to be ~1205 m<sup>2</sup>.g<sup>-1</sup> and ~0.47 cm<sup>3</sup>.g<sup>-1</sup>, respectively. The prepared adsorbents were evaluated for three important applications, including (i) gas storage, (ii) selective separation of CO<sub>2</sub> over CH<sub>4</sub> based on the IAST model and (iii) electrochemical energy storage in supercapacitor devices. In the H<sub>2</sub> and CH<sub>4</sub> uptake case, the fabric-based carbon showed acceptable values of 1.68 wt.% (at -196 °C & 1 bar) and 0.72 mmol.g<sup>-1</sup> (at 25 °C and 1 bar), respectively.



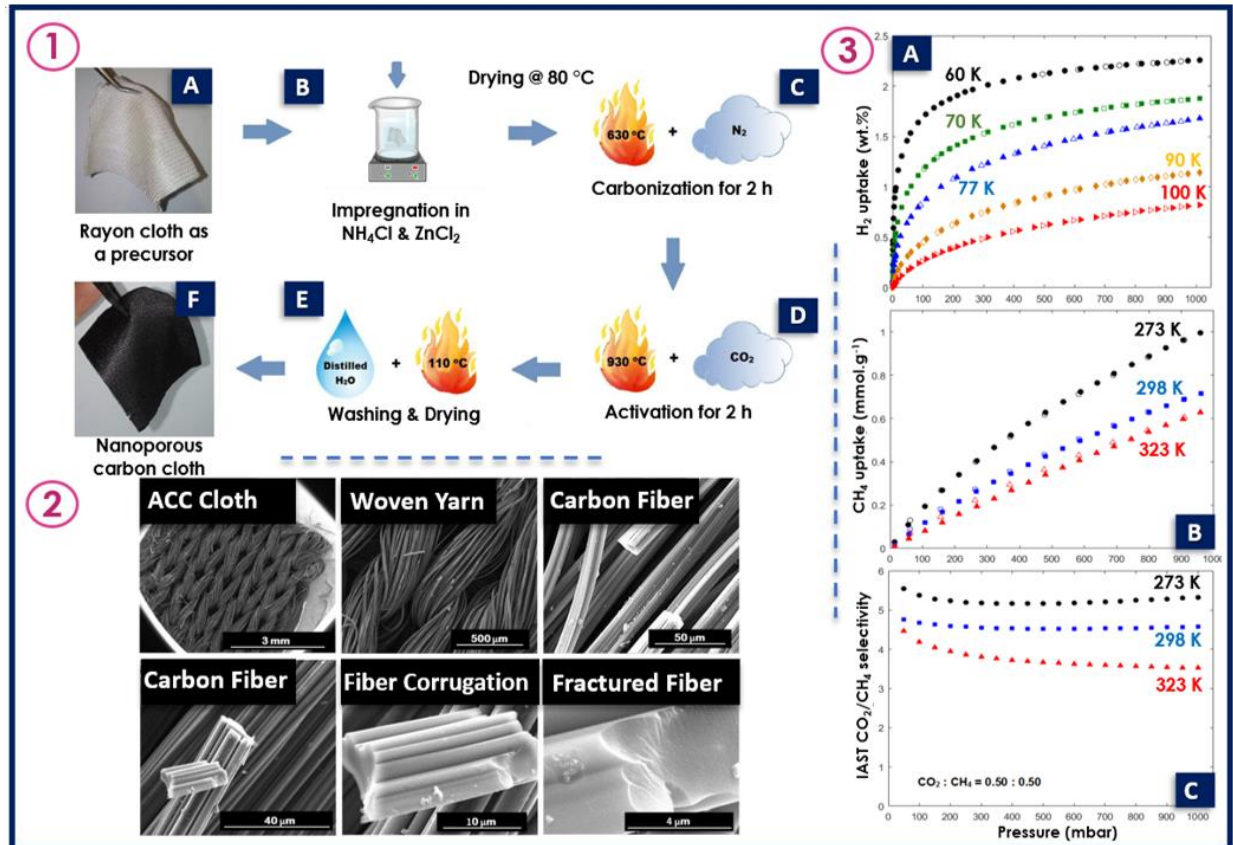


**Figure 14.** 1) Synthesis of the nanoporous material, carbonization and CO<sub>2</sub> activation procedures. 2) SEM images at different magnifications showing ACC cloth, woven yarns, carbon fibers, fiber corrugations and fractured fiber surface. 3) H<sub>2</sub> and CH<sub>4</sub> adsorption (solid symbols) and desorption (open symbols) isotherms together with CO<sub>2</sub> over CH<sub>4</sub> gas selectivity plots. Reproduced from ref [92]. Copyright 2017, Elsevier Ltd.

### 3. Carbon Nano-allotropes

ACs possess amorphous nature, disorderliness inside their framework and complicated crystalline structures originating from defects, curvatures, edges, heteroatoms or even randomly arranged stacked-carbon fragments [169]. However, carbon nano-allotropes family is a highly ordered material organized in particular carbon unit cells interconnected to adjacent cells [170]. The exceptional capability of carbon atoms to participate in robust covalent bonds with other carbon atoms in various hybridization states ( $sp$ ,  $sp^2$ ,  $sp^3$ ) enables them to create a wide range of nanostructures, from small molecules to long chains [169]. As a result, as demonstrated in Figure

15, different types of ordered nanostructure carbons of 0D carbon fullerene, 1D carbon nanotube, 2D graphene and 3D graphite, can be formed. Desirable properties such as high specific surface area, superior electron mobility, easy self-assembly with controlled microstructures, high mechanical, chemical, thermal, and electrochemical stability make these ordered adsorbent promising candidates for gas sorption, separation and storage. The following section discussed these novel structures and their gas adsorption properties.

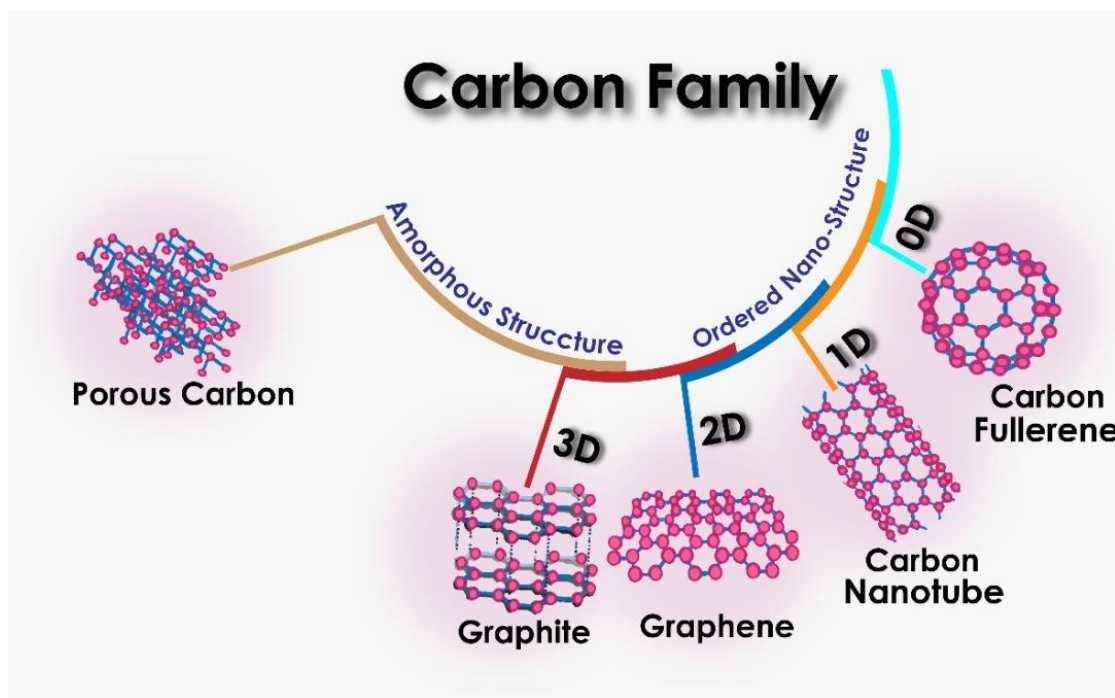


**Figure 15.** Different classes of porous carbons family

### 3.1 0D Carbon fullerenes

The discovery of carbon nano-allotrope structures began with the detection of fullerenes (e.g.  $C_{60}$ ), known as the smallest carbon nanostructure and a representative of 0D carbon nano-allotrope [171]. Besides  $C_{60}$  molecule, several other fullerenes such as  $C_{20}$ ,  $C_{70}$ ,  $C_{82}$  and  $C_{84}$  were subsequently discovered and introduced by researchers [169, 172]. However, most relevant studies focus on the synthesis and applications of  $C_{60}$  [173-176].

Fullerenes have closed-cage structures composed of  $sp^2$  hybridized carbon atoms connected by single and double bonds. Each  $C_{60}$  molecule comprises 60  $sp^2$  carbon atoms organized in a series of hexagons to develop diverse structures such as a hollow sphere, ellipsoid, tube, or any other configuration. The most famous member of this family is buckminsterfullerene ( $C_{60}$ )<sup>5</sup>. The closed fullerenes, especially  $C_{60}$ , which is so-called buckyballs, have the shape of a soccer ball with twelve pentagons and twenty hexagons in its particular framework (Figure 16).

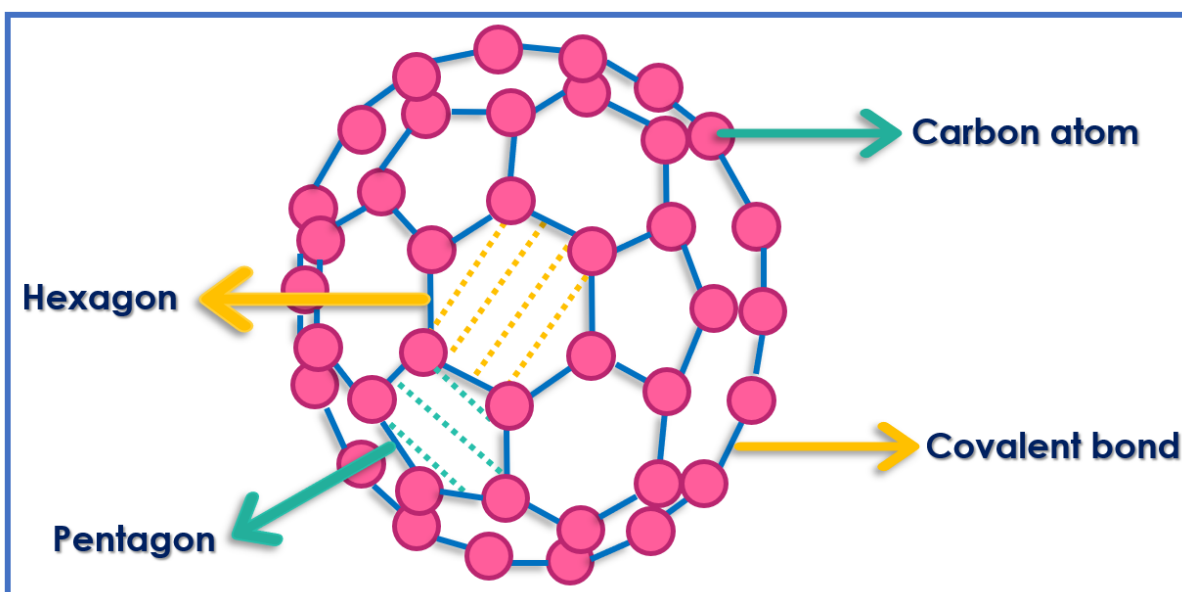


**Figure 16.** Configuration of buckyballs  $C_{60}$

Generally, carbon fullerenes (i.e.  $C_{60}$ ,  $C_{70}$  and other configurations) are synthesized via two basic synthesis methods, including (i) vaporization through the arc and plasma discharges [171, 172, 177-179] and (ii) laser irradiation [171, 180]. The arc method, also called plasma arcing, is the first and most convenient way to fabricate fullerenes in reasonable quantities; the process is conducted using an electric current across two carbon-based electrodes under inert gas conditions.

<sup>5</sup> The buckminsterfullerene ( $C_{60}$ ) was discovered in 1960 by Kroto et al. and named in honor of the famous architect Buckminster Fuller.

[171] H.W. Kroto, J.R. Heath, S.C. O'Brien, R.F. Curl, R.E. Smalley,  $C_{60}$ : buckminsterfullerene, nature 318(6042) (1985) 162-163..

Fullerenes are created in the appearance of soot by plasma arcing of carbonaceous materials, especially graphite, as raw material. One drawback associated with the technique is producing a complex mixture of components, so additional purification is recommended to separate fullerene from the mixture [179, 181]. The laser irradiation method involves several steps; first, the sample becomes ready using laser evaporation of graphite rods with a catalyst mixture (ratio of 50:50) at 1200 °C under argon atmosphere, then thermal treatment in a vacuum condition is applied, and finally, purification will be conducted to remove the fullerene from carbon deposits (i.e. soot)[181].

Moreover, alternative preparation techniques such as naphthalene pyrolysis[182] and hydrocarbon combustion [183, 184] have been proposed; the last one is useful for the extensive commercial production of fullerenes. The associated drawbacks of most fullerene preparation techniques are (1) low yields and (2) difficulty of isolation/purification of the final products. As a result, although carbon fullerene originates from cheap and abundant raw materials such as graphite, its production is a high-cost process with undesired environmental impacts.

Fullerene's curved geometry helps these structures to store guest species either outside their spherical surface, known as exohedral adsorption, or inside the nano-cages cavity called endohedral adsorption or encapsulation. C<sub>60</sub> molecules can form monolayer and multilayer films of gas adsorbate inside their particular framework. Methane and hydrogen adsorption on the C<sub>60</sub> film seems to yield well due to the large curved C<sub>60</sub> molecules (1 nm diameter), with a highly corrugated adsorption potential [185].

So far, gas adsorption properties of the fullerene-based adsorbents have been mostly explored through theoretical studies [175, 186-190], and limited experimental information is reported in the literature [191, 192]. Saha and Deng proposed an effective process to truncate C<sub>60</sub> buckyball

molecules partially and create suitable pore textures for hydrogen adsorption by controlled oxidation at 400 °C and 2 bar oxygen pressure [191]. They made “real pores” within the carbon fullerene by rupturing the C<sub>60</sub> structure, and opening closed cages. The hydrogen storage capacity of pure and ruptured C<sub>60</sub> samples was measured using a magnetic suspension microbalance at different temperatures of -196, -130 and -50 °C and pressure ranges of 120 and 150 bar. The results indicated that the gas adsorption capacity of truncated fullerene molecules at -196 °C at 120 bar was enhanced more than three times from 3.9 wt.% to 13 wt.% compared to the pristine C<sub>60</sub> structure. Such an adsorption capacity strongly suggests that partial oxidation has opened the fullerene cages and made the buckyballs' inner surface area accessible to hydrogen molecules. The increased density of the partially truncated fullerene sample (2.52 g.cm<sup>-3</sup>) compared to that of pristine fullerene (1.97 g.cm<sup>-3</sup>) measured by helium pycnometry confirmed accessibility of gas molecules to the internal volume of the partially truncated C<sub>60</sub> fullerene after opening the cages. The robust spherical cage-like structure of fullerenes theoretically provides ample space for capturing/storing certain gases such as H<sub>2</sub> and CH<sub>4</sub>. However, the challenging question for onboard gas storage application of these materials is the gas accessibility and the presence of active and selective adsorption sites in their spherical structure. Zottel et al. investigated available adsorption sites for CH<sub>4</sub> storage on fullerenes C<sub>60</sub> by a combined theoretical and experimental analysis [192]. They measured the adsorption capacity of different sites by mass spectrometry analysis, density functional theory and molecular dynamics (MD) simulations. They distinguished four different adsorption sites, including (1) registered sites above the carbon hexagons and pentagons, (2) groove sites between adjacent fullerenes, (3) dimple sites between three adjacent fullerenes, and (4) exterior sites.

Besides, it should be noted that confinement of a guest in the cavity of a fullerene cage would affect both the host and the guest molecules. Lately, the stability of “endohedral fullerenes” (so-called  $\text{gas}@C_{60}$ ), where guest gas molecules are enclosed inside the fullerene cage, has been investigated experimentally and theoretically [173-175, 193-195]. The term “endohedral” originates from a combination of Greek words “endon” – within, and “hedra” – face of a geometrical figure [195]. Endohedral fullerenes can be formed in different ways; however, one effective way might be forming the fullerene in the presence of the endohedral species under high temperature and pressure [195]. Mohajeri et al. studied the  $\text{CH}_4$  storage capacity of three different carbon fullerenes ( $C_{60}$ ,  $C_{84}$  and  $C_{180}$ ) as well as the stability of these structures with confined  $\text{CH}_4$  molecule(s)[175]. They analysed the empty cages and the formed complexes stability via electronic properties of the carbon fullerenes before and after  $\text{CH}_4$  encapsulation based on first-principle density functional theory (DFT) calculations (see Figure 17). The binding energy values proved that  $C_{60}$  (0.638 eV) and  $C_{84}$  (0.559 eV) cages with one confined  $\text{CH}_4$  molecule were stable. In the case of  $C_{180}$  fullerene, the most stable configuration<sup>6</sup> was found when six  $\text{CH}_4$  molecules were involved with the complex. To investigate the mechanical strength of  $C_{60}$  and  $C_{84}$  and their complexes, Mohajeri et al. performed Young’s modulus analysis, which characterises how easily the structure can stretch and deform [175]. The results indicated that the strength of fullerenes with confined  $\text{CH}_4$  molecules drastically decreases. In a similar study, the stability of endohedral  $n\text{CH}_4@C_{60}$  was investigated through the combined DFT-based computation methods [173] and it was shown that the deposition of one  $\text{CH}_4$  molecule in the spherical fullerene might be the only stable complex that ever formed for the  $C_{60}$  cages.

---

<sup>6</sup> The most stable configuration of  $\text{gas}@fullerene$  complex demonstrate the geometry with the lowest mean polarizability.

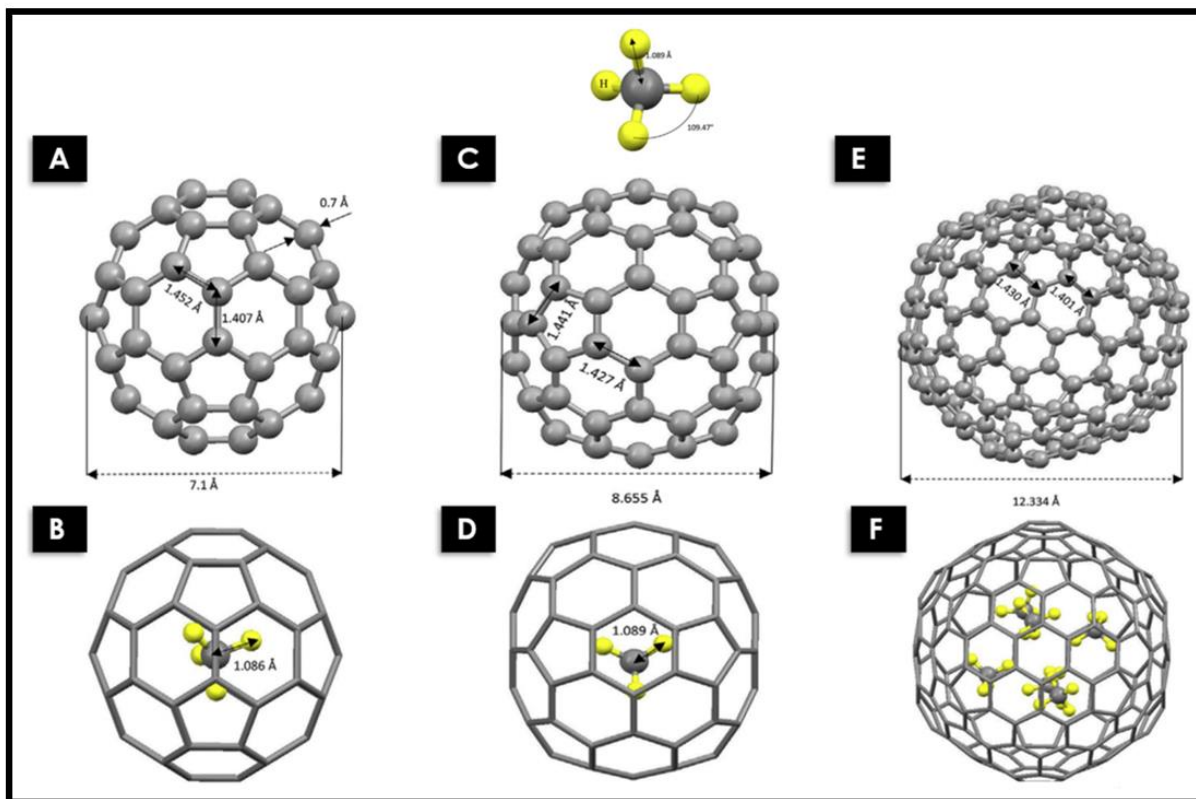


**Figure 17.** Optimized structures of  $\text{CH}_4$  as well as A)  $\text{C}_{60}$ , B)  $1\text{CH}_4@C_{60}$ , C)  $\text{C}_{84}$ , D)  $1\text{CH}_4@C_{84}$ , E)  $\text{C}_{180}$  and F)  $6\text{CH}_4@C_{180}$  calculated by DFTB + code. Reproduced from ref [175]. Copyright 2018, Elsevier Ltd.

One of the other approaches for forming endohedral fullerenes is “molecular surgery”, wherein an orifice will be created on the nanocage to make open-cage fullerene accessible to atoms or small molecules (Figures 18 and 19). After a series of chemical reactions, the orifice becomes smaller and eventually closed to isolate the guest species [193, 194]. The orifice's opening size might be considered a limiting factor that restricts the insertion of the guest species inside the nanocage. As shown in Figure 18, in the synthesis of  $\text{H}_2@C_{60}$ , Komatsu et al. proposed a four-step organic reaction (A-D) in which a 13-membered ring orifice of an open-cage fullerene gently reduced and finally closed [194]. During each of these steps, complete retention of encapsulated  $\text{H}_2$  was confirmed by observing the characteristically upfield-shifted NMR signal of the incorporated  $\text{H}_2$ . The stability of the endohedral fullerene  $\text{H}_2@C_{60}$  was assessed, and the results proved that the

complex was nearly as stable as  $C_{60}$  itself; for instance, the encapsulated  $H_2$  did not escape even when the temperature rose up to  $500\text{ }^\circ\text{C}$  for 10 min.

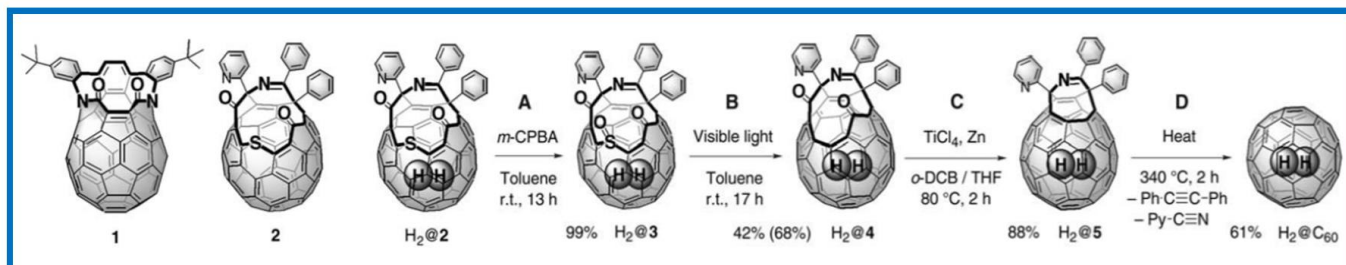


**Figure 18.** Size reduction and closure of the orifice of the open cage fullerene encapsulating hydrogen in a four-step process. Percentage values are product yields; shown in parenthesis is based on the consumed precursor. *m*-CPBA, r.t., and *o*-DCB stand for *m*-chloroperbenzoic acid, room temperature, and *o*-dichlorobenzene, respectively. Reproduced from ref [194]. Copyright 2005, American Association for the Advancement of Science.

In a similar study, Bloodworth and co-workers fabricated an endohedral fullerene of  $CH_4@C_{60}$  [174]. They successfully encapsulated a single  $CH_4$  molecule, as a large organic molecule, inside the  $C_{60}$  fullerene cage (Figure 19). Also, the vital stage of the orifice contraction was conducted via a photochemical desulfinylation of an open fullerene, even though the presence of the endohedral molecule significantly inhibits the process. The  $CH_4@C_{60}$  was characterized by high-resolution mass spectrometry, NMR spectroscopy and X-ray crystallography. The  $^1\text{H}$  and  $^{13}\text{C}$  spin-lattice relaxation times for endohedral  $CH_4$  were measured and it was shown that  $CH_4$  is freely rotating inside the  $C_{60}$  cage.



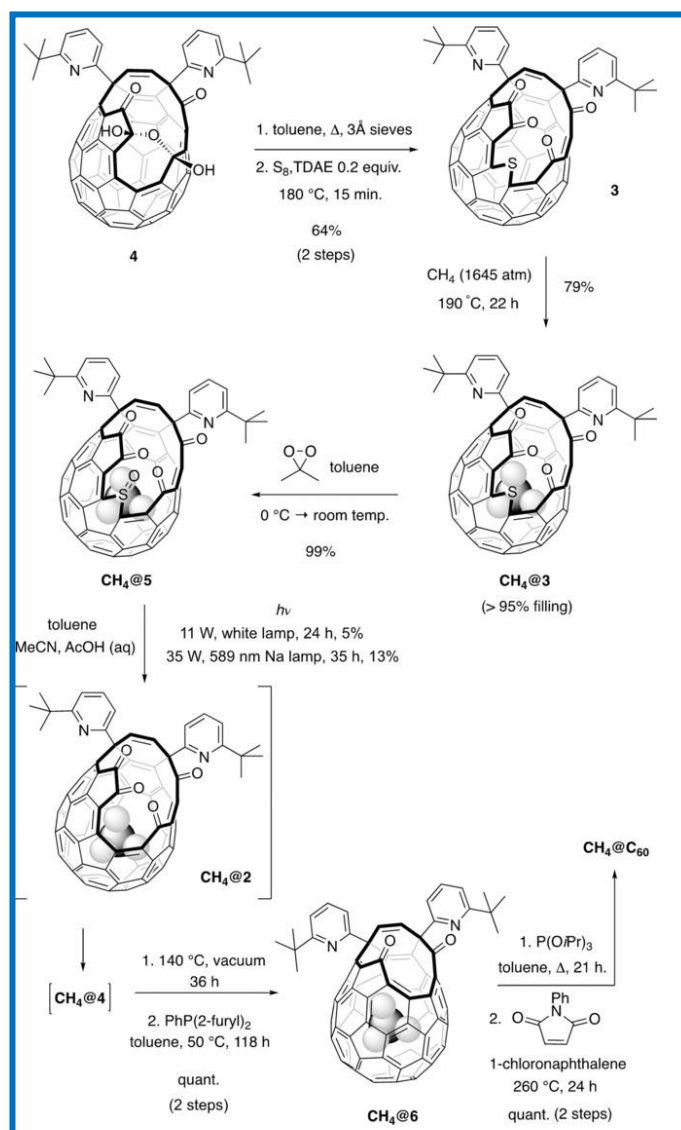


**Figure 19.** Synthesis of  $\text{CH}_4@C_{60}$ . Optimized  $\text{CH}_4$  encapsulation by **3** successful closure sequences, including photochemical desulfinylation, applied to the first synthesis of  $\text{CH}_4@C_{60}$ . Reproduced from ref [174]. Copyright 2019, Wiley Online Library.

### 3.2 1D Carbon nanotube

The second class of carbon nano allotropes adsorbents, “Carbon Nanotubes” (CNTs) were discovered independently in 1993 by Iijima and Ichihashi[196]. CNTs generally are a wide range of carbon-made nanoscale diameter tubes. No matter the shape of the carbon tubular structure, CNTs are usually developed based on a hexagonal lattice of  $\text{sp}^2$  carbon atoms, just like graphene

sheets [169]. The edge of these sheets becomes a curve to form a final cylindrical tube with a high aspect ratio (i.e. length-to-diameter ratio). From the structural point of view, CTNs are compared to “rolled up” one-atom-thick sheets of graphene. Due to the difference in size and shape of CNTs and C<sub>60</sub>, there is a significant difference between their inherent properties.

The most elementary form of CNT is a single graphenic wall with a closed cap at both end sides (Figure 20). The next type of CNTs member is single-walled carbon nanotubes (SWNTs), which are hollow tubes with about 0.4 to 2 nm diameter and several micrometers long. Furthermore, CNTs may be configured in double-walled (DWNTs) or multi-walled (MWNTs) carbon nanotubes based on the number of graphenic layers in the walls of the cylindrical structure [169]. Besides CNTs, other 1D carbon nanostructures such as carbon nanohorns [197, 198] and carbon nanoscrolls [199] have also been reported as potential adsorbents for gas storage (see Figure 20). Although various CNTs hold the same basic structure as graphene, they are prepared entirely differently. CNTs are produced via several well-established methods, including a simple high-temperature (> 800 °C) synthesis using arc discharge or laser ablation and novel low-temperature (< 800 °C) techniques such as chemical vapour deposition (CVD) approach [200]. The CVD technique benefits from precisely controlling CNT's important parameters such as orientation, alignment, nanotube length, diameter, purity, and density.

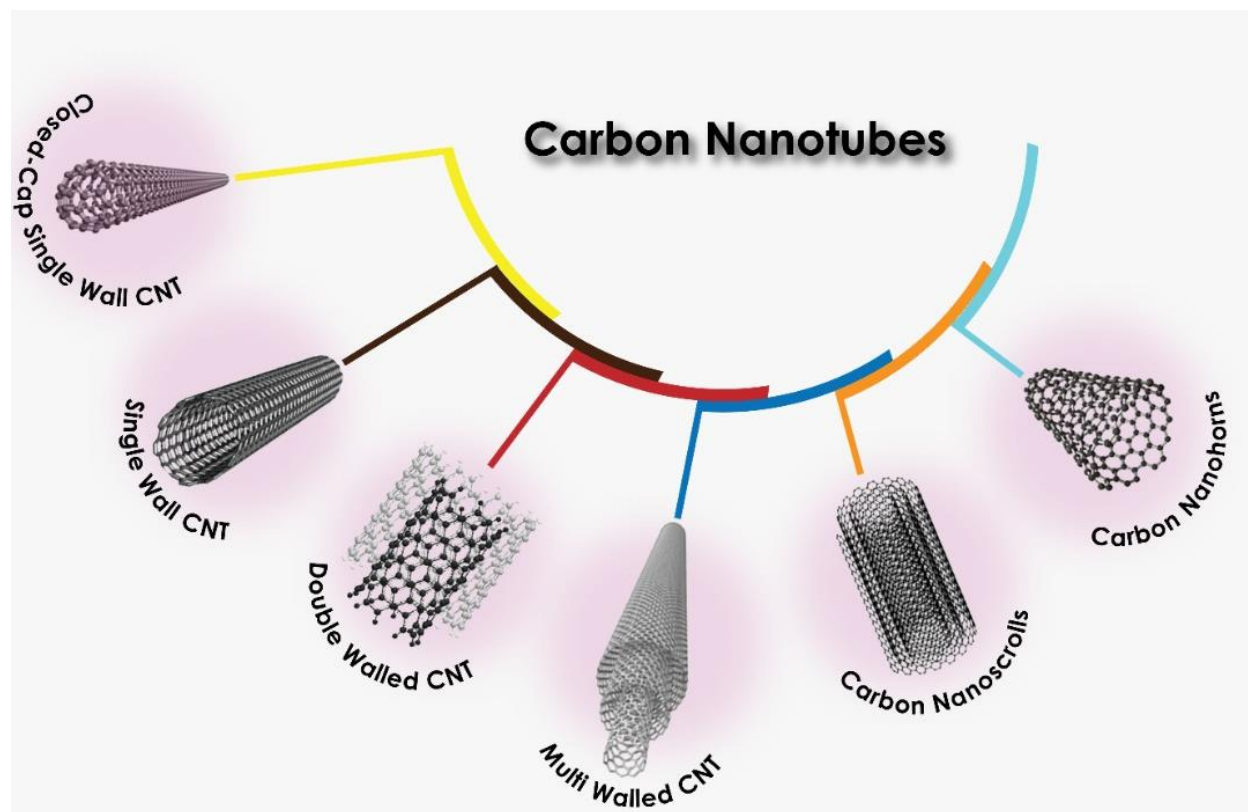


**Figure 20.** Different types of carbon nanotubes

Several attempts have been made to examine the impact of structural properties of curved graphenic surfaces for gas adsorption requests [201-203]. Bekyarova and colleagues fabricated open single-wall carbon nanohorns (SWNHs) as promising candidates for CH<sub>4</sub> storage through laser-ablating of graphite without a catalyst at room temperature [201]. The characterization of the prepared sample by TEM analysis and Raman spectroscopy showed a significant distortion in the structure of the compressed SWNHs. Such a disorderliness in the nanostructured carbons provided potential spots for storing CH<sub>4</sub> molecules. Thus, the obtained compound with high purity (~95%) and specific morphology illustrated a high ability to adsorb CH<sub>4</sub> (160 cm<sup>3</sup>.cm<sup>-3</sup>) at 35 bar and 30 °C.

Delavar et al. investigated the CH<sub>4</sub> adsorption capacity of two different types of MWCNTs adsorbents experimentally [202]. ‘Type I’ samples were prepared with the CVD method, with a

purity of about 90%, the specific surface area of  $126 \text{ m}^2 \cdot \text{g}^{-1}$ , a mean pore diameter of 16 nm and a total pore volume of  $0.5140 \text{ cm}^3 \cdot \text{g}^{-1}$ . With 95% purity, the other prepared sample (Type II) was purchased from Alpha Nanotechnologies Company in China. The second sample possessed an outside diameter of 15-20 nm, inside diameter of  $\sim 4$  nm, length of 30 nm, the specific surface area of  $294 \text{ m}^2 \cdot \text{g}^{-1}$  and a total pore volume of  $0.6231 \text{ cm}^3 \cdot \text{g}^{-1}$ . The performance of MWCNT Type I with the developed mesoporous structure was not quite satisfactory for  $\text{CH}_4$  adsorption ( $4.5 \text{ mmol} \cdot \text{g}^{-1}$  @ 50 bar and  $10^\circ \text{C}$ ). In contrast, the MWCNT type II stored a considerably significant amount of  $\text{CH}_4$  ( $33 \text{ mmol} \cdot \text{g}^{-1}$ ) at the same condition. Such an exceptional  $\text{CH}_4$  storage capacity can be justified by the unique surface properties of Type II MWCTs such as their highly uniform pore size and high pore volume.

Numerous studies have suggested that defects in CNTs structures increase the possibility of their gas storage capacity [201, 204, 205]. Defects or disorder cavities on the CNT framework may develop the surface area and pore volume of CNTs, act as entry points for gases, and shorten the diffusion pathway. Orimo and coworkers proposed the technique of “mechanical milling” to promote the hydrogen uptake of a nanostructure materials [206]. In a similar study, Liu and coworkers observed that the hydrogen loading was enhanced effectively as the milling time increased [207]. Moreover, some authors proposed the “post-activation” treatment for improving the porosity of CNTs and enhancing the deflection and irregularity inside the nanotube structure [97, 208]. Adeniran and Mokaya made a series of carbon nanotubes at low temperature ( $180^\circ \text{C}$ ) using carbon tetrachloride as precursor and ferrocene/Ni as substrate/catalyst [97]. The obtained CNTs showed a predominantly amorphous framework with large tube diameters of 180–300 nm, a wall thickness of *ca.* 25 nm, a surface area of  $470 \text{ m}^2 \cdot \text{g}^{-1}$  and pore volume of  $0.39 \text{ cm}^3 \cdot \text{g}^{-1}$ . After KOH-activation, the surface area and micropore volume were increased to  $1479\text{--}3802 \text{ m}^2 \cdot \text{g}^{-1}$  and  $1.65\text{--}$

2.98 cm<sup>3</sup>.g<sup>-1</sup>, respectively. They reported that the activated-CTN with KOH/carbon ratio of 4, contained large micropores and a significant proportion of mesopores and exhibited hydrogen storage of up to 7.5 wt%, 9.7 wt.% and 14.9 wt.% at -196 °C and 20, 40 and 150 bar, respectively. Due to practical difficulties associated with experiments in controlling/adjusting the geometrical properties of CNTs, the reported results in the literature are often controversial. One best way to precisely clarify the impact of the design parameters on the gas storage capacity of carbon nanotubes is using theoretical molecular studies. This method makes it possible to describe the nature of the interactions between gas and host nanomaterials, which helps to better understand the basic mechanisms of gas storage. As an example, the physisorption of pure CH<sub>4</sub> on bundles of single-wall carbon nanotubes (SWCNT) was studied by computational methods to investigate the influence of the material's porosity on the storage capacity and the adsorbate distribution [209]. In this research, the concept of CNT porosity was considered in two ways based on different (i) diameters of the nanotube inner cavity and (ii) the volume of the interstitial channels. The maximum load capacity was observed for the selected nanotubes with a smaller diameter. The small inner cavities efficiently trap CH<sub>4</sub> molecules and present a larger van der Waals (vdW) stabilization energy. The simulation results also proved that there is a significant chance of improving SWCNT-bundles' load capacity if the gap between the tubes can be controlled accurately.

In another theoretical study, Peng et al. performed a molecular simulation on CH<sub>4</sub> and CO<sub>2</sub> storage/separation on carbon nanoscrolls [199]. They analysed the effects of temperature and pressure, interlayer spacing, vdW gap and innermost radius systematically on the gas storage of these curve-shaped nanostructured materials. It was found that the adsorption of gases on pristine nanoscrolls is relatively low. However, both CH<sub>4</sub> and CO<sub>2</sub> adsorption capacities experience a

significant improvement after expanding the interlayer spacing (see Figure 21). In similar research, Mpourmpakis and co-workers performed a multiscale theoretical approach to investigate the hydrogen storage capacity of recently synthesized carbon nanoscrolls [210]. They found that pure carbon nanoscrolls cannot properly accumulate hydrogen because of their small interlayer distance. However, opening the spiral structure to approximately 0.7 nm followed by alkali doping can make them auspicious materials for hydrogen storage application, reaching 3 wt.% at ambient temperature and pressure (Figure 22).

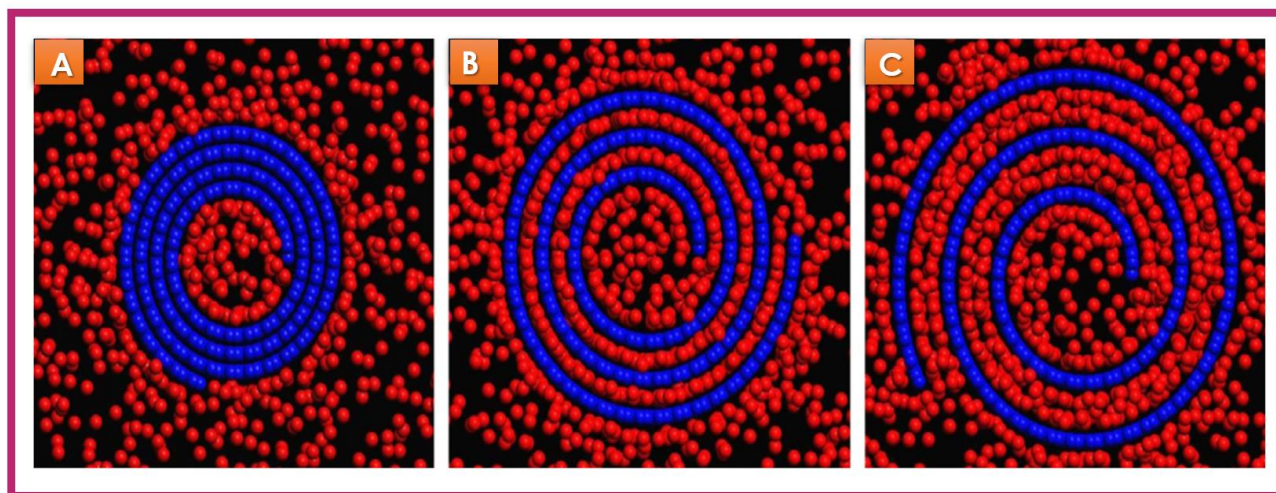


**Figure 21.** Snapshots of CH<sub>4</sub> adsorbed on isolated carbon nanoscrolls at 25 °C and 90 bar: (A)  $D = 0.34$  nm; (B)  $D = 0.7$  nm; (C)  $D = 1.1$  nm. The blue and red spheres denote carbon atoms on nanoscrolls and CH<sub>4</sub> molecules, respectively. Reproduced from ref [199]. Copyright 2010, Elsevier Ltd.

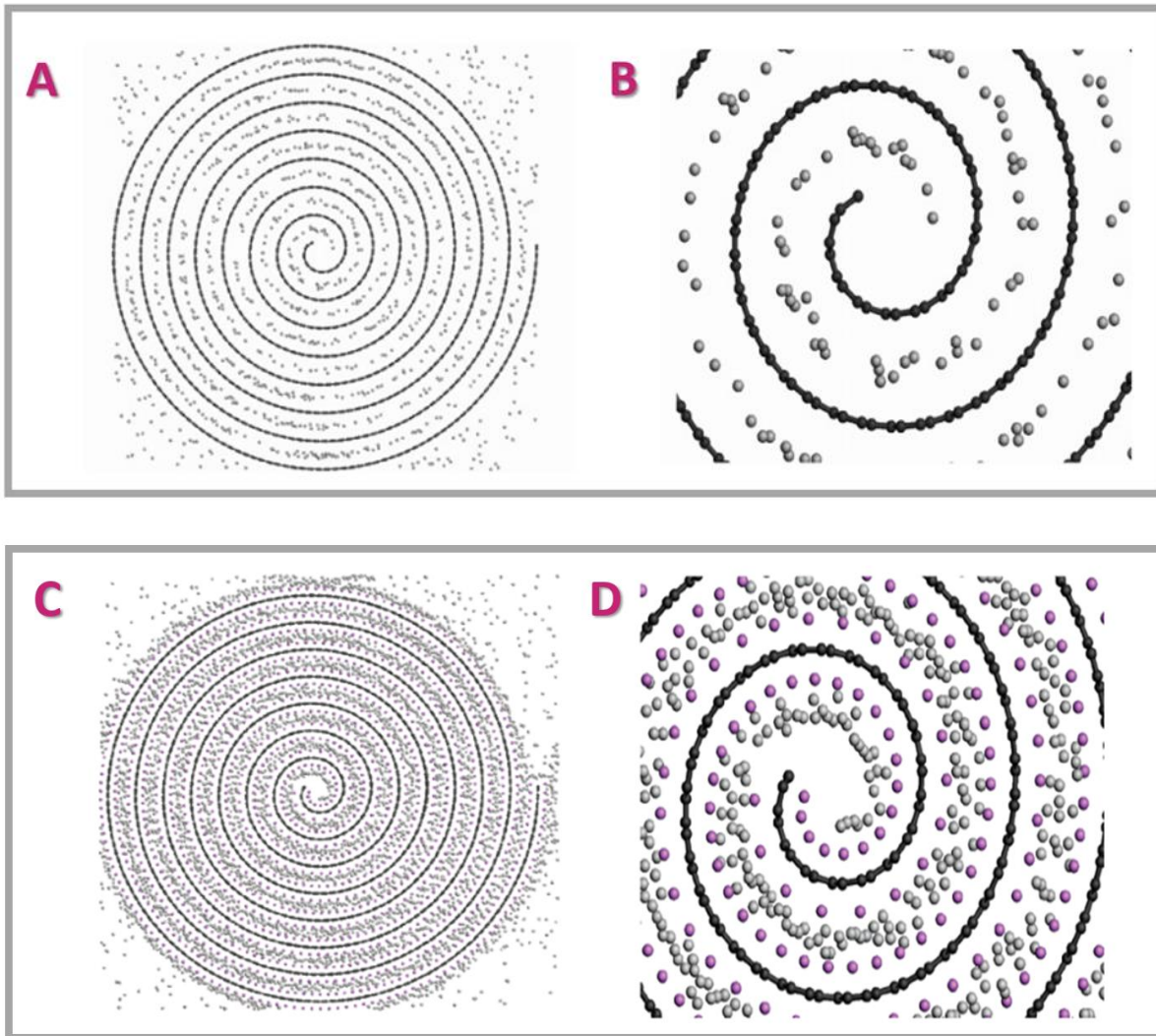


**Figure 22.** Snapshots from GCMC simulations of hydrogen adsorption on undoped CNS structures of (A) 0.7 nm interlayer distance and (B) zooming of the central part at room temperature and 100 bar pressure. The GCMC simulation of hydrogen adsorption on (C) alkali doping of CNS structures with 0.7 nm interlayer distance and (D) zooming of the central part at room temperature and 100 bar pressure. Reproduced from ref [210]. Copyright 2007, American Chemical Society.

The configuration arrangement of CTNs affects the gas uptake characteristics of these nanomaterials. In other words, the gas adsorption in interstices of nanotube arrays plays a significant role in their total volumetric and gravimetric gas capacity. A grand canonical Monte Carlo (GCMC) simulation was performed to optimize an array of armchair SWCNTs arrangements in a triangular shape for gas storage [211]. The results further confirmed that the interstitial

adsorption highly depends on the van der Waals gap between the tubular arrays. From a theoretical point of view, the interstitial adsorption process is tricky and varies with the size of tubes in addition to the distance between the tubes in a triangular array [212]. It has been demonstrated in Figure 23 that a triangular array of (14,14) nanotubes with a diameter of 1.9 nm separated by a vdW distance of 0.34 nm, possesses the volumetric storage capacity of up to 173 V.V<sup>-1</sup> at 35 bar and 298 K, which is 96% of the landmark value 180 V.V<sup>-1</sup> introduced as DOE target in 2015. Zhang and Wang used GCMC simulations and DFT calculations to explore the adsorption of CH<sub>4</sub> in a square lattice of nanotubes array with different diameters of 2.04-4.077 nm, wherein the tubes were separated by a van der Waals distance of 0.334 nm [213]. They found that an array of nanotubes with diameters of 4.077 nm can store about 22 mmol.g<sup>-1</sup> (35 wt %) at 300 K and 60 bar. Most of the reported values from theoretical studies seem promising for gas storage in CNTs (Table 7). Still, experimental attempts to reach or even approach such values in this class of nanomaterials have been unsuccessful. Under actual conditions, none of the carbon nanotubes synthesized have exhibited such ideal storage values. The conflicts between theory and experiments are most probably due to the fact that the nanotubes used in experiments are far from ideal theoretical structures. The synthesized CNTs are often distorted, contain mixtures of opened and unopened and single-walled and multiwalled nanotubes of various diameters and helicities [214].



**Table 7.** Gas storage properties of CNTs designed by theoretical and experimental study.

Adsorbent	Study Condition	$S_{BET}$ ( $m^2.g^{-1}$ )	$H_2$ Uptake (wt.%)	$CH_4$ Storage Capacity ( $V.V^{-1}$ )	Selective Separation Capacity (SSC)		Measurement Condition	Reference
					$CO_2/CH_4$	$CH_4/N_2$		
Commercial MWCNT	Experiment	> 500	-	0.98 $mmol.g^{-1}$	2.39	-	$CH_4$ @ 30 °C, 3.5 bar SSC@ 30 °C , 1 bar	Molyanyan et al.[203] (2016)
SWCNT with chirality (10,0)	Dynamics simulations with DLPOLY method	-	-	3.9	-	-	$CH_4$ @ 0 °C , 35 bar	Vela et al.[209] (2011)
Isolated carbon nanoscrolls	Molecular GCMC & GEMC simulations	-	-	262.70	1.57	-	$CH_4$ @ 25 °C , 65 bar SSC@ 25 °C, 60 bar	Peng et al. [199] (2010)
Commercial MWCNT	Experiment	126	-	4.02 $mmol.g^{-1}$	-	-	$CH_4$ @ 25 °C, 50 bar	Delavar et al.[202] (2014)
MWCNT	Prepared by CVD method	294	-	28.44 $mmol.g^{-1}$	-	-	$CH_4$ @ 25 °C, 50 bar	Delavar et al.[152] (2014)
SWNHs	Prepared by laser-ablating graphite	1030	-	96	-	-	$CH_4$ @ 30 °C, 35 bar	Bekyarova et al.[201] (2003)
CNT	Multiscale theoretical approach based on DFT calculation	-	5.24	-	-	-	$H_2$ @ -196 °C, 10 bar	Mpourmpakis et al.[210] (2007)
Scroll	Multiscale theoretical approach based on DFT calculation	-	3.08	-	-	-	$H_2$ @ -196 °C, 10 bar	Mpourmpakis et al. [160] (2007)
CNT	GCMC simulations	759	0.44 $mmol.g^{-1}$	2 $mmol.g^{-1}$	-	-	$H_2$ @ 25 °C, 25 bar $CH_4$ @ 25 °C, 25 bar	Kumar et al.[215] (2012)
CNT4700	Prepared by hydrothermal method	3202	6.7	-	-	-	$H_2$ @ -196 °C, 20 bar	Adeniran & Mokaya[112] (2015)

### 3.3 2D Graphene

Another important group of graphitic nanostructures is the building block of graphite known as “Graphene”. Graphene is an ideal one-atom-thick two-dimensional (2D)  $sp^2$  bonded carbon sheet arranged in a hexagonal honeycomb lattice [169]. Although the structure of graphene had been experimentally identified in 1962 by Boehm et al [216] and predicted decades ago [217], graphene was isolated and characterized as a 2D carbon nano-allotrope for the first time by the efforts of Novoselov and Geim in 2004 [218]. About six years later, in 2010, Novoselov and Geim received the Nobel prize in physics for detecting such a fantastic carbon-based material [169].

These particular 2D carbon nano-allotropes have attracted interest in various research areas such as medicine, aviation, as well as automotive and aerospace industry, and military applications because of their unique structure and exceptional characteristics. Recently, a significant number of investigations have been focused on applying graphene and its oxygen-containing derivatives, so-called graphene oxide (GO), for gas storage/separation requests. These carbonaceous structures usually possess a large surface area with adjustable microstructures, excellent electronic conductivity, and remarkable mechanical, chemical, thermal, and electrochemical stability.

The graphene’s quality is affected strongly by its production method. Briefly, the fabrication technics can be classified as chemical vapour deposition (CVD), plasma-enhanced CVD, graphitization, solvothermal, thermal and chemical exfoliation [219]. Generally, high-quality graphene is made of more expensive procedures (i.g. graphitization and exfoliation), while affordable synthesis technics (e.g. chemical vapour deposition and solvothermal) result in materials with poor electrical conductivity or mechanical strength. A few recently published review articles reported more details on graphene-based adsorbent synthesis procedures [219-221].

In relevant research, the hydrogen storage capacity of the so-called “pristine single-layer graphene sheet” with a BET specific surface area of  $156 \text{ m}^2.\text{g}^{-1}$ , was evaluated [222]. The results showed that the  $\text{H}_2$  adsorption is about 0.4 wt.% (at  $-196 \text{ }^\circ\text{C}$  and 1 bar) and 0.2 wt.% (at  $25 \text{ }^\circ\text{C}$  and 60 bar), respectively. As it can be seen, the hydrogen adsorption capacities are far below the DOE target expectation of 5.5 wt.%. Therefore, attempts have been made to improve the graphene nanosheet's gas adsorption capacity via different modification approaches [223-225]. Post chemical/physical activation of graphene sheets seems to be a successful approach to improving gas capacity. Using a facile and scalable synthetic approach, Huang et al. fabricated graphene nanosheets with hierarchically porous structures [226]. The produced steam-activated graphene sheets showed appropriate interconnected micro-meso-macroporous structures with high specific surface areas up to  $1238 \text{ m}^2.\text{g}^{-1}$ , and ultra-large pore volumes up to  $4.28 \text{ cm}^3.\text{g}^{-1}$ . These materials showed a high hydrogen storage capacity of 1.47 wt.% at  $-196 \text{ }^\circ\text{C}$  and 1 bar. Klechikov et al. optimized a post-KOH-activation procedure to enhance the graphene scaffold's porosity and gas adsorption properties (Figure 24) [227]. As-prepared adsorbent showed high BET surface area (values up to  $3400 \text{ m}^2.\text{g}^{-1}$ ) and pore volume up to  $2.2 \text{ cm}^3.\text{g}^{-1}$ . The maximum hydrogen uptake of  $\sim 7 \text{ wt.}\%$  (at  $-196 \text{ }^\circ\text{C}$  and 129 bar) was observed for these activated graphenes.

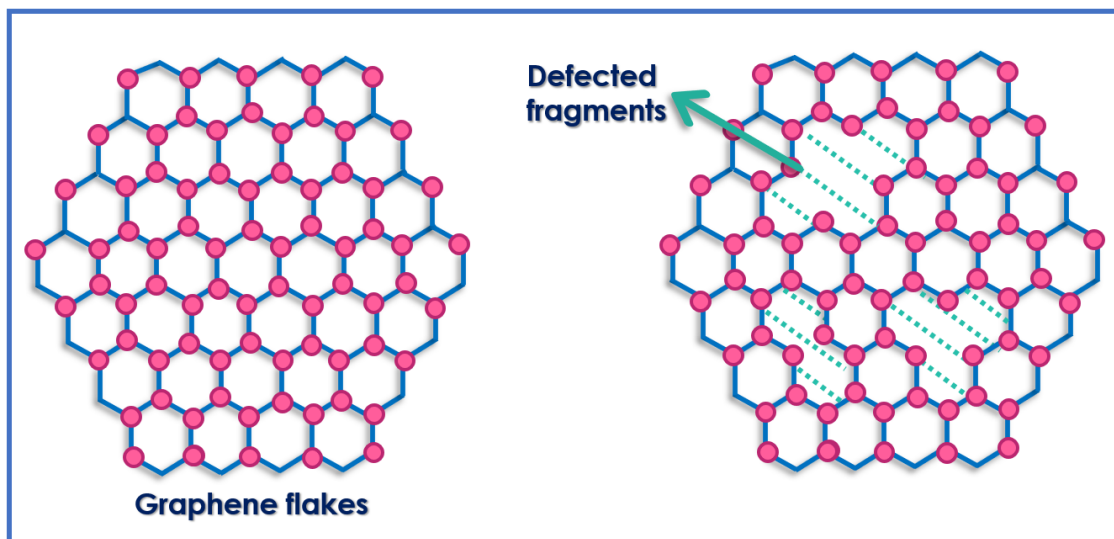


**Figure 24.** Schematic representation of possible defected fragments of graphene flakes.

A series of porous graphene-based adsorbents were fabricated by Srinivas et al. using KOH-activation of thermally exfoliated GO (exf-GO) and solvothermal reduced GO (rGO) precursors [228]. They reported an efficient approach to significantly increasing the graphene oxide surface area from  $10 \text{ m}^2.\text{g}^{-1}$  up to about  $1900 \text{ m}^2.\text{g}^{-1}$ . Besides, a linear trend between the BET surface area of graphene-based adsorbents and their  $\text{CH}_4$  adsorption capacity was observed. The optimum activation condition of  $800^\circ\text{C}$  and GO(1): KOH(9) ratio was reported to obtain a sample with hierarchical pore structure ( $1.65 \text{ cm}^3.\text{g}^{-1}$ ) and high  $\text{CH}_4$  storage capacity ( $0.175 \text{ mg}.\text{g}^{-1}$ ). The feasibility of layer spacing and adding dopants on multilayer graphene sheets to improve their  $\text{CH}_4$  adsorption was theoretically investigated in another study [229]. As depicted in Figure 25, simulation results indicated that the number of adsorbed  $\text{CH}_4$  molecules increases with the expansion of the graphene layer gap. However, the volumetric storage capacity might be reduced due to the increase in the volume space.

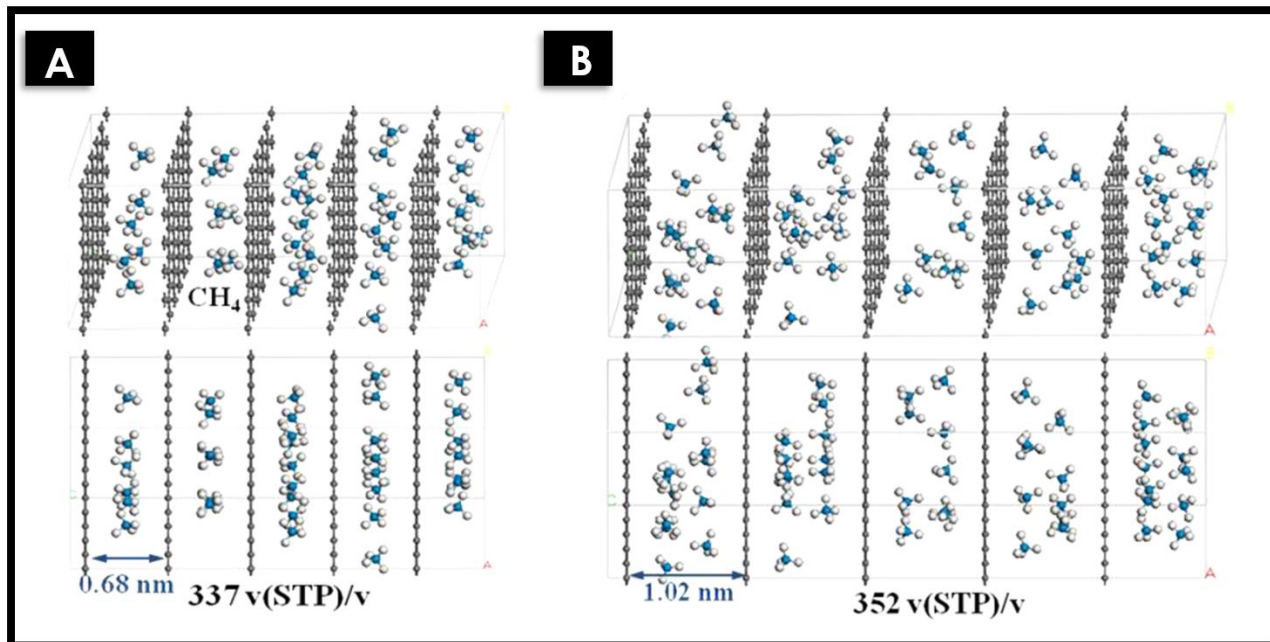


**Figure 25.** Snapshots and adsorption capacities of CH<sub>4</sub> in MGN with a dGL of (A) 0.68 nm and (B) 1.02 nm at 25 °C and 100 bar, including the three-dimensional view and front view. Reproduced from ref [229]. Copyright 2012, American Chemical Society.

The reported CH<sub>4</sub> and H<sub>2</sub> capacity of graphene sheets is well below the recent DOE targets in either of the theoretical and experimental studies. As mentioned, the linear relationship between the porous textural properties and gas adsorption capacity of the graphene sheet was reported in the literature. Theoretical studies showed that ideally, one particular graphene sheet can have a BET surface area as high as 2630 m<sup>2</sup>.g<sup>-1</sup>, which means about 1315 m<sup>2</sup>.g<sup>-1</sup> for each side of the sheet [230]. One best solution to fully exploiting the gas storage properties of 2D graphene sheets is to generate three-dimensional structures by introducing “spacers” among the graphene layers and producing interconnected defected graphene sheets [221, 231, 232]. The following section presents progress on the fabrication of 3D graphene-based structures for gas adsorption purposes.

### 3.4 3D Graphene

When it comes to practical applications, 2D graphene sheets might lose their inherent properties and consequently show poor performances far below the theoretical targets. One effective way to promote graphene sheets' processability and practical application in energy storage is to convert them into well-organized and interconnected three-dimensional (3D) structures made up of more than ten stacked layers of graphene. With such a solution, the exceptional properties of 2D graphene materials will be preserved, and the obtained 3D samples can be easily used without the concern of restacking.

Accordingly, the last but not the least member of the large family of carbon nano-allotropes is defined as a graphitic framework, where graphene layers weakly interact through van der Waals (vdW) forces. Different classifications of 3D graphene architecture have been presented since 2009, including pillared graphene frameworks (PGFs) [233], graphene oxide frameworks (GOFs) [234], multilayer graphene frameworks (MGFs) [221], graphene foams [235], and graphene sponges [236]. Different preparation methods of hydrothermal reduction [231, 237], chemical reduction [238, 239], laser casting [240, 241], 3D printing [242, 243], chemical vapour deposition (CVD) [221, 244] and on-site polymerization processes [245, 246] have been reported to produce these carbonaceous adsorbents.

Different types of 3D nanoporous graphene structures have been screened computationally and experimentally to find adsorbents with capacity close to the DOE target for CH<sub>4</sub> and H<sub>2</sub> storage [234, 247-249]. Hassani et al. employed hybrid molecular dynamics simulations to investigate the CH<sub>4</sub> storage capacity of nanostructure adsorbents of pillared graphene frameworks (PGFs) [247]. These frameworks are composed of parallel multi-layers of graphene, connected by vertical

organic linkers (so-called holders). They found the CH<sub>4</sub> uptake of the PGFs is about 22% higher than the pristine graphene sheets. In another study, the impact of length of linker inter-space on the CH<sub>4</sub> adsorption capacity of hypothetical graphene oxide framework was assessed by simulation [234]. Results showed that neither large linker interspace of 1.4 nm nor small linker interspace of 0.8 nm, but an optimum linker interspace distance (1.1 nm) results in the highest CH<sub>4</sub> adsorption capacity (19.70 mmol.g<sup>-1</sup> at 25 °C and 60 bar).

The highest volumetric CH<sub>4</sub> uptake value of 317 V.V<sup>-1</sup> was reported in a simulation study of general multilayer frameworks (GMFs), multilayer graphene frameworks (MGFs) and pillared graphene frameworks [248]. The stored gas amount reported for these 3D graphene-based structures remarkably can meet the latest value of the DOE target. In an experimental study, a novel, cost-effective and single-step technique was reported for mass production of 3D porous graphenes, using bagasse as a source of carbon [249]. In this research, bagasse was chemically activated using KOH at 850 °C with a ratio of 1(bagasse):6(KOH). The final microporous adsorbent showed large micropore volume of 1.45 cm<sup>3</sup>.g<sup>-1</sup>, an unprecedented surface area of ~3000 m<sup>2</sup>.g<sup>-1</sup> and a promising methane storage capacity of 193 V.V<sup>-1</sup> at 25 °C and 35 bar.

Recent advances in hydrogen storage on 3D graphene materials confirm their possible high capacity and acceptable stability for practical usage. In a simulation study, using idealised models, Garberoglio et al. assessed the amount of H<sub>2</sub> uptake of hypothetical organic pillared reduced-graphene-oxide sheets [169]. It was found that two important factors of (i) the density of the pillars and also (ii) the corrugation of graphene sheets have a profound impact on the gas adsorption properties of these materials. Another approach was adopted by Kumar and colleagues, where the H<sub>2</sub> storage of two different porous graphene frameworks (PGFs) was investigated via theoretical and experimental assessment [250]. Both of the Three-dimensional frameworks exhibited high

surface area ( $825 \text{ m}^2.\text{g}^{-1}$ ), pore volumes ( $0.74 \text{ cm}^3.\text{g}^{-1}$ ) and  $\text{H}_2$  uptake (1.2 wt.% at  $-196 \text{ }^\circ\text{C}$  and 1 bar) due to the effect of pillaring.

Macroscopic 3D graphene sponges and foams are also attractive materials for gas storage/separation. Lyth and coworkers reported a low-cost and scalable technique for fabricating 3D graphene foams through the combustion of sodium ethoxide [251]. As-prepared graphene foams showed a surface area of  $1296 \text{ m}^2.\text{g}^{-1}$  and  $\text{H}_2$  storage capacity of 2.1 wt.% at  $-196 \text{ }^\circ\text{C}$  and 10 bar pressure. The prepared 3D graphene foams also showed a higher  $\text{H}_2$  uptake value than the commercially obtained graphene sample (1.2 wt.% at  $-196 \text{ }^\circ\text{C}$  and 10 bar), which might be attributed to the higher surface area of the graphene foam. In another study, nanoporous spongy graphene oxides were synthesized using combined wet chemical reduction and freeze-drying techniques [252]. Potential application of these spongy graphenes for the gas storage/separation uses was analyzed by  $\text{H}_2$ ,  $\text{CO}_2$  and  $\text{CH}_4$  sorption measurements at different temperatures. The measured gas storage capacity of the samples at 1 bar was about 0.5 wt.% for hydrogen ( $-196 \text{ }^\circ\text{C}$ ), 3.7 wt.% for carbon dioxide ( $0 \text{ }^\circ\text{C}$ ) and 0.4 wt.% for  $\text{CH}_4$  ( $0 \text{ }^\circ\text{C}$ ). Moreover, the 3D sponges showed high  $\text{CO}_2$  over  $\text{CH}_4$  selectivity of 95:1 at  $0 \text{ }^\circ\text{C}$  and 0.7 bar pressure.

#### **4. Summary and outlook**

Considering the energy crisis and environmental pollution as the current global threats, developing practical, clean, affordable, and available energy storage systems becomes vital. High-pressure storage of energy carrier gases such as  $\text{CH}_4$  and  $\text{H}_2$ , as adsorbed phase on porous materials, is a promising safe alternative for current expensive and energy-consuming techniques. The porous carbons family, particularly activated carbons, has a long usage history in energy storage systems. These tunable structures, with unique inherent properties, are experiencing continual development



to satisfy the requirements of emergent applications. This paper reviewed various recent design strategies to synthesise carbonaceous adsorbents for CH<sub>4</sub> and H<sub>2</sub> storage.

Carbon-based adsorbents in different forms of granule, powder, fibres, foam, pellet and monoliths, with a high surface area and good packing density, can play a meaningful role in gas storage/separation applications. The key factor for gravimetric gas uptake of these adsorbents is their porosity; however, for the volumetric gas storage capacity, another critical parameter of packing density should be counted simultaneously. Between these two different storage capacity scales, the volumetric uptake of energy carriers is more important and applicable for onboard vehicular applications. In the case of methane storage, the highest volumetric uptake can reach up to 200 cm<sup>3</sup>.cm<sup>-3</sup> at 25 °C and 65 bar, getting closer to or meeting the new DOE targets. For hydrogen storage, the adsorbent with a well-developed microporosity exhibits high storage capacity of 4 wt.% at -196 °C and 1 bar condition.

Traditional activation of carbon materials enlarges the pores to prepare adsorbents with high surface area. However, to better control and tune the porosity, new techniques such as HTC, templating, and CDC methods have been developed to fabricate carbonaceous materials. These methods showed repeatable results, and products with relatively well-controlled structural characteristics (i.e. surface area, pore-volume, pore size, particle size, morphology, etc.), and, as a result, higher gas uptake. For example, some zeolite-templated carbons showed to have a high pore volume, fined-tuned PSD and exceptionally high methane storage of up to 210 cm<sup>3</sup>.cm<sup>-3</sup> at 25 °C and 65 bar.

Activated carbons are recognized as well-studied adsorbents in many application fields. Still, limitations such as their relatively low gas storage efficiency, disorder pore geomorphology, and even etching contamination during the activation procedure are associated with these adsorbents.

It is essential to explore new configurations of carbons with fewer inherent problems to overcome the limitation of these valuable materials. Over the past decade, carbon nano-allotrope adsorbents with highly ordered organized structures were introduced to compete with conventional amorphous disorder activated carbons. These novel adsorbents with different classes of zero (0D, carbon fullerenes), one (1D, carbon nanotubes), two (2D, graphenes) and three (3D, graphitic carbons) dimensions show great potential to serve as a suitable platform for loading gases such as methane and hydrogen. There is a strong possibility of significantly improving gas adsorption on carbon nano-allotropes structures due to defects inside their unique carbon cell. Recent studies on carbon nano-allotropes have revealed that the gas storage capacity of these materials can be enhanced by treating them with acids/basic media under different thermal conditions. However, most of the promising reported gas storage on this class of nanomaterials is based on theoretical studies. It seems experimental attempts to reach or even approach such values have been unsuccessful and need further investigation.

In the end, it should be acknowledged that despite the latest progress on developing novel materials, activated carbons remain a primary option for the fabrication of gas molecular adsorbent due to their accessibility, low cost, and ability to mass production and facile preparation methods. However, as motioned earlier, these materials also associated with some drawbacks and further technological and scientific research is required to improve carbon-based adsorbents:

For instance, new-faced materials like hybrid nanocomposite structures can be used as an energy-efficient platform for advancing porous carbon sorbents. One advantage of using such novel structures' is to benefit the unique properties of its two (or even more) pristine components at the same time, however, more precise research and study should be done to economize and facile the fabrication methods of these adsorbents. Furthermore, the exact mechanism of gas adsorption on,

inside or outside, curved-carbon structured or pillared graphene adsorbents is still controversial. Thus, further investigation should be performed to find fundamental molecular gas adsorption mechanisms inside the skeleton or on the surface of these carbon structures as next-generation gas adsorbers. Finally, we hope the topic of carbon-based materials continuously develops in other emerging regimes and attracts more scientists to join.

## References

- [1] S. Deutz, D. Bongartz, B. Heuser, A. Kätelhön, L.S. Langenhorst, A. Omari, M. Walters, J. Klankermayer, W. Leitner, A. Mitsos, Cleaner production of cleaner fuels: wind-to-wheel–environmental assessment of CO<sub>2</sub>-based oxymethylene ether as a drop-in fuel, *Energy & Environmental Science* 11(2) (2018) 331-343.
- [2] M.Z. Jacobson, The health and climate impacts of carbon capture and direct air capture, *Energy & Environmental Science* 12(12) (2019) 3567-3574.
- [3] Y.-J. Heo, S.-H. Yeon, S.-J. Park, Defining contribution of micropore size to hydrogen physisorption behaviors: A new approach based on DFT pore volumes, *Carbon* 143 (2019) 288-293.
- [4] G. Sdanghi, V. Nicolas, K. Mozet, S. Schaefer, G. Maranzana, A. Celzard, V. Fierro, A 70 MPa hydrogen thermally driven compressor based on cyclic adsorption-desorption on activated carbon, *Carbon* 161 (2020) 466-478.
- [5] K. Kaneko, F. Rodríguez-Reinoso, *Nanoporous materials for gas storage*, Springer 2019.
- [6] L. Wagner, I. Ross, J. Foster, B. Hankamer, Trading off global fuel supply, CO<sub>2</sub> emissions and sustainable development, *PloS one* 11(3) (2016) e0149406.
- [7] <https://energi.media/usa/natural-gas-consumed-fuel-industrial-sector-2018mar01/>.

- [8] EIA Projects that Natural Gas Consumption in Asia Will Continue to Outpace Supply [WWW Document]. <https://www.eia.gov/todayinenergy/detail>. Accessed Oct 2019.
- [9] How you can benefit from CNG conversion. CNG United, San Clemente, CA. <http://www.cngunited.com/support/howyoucanbenefitfromcngconversion>. Accessed Mar 2018.
- [10] M. Smith, J. Gonzales, Costs associated with compressed natural gas vehicle fueling infrastructure, National Renewable Energy Lab.(NREL), Golden, CO (United States), 2014.
- [11] J. Cho, G.J. Lim, S.J. Kim, T. Biobaku, Liquefied natural gas inventory routing problem under uncertain weather conditions, *International Journal of Production Economics* 204 (2018) 18-29.
- [12] V. Rozyyev, D. Thirion, R. Ullah, J. Lee, M. Jung, H. Oh, M. Atilhan, C.T. Yavuz, High-capacity methane storage in flexible alkane-linked porous aromatic network polymers, *Nature Energy* 4(7) (2019) 604-611.
- [13] F. Rodríguez-Reinoso, J. Silvestre-Albero, Methane Storage on Nanoporous Carbons, *Nanoporous Materials for Gas Storage*, Springer2019, pp. 209-226.
- [14] J. Wang, I. Senkovska, S. Kaskel, Q. Liu, Chemically activated fungi-based porous carbons for hydrogen storage, *Carbon* 75 (2014) 372-380.
- [15] D.Lozano-Castello, D. Cazorla-Amoros, A. Linares-Solano, and D. F. Quinn., Influence of pore size distribution on methane storage at relatively low pressure: preparation of activated carbon with optimum pore size. *Carbon* 40, no. 7 (2002): 989-1002.
- [16] S. Choi, M. A. Alkhabbaz, Y. Wang, R.M. Othman, M. Choi. Unique thermal contraction of zeolite-templated carbons enabling micropore size tailoring and its effects on methane storage. *Carbon* 141 (2019): 143-153.
- [17] M. Ghazvini, M. Vahedi, Sh. Najafi Nobar, F. Sabouri. Investigation of the MOF adsorbents and the gas adsorptive separation mechanisms. *Journal of Environmental Chemical Engineering* 9, no. 1 (2021): 104790.

- [18] Y. Tian, G. Zhu, Porous aromatic frameworks (PAFs), *Chemical reviews* 120(16) (2020) 8934-8986.
- [19] K. Otsuka, A. Mito, S. Takenaka, I. Yamanaka, Production and storage of hydrogen from methane mediated by metal, *Natural Gas Conversion VI* (2001) 215.
- [20] J. Moellmer, A. Moeller, F. Dreisbach, R. Glaeser, R. Staudt, High pressure adsorption of hydrogen, nitrogen, carbon dioxide and methane on the metal-organic framework HKUST-1, *Microporous and Mesoporous Materials* 138(1-3) (2011) 140-148.
- [21] M. Sevilla, R. Mokaya, Energy storage applications of activated carbons: supercapacitors and hydrogen storage, *Energy & Environmental Science* 7(4) (2014) 1250-1280.
- [22] N. Texier-Mandoki, J. Dentzer, T. Piquero, S. Saadallah, P. David, Hydrogen storage in activated carbon materials: role of the nanoporous texture, *Carbon (New York, NY)* 42(12-13) (2004) 2744-2747.
- [23] D. Lozano-Castello, D. Cazorla-Amoros, A. Linares-Solano, D. Quinn, Influence of pore size distribution on methane storage at relatively low pressure: preparation of activated carbon with optimum pore size, *Carbon* 40(7) (2002) 989-1002.
- [24] S. Mirzaei, A. Ahmadpour, A. Shahsavand, H. Rashidi, A. Arami-Niya, A Comparative study between regression and soft computing models to maximize methane storage capacity of anthracite-based adsorbents, *Industrial & Engineering Chemistry Research* (2020).
- [25] S. Mirzaei, A. Ahmadpour, A. Shahsavand, A.N. Pour, L. LotfiKatooli, A.G. Asil, B. Pouladi, A. Arami-Niya, Experimental and simulation study of the effect of surface functional groups decoration on CH<sub>4</sub> and H<sub>2</sub> storage capacity of microporous carbons, *Applied Surface Science* 533 (2020) 147487.

- [26] D. Lozano-Castello, M. Lillo-Rodenas, D. Cazorla-Amorós, A. Linares-Solano, Preparation of activated carbons from Spanish anthracite: I. Activation by KOH, *Carbon* 39(5) (2001) 741-749.
- [27] M. Lillo-Ródenas, D. Lozano-Castelló, D. Cazorla-Amorós, A. Linares-Solano, Preparation of activated carbons from Spanish anthracite: II. Activation by NaOH, *Carbon* 39(5) (2001) 751-759.
- [28] F.N. Ridha, R.M. Yunus, M. Rashid, A.F. Ismail, Thermal analysis of adsorptive natural gas storages during dynamic charge phase at room temperature, *Experimental thermal and fluid science* 32(1) (2007) 14-22.
- [29] S. Mirzaei, A. Shahsavand, A. Ahmadpour, A.G. Asil, A. Arami-Niya, Dynamic simulation and experimental performance of an adsorbed natural gas system under variable charging conditions, *Applied Thermal Engineering* (2022) 118067.
- [30] D. Lozano-Castelló, D. Cazorla-Amorós, A. Linares-Solano, D. Quinn, Activated carbon monoliths for methane storage: influence of binder, *Carbon* 40(15) (2002) 2817-2825.
- [31] J. Alcañiz-Monge, D. Lozano-Castelló, D. Cazorla-Amorós, A. Linares-Solano, Fundamentals of methane adsorption in microporous carbons, *Microporous and mesoporous materials* 124(1-3) (2009) 110-116.
- [32] M.E. Casco, M. Martinez-Escandell, K. Kaneko, J. Silvestre-Albero, F. Rodríguez-Reinoso, Very high methane uptake on activated carbons prepared from mesophase pitch: a compromise between microporosity and bulk density, *Carbon* 93 (2015) 11-21.
- [33] Y. Peng, V. Krungleviciute, I. Eryazici, J.T. Hupp, O.K. Farha, T. Yildirim, Methane storage in metal–organic frameworks: current records, surprise findings, and challenges, *Journal of the American Chemical Society* 135(32) (2013) 11887-11894.

- [34] F. Rodríguez-Reinoso, Y. Nakagawa, J. Silvestre-Albero, J. Juárez-Galán, M. Molina-Sabio, Correlation of methane uptake with microporosity and surface area of chemically activated carbons, *Microporous and mesoporous Materials* 115(3) (2008) 603-608.
- [35] h.c.c.w.s.w.-o.-s. Web of Science; Web of Science Group.
- [36] E. Lee, S.H. Kwon, P.R. Choi, J.C. Jung, M.-S. Kim, Activated carbons prepared from mixtures of coal tar pitch and petroleum pitch and their electrochemical performance as electrode materials for electric double-layer capacitor, *Carbon Letters (Carbon Lett.)* 16(2) (2015) 78-85.
- [37] P.R. Choi, E. Lee, S.H. Kwon, J.C. Jung, M.-S. Kim, Characterization and organic electric-double-layer-capacitor application of KOH activated coal-tar-pitch-based carbons: Effect of carbonization temperature, *Journal of Physics and Chemistry of Solids* 87 (2015) 72-79.
- [38] X. Lu, D. Jin, S. Wei, M. Zhang, Q. Zhu, X. Shi, Z. Deng, W. Guo, W. Shen, Competitive adsorption of a binary CO<sub>2</sub>-CH<sub>4</sub> mixture in nanoporous carbons: effects of edge-functionalization, *Nanoscale* 7(3) (2015) 1002-1012.
- [39] M.E. Casco, M. Martínez-Escandell, E. Gadea-Ramos, K. Kaneko, J. Silvestre-Albero, F. Rodríguez-Reinoso, High-pressure methane storage in porous materials: are carbon materials in the pole position?, *Chemistry of materials* 27(3) (2015) 959-964.
- [40] M.S. Shafeeyan, A. Houshmand, A. Arami-Niya, H. Razaghizadeh, W.M.A.W. Daud, Modification of activated carbon using nitration followed by reduction for carbon dioxide capture, *Bulletin of the Korean Chemical Society* 36(2) (2015) 533-538.
- [41] J. Shi, W. Li, D. Li, Rapidly reversible adsorption of methane with a high storage capacity on the zeolite templated carbons with glucose as carbon precursors, *Colloids and Surfaces A: Physicochemical and Engineering Aspects* 485 (2015) 11-17.

- [42] S.A. Mirzaei, A.; Shahsavand, A.; Rashidi, H.; Arami-Niya, A., Superior performance of modified pitch-based adsorbents for cyclic methane storage, *Journal of Energy Storage* (2020).
- [43] Y. Zheng, Q. Li, C. Yuan, Q. Tao, Y. Zhao, G. Zhang, J. Liu, G. Qi, Thermodynamic analysis of high-pressure methane adsorption on coal-based activated carbon, *Fuel* 230 (2018) 172-184.
- [44] H. Zhang, J. Chen, S. Guo, Preparation of natural gas adsorbents from high-sulfur petroleum coke, *Fuel* 87(3) (2008) 304-311.
- [45] S.Y. Sawant, K. Munusamy, R.S. Somani, M. John, B.L. Newalkar, H.C. Bajaj, Precursor suitability and pilot scale production of super activated carbon for greenhouse gas adsorption and fuel gas storage, *Chemical Engineering Journal* 315 (2017) 415-425.
- [46] A. Arami-Niya, T.E. Rufford, Z. Zhu, Activated carbon monoliths with hierarchical pore structure from tar pitch and coal powder for the adsorption of CO<sub>2</sub>, CH<sub>4</sub> and N<sub>2</sub>, *Carbon* 103 (2016) 115-124.
- [47] C. Zhang, R. Kong, X. Wang, Y. Xu, F. Wang, W. Ren, Y. Wang, F. Su, J.-X. Jiang, Porous carbons derived from hypercrosslinked porous polymers for gas adsorption and energy storage, *Carbon* 114 (2017) 608-618.
- [48] B. Ashourirad, A.K. Sekizkardes, S. Altarawneh, H.M. El-Kaderi, Exceptional gas adsorption properties by nitrogen-doped porous carbons derived from benzimidazole-linked polymers, *Chemistry of Materials* 27(4) (2015) 1349-1358.
- [49] M.T. Shirazani, H. Bakhshi, A. Rashidi, M. Taghizadeh, Starch-based Activated Carbon Micro-spheres for Adsorption of Methane with Superior Performance in ANG Technology, *Journal of Environmental Chemical Engineering* (2020) 103910.
- [50] I. Wróbel-Iwaniec, N. Díez, G. Gryglewicz, Chitosan-based highly activated carbons for hydrogen storage, *International Journal of Hydrogen Energy* 40(17) (2015) 5788-5796.



- [51] A. Altwala, R. Mokaya, Predictable and targeted activation of biomass to carbons with high surface area density and enhanced methane storage capacity, *Energy & Environmental Science* 13(9) (2020) 2967-2978.
- [52] M. Jung, J. Park, K. Lee, N.F. Attia, H. Oh, Effective synthesis route of renewable nanoporous carbon adsorbent for high energy gas storage and CO<sub>2</sub>/N<sub>2</sub> selectivity, *Renewable Energy* 161 (2020) 30-42.
- [53] J. Wang, P. Zhang, L. Liu, Y. Zhang, J. Yang, Z. Zeng, S. Deng, Controllable synthesis of bifunctional porous carbon for efficient gas-mixture separation and high-performance supercapacitor, *Chemical Engineering Journal* 348 (2018) 57-66.
- [54] Z. Heidarinejad, M.H. Dehghani, M. Heidari, G. Javedan, I. Ali, M. Sillanpää, Methods for preparation and activation of activated carbon: a review, *Environmental Chemistry Letters* 18(2) (2020) 393-415.
- [55] N. Byamba-Ochir, W.G. Shim, M. Balathanigaimani, H. Moon, Highly porous activated carbons prepared from carbon rich Mongolian anthracite by direct NaOH activation, *Applied Surface Science* 379 (2016) 331-337.
- [56] Y.-D. Chen, W.-Q. Chen, B. Huang, M.-J. Huang, Process optimization of K<sub>2</sub>C<sub>2</sub>O<sub>4</sub>-activated carbon from kenaf core using Box–Behnken design, *Chemical Engineering Research and Design* 91(9) (2013) 1783-1789.
- [57] A. Ahmadpour, D. Do, The preparation of active carbons from coal by chemical and physical activation, *Carbon* 34(4) (1996) 471-479.
- [58] H.S. Kim, M.S. Kang, S. Lee, Y.-W. Lee, W.C. Yoo, N-doping and ultramicroporosity-controlled crab shell derived carbons for enhanced CO<sub>2</sub> and CH<sub>4</sub> sorption, *Microporous and Mesoporous Materials* 272 (2018) 92-100.

- [59] C. Bouchelta, M.S. Medjram, O. Bertrand, J.-P. Bellat, Preparation and characterization of activated carbon from date stones by physical activation with steam, *Journal of Analytical and Applied Pyrolysis* 82(1) (2008) 70-77.
- [60] H. Marsh, F. Rodriguez-Reinoso, Chapter 5—Activation processes (thermal or physical), *Activated Carbon*; Elsevier Science Ltd.: Oxford, UK (2006) 243-321.
- [61] J. Park, N.F. Attia, M. Jung, M.E. Lee, K. Lee, J. Chung, H. Oh, Sustainable nanoporous carbon for CO<sub>2</sub>, CH<sub>4</sub>, N<sub>2</sub>, H<sub>2</sub> adsorption and CO<sub>2</sub>/CH<sub>4</sub> and CO<sub>2</sub>/N<sub>2</sub> separation, *Energy* 158 (2018) 9-16.
- [62] Y. Li, D. Li, Y. Rao, X. Zhao, M. Wu, Superior CO<sub>2</sub>, CH<sub>4</sub>, and H<sub>2</sub> uptakes over ultrahigh-surface-area carbon spheres prepared from sustainable biomass-derived char by CO<sub>2</sub> activation, *Carbon* 105 (2016) 454-462.
- [63] C. Nguyen, A. Ahmadpour, D. Do, Effects of gasifying agents on the characterization of nut shell-derived activated carbon, *Adsorption Science & Technology* 12(3) (1995) 247-258.
- [64] K.X. Yao, Y. Chen, Y. Lu, Y. Zhao, Y. Ding, Ultramicroporous carbon with extremely narrow pore distribution and very high nitrogen doping for efficient methane mixture gases upgrading, *Carbon* 122 (2017) 258-265.
- [65] T. Yang, A.C. Lua, Characteristics of activated carbons prepared from pistachio-nut shells by physical activation, *Journal of Colloid and Interface Science* 267(2) (2003) 408-417.
- [66] S. Zhao, J. Xiang, C.-Y. Wang, M.-M. Chen, Characterization and electrochemical performance of activated carbon spheres prepared from potato starch by CO<sub>2</sub> activation, *Journal of Porous Materials* 20(1) (2013) 15-20.

- [67] F.-L. Wang, L.-L. Pang, Y.-Y. Jiang, B. Chen, D. Lin, N. Lun, H.-L. Zhu, R. Liu, X.-L. Meng, Y. Wang, Simple synthesis of hollow carbon spheres from glucose, *Materials Letters* 63(29) (2009) 2564-2566.
- [68] A. Ahmadpour, H. Rashidi, M.J.D. Mahboub, M.R. Farmad, Comparing the performance of KOH with NaOH-activated anthracites in terms of methane storage, *Adsorption Science & Technology* 31(8) (2013) 729-745.
- [69] D. Lozano-Castello, D. Cazorla-Amoros, A. Linares-Solano, Powdered activated carbons and activated carbon fibers for methane storage: a comparative study, *Energy & fuels* 16(5) (2002) 1321-1328.
- [70] M.A. Yahya, Z. Al-Qodah, C.Z. Ngah, Agricultural bio-waste materials as potential sustainable precursors used for activated carbon production: A review, *Renewable and Sustainable Energy Reviews* 46 (2015) 218-235.
- [71] M. Molina-Sabio, F. Rodriguez-Reinoso, Role of chemical activation in the development of carbon porosity, *Colloids and Surfaces A: Physicochemical and Engineering Aspects* 241(1-3) (2004) 15-25.
- [72] A. Ahmadpour, B.A. King, D.D. Do, Comparison of equilibria and kinetics of high surface area activated carbon produced from different precursors and by different chemical treatments, *Industrial & engineering chemistry research* 37(4) (1998) 1329-1334.
- [73] A. Okhovat, A. Ahmadpour, A comparative study of the effects of different chemical agents on the pore-size distributions of macadamia nutshell-based activated carbons using different models, *Adsorption Science & Technology* 30(2) (2012) 159-169.

- [74] A. Perrin, A. Celzard, A. Albinia, J. Kaczmarczyk, J. Mareche, G. Furdin, NaOH activation of anthracites: effect of temperature on pore textures and methane storage ability, *Carbon* 42(14) (2004) 2855-2866.
- [75] A. Silvestre-Albero, J. Silvestre-Albero, M. Martínez-Escandell, F. Rodríguez-Reinoso, Micro/mesoporous activated carbons derived from polyaniline: promising candidates for CO<sub>2</sub> adsorption, *Industrial & Engineering Chemistry Research* 53(40) (2014) 15398-15405.
- [76] A.S. Mestre, C. Freire, J. Pires, A.P. Carvalho, M.L. Pinto, High performance microspherical activated carbons for methane storage and landfill gas or biogas upgrade, *Journal of Materials Chemistry A* 2(37) (2014) 15337-15344.
- [77] Y. Mao, H. Xie, X. Chen, Y. Zhao, J. Qu, Q. Song, Z. Ning, P. Xing, H. Yin, A combined leaching and electrochemical activation approach to converting coal to capacitive carbon in molten carbonates, *Journal of Cleaner Production* 248 (2020) 119218.
- [78] A. Ahmadpour, D. Do, The preparation of activated carbon from macadamia nutshell by chemical activation, *Carbon* 35(12) (1997) 1723-1732.
- [79] A. Okhovat, A. Ahmadpour, F. Ahmadpour, Z. Khaki Yadegar, Pore size distribution analysis of coal-based activated carbons: investigating the effects of activating agent and chemical ratio, *International Scholarly Research Notices* 2012 (2012).
- [80] A. Arami-Niya, W.M.A.W. Daud, F.S. Mjalli, Using granular activated carbon prepared from oil palm shell by ZnCl<sub>2</sub> and physical activation for methane adsorption, *Journal of Analytical and Applied Pyrolysis* 89(2) (2010) 197-203.
- [81] R.H. Hesas, A. Arami-Niya, W.M.A.W. Daud, J. Sahu, Comparison of oil palm shell-based activated carbons produced by microwave and conventional heating methods using zinc chloride activation, *Journal of Analytical and Applied Pyrolysis* 104 (2013) 176-184.

- [82] A. Arami-Niya, W.M.A.W. Daud, F.S. Mjalli, F. Abnisa, M.S. Shafeeyan, Production of microporous palm shell based activated carbon for methane adsorption: modeling and optimization using response surface methodology, *Chemical engineering research and design* 90(6) (2012) 776-784.
- [83] Y. Gao, Q. Yue, B. Gao, A. Li, Insight into activated carbon from different kinds of chemical activating agents: A review, *Science of The Total Environment* (2020) 141094.
- [84] A. Ahmadpour, N. Jahanshahi, S. Rashidi, N. Chenarani, M.J.D. Mahboub, Application of artificial neural networks and adaptive neuro-fuzzy inference systems to predict activated carbon properties for methane storage, *Adsorption Science & Technology* 32(4) (2014) 275-290.
- [85] A. Shahsavand, A. Ahmadpour, Application of optimal RBF neural networks for optimization and characterization of porous materials, *Computers & Chemical Engineering* 29(10) (2005) 2134-2143.
- [86] J. Cai, J. Qi, C. Yang, X. Zhao, Poly (vinylidene chloride)-based carbon with ultrahigh microporosity and outstanding performance for CH<sub>4</sub> and H<sub>2</sub> storage and CO<sub>2</sub> capture, *ACS applied materials & interfaces* 6(5) (2014) 3703-3711.
- [87] N.F. Attia, M. Jung, J. Park, H. Jang, K. Lee, H. Oh, Flexible nanoporous activated carbon cloth for achieving high H<sub>2</sub>, CH<sub>4</sub>, and CO<sub>2</sub> storage capacities and selective CO<sub>2</sub>/CH<sub>4</sub> separation, *Chemical Engineering Journal* 379 (2020) 122367.
- [88] J. Wang, R. Krishna, T. Yang, S. Deng, Nitrogen-rich microporous carbons for highly selective separation of light hydrocarbons, *Journal of Materials Chemistry A* 4(36) (2016) 13957-13966.

- [89] M. Sevilla, A. Fuertes, R. Mokaya, Preparation and hydrogen storage capacity of highly porous activated carbon materials derived from polythiophene, *International journal of hydrogen energy* 36(24) (2011) 15658-15663.
- [90] S. Horike, Y. Inubushi, T. Hori, T. Fukushima, S. Kitagawa, A solid solution approach to 2D coordination polymers for CH<sub>4</sub>/CO<sub>2</sub> and CH<sub>4</sub>/C<sub>2</sub>H<sub>6</sub> gas separation: equilibrium and kinetic studies, *Chemical Science* 3(1) (2012) 116-120.
- [91] M.J. Prauchner, K. Sapag, F. Rodríguez-Reinoso, Tailoring biomass-based activated carbon for CH<sub>4</sub> storage by combining chemical activation with H<sub>3</sub>PO<sub>4</sub> or ZnCl<sub>2</sub> and physical activation with CO<sub>2</sub>, *Carbon* 110 (2016) 138-147.
- [92] N. Kostoglou, C. Koczwar, C. Prehal, V. Terziyska, B. Babic, B. Matovic, G. Constantinides, C. Tampaxis, G. Charalambopoulou, T. Steriotis, Nanoporous activated carbon cloth as a versatile material for hydrogen adsorption, selective gas separation and electrochemical energy storage, *Nano Energy* 40 (2017) 49-64.
- [93] M.J. Prauchner, F. Rodríguez-Reinoso, Chemical versus physical activation of coconut shell: A comparative study, *Microporous and Mesoporous Materials* 152 (2012) 163-171.
- [94] US Department Of Energy, vehicles. 2012, [http://energy.gov/sites/prod/files/2015/01/f19/fcto\\_myRDD\\_table\\_onboard\\_h2\\_storage\\_systems\\_doe\\_targets\\_ldv.pdf](http://energy.gov/sites/prod/files/2015/01/f19/fcto_myRDD_table_onboard_h2_storage_systems_doe_targets_ldv.pdf).
- [95] Advanced Research Project Agency-Energy (ARPA-E), overview., [https://arpa.e.energy.gov/sites/default/files/documents/files/MOVE\\_ProgramOverview.pdf](https://arpa.e.energy.gov/sites/default/files/documents/files/MOVE_ProgramOverview.pdf).
- [96] G. Sethia, A. Sayari, Activated carbon with optimum pore size distribution for hydrogen storage, *Carbon* 99 (2016) 289-294.

- [97] B. Adeniran, R. Mokaya, Compaction: a mechanochemical approach to carbons with superior porosity and exceptional performance for hydrogen and CO<sub>2</sub> storage, *Nano Energy* 16 (2015) 173-185.
- [98] Y. Zhang, L. Liu, P. Zhang, J. Wang, M. Xu, Q. Deng, Z. Zeng, S. Deng, Ultra-high surface area and nitrogen-rich porous carbons prepared by a low-temperature activation method with superior gas selective adsorption and outstanding supercapacitance performance, *Chemical Engineering Journal* 355 (2019) 309-319.
- [99] J.-H. Park, S.-J. Park, Expansion of effective pore size on hydrogen physisorption of porous carbons at low temperatures with high pressures, *Carbon* 158 (2020) 364-371.
- [100] W. Hu, J. Huang, P. Yu, M. Zheng, Y. Xiao, H. Dong, Y. Liang, H. Hu, Y. Liu, Hierarchically Porous Carbon Derived from *Neolamarckia cadamba* for Electrochemical Capacitance and Hydrogen Storage, *ACS Sustainable Chemistry & Engineering* 7(18) (2019) 15385-15393.
- [101] M. Tian, M.J. Lennox, A.J. O'Malley, A.J. Porter, B. Krüner, S. Rudić, T.J. Mays, T. Düren, V. Presser, L.R. Terry, Effect of pore geometry on ultra-densified hydrogen in microporous carbons, *Carbon* 173 (2020) 968-979.
- [102] L. He, Y.B. Melnichenko, N.C. Gallego, C.I. Contescu, J. Guo, J. Bahadur, Investigation of morphology and hydrogen adsorption capacity of disordered carbons, *Carbon* 80 (2014) 82-90.
- [103] C.A. Grande, Ø. Vistad, Adequacy versus complexity of mathematical models for engineering an adsorbed natural gas device, *Journal of Energy Storage* 28 (2020) 101200.
- [104] T.S. Blankenship II, N. Balahmar, R. Mokaya, Oxygen-rich microporous carbons with exceptional hydrogen storage capacity, *Nature communications* 8(1) (2017) 1545.

- [105] T.K. Das, S. Banerjee, P. Sharma, V. Sudarsan, P. Sastry, Nitrogen doped porous carbon derived from EDTA: Effect of pores on hydrogen storage properties, *International Journal of Hydrogen Energy* 43(17) (2018) 8385-8394.
- [106] Y. Li, N. Liu, T. Zhang, B. Wang, Y. Wang, L. Wang, J. Wei, Highly microporous nitrogen-doped carbons from anthracite for effective CO<sub>2</sub> capture and CO<sub>2</sub>/CH<sub>4</sub> separation, *Energy* 211 (2020) 118561.
- [107] S. Ghosh, R. Sarathi, S. Ramaprabhu, Magnesium oxide modified nitrogen-doped porous carbon composite as an efficient candidate for high pressure carbon dioxide capture and methane storage, *Journal of colloid and interface science* 539 (2019) 245-256.
- [108] P. Ariyageadsakul, V. Vchirawongkwin, C. Kritayakornupong, Determination of toxic carbonyl species including acetone, formaldehyde, and phosgene by polyaniline emeraldine gas sensor using DFT calculation, *Sensors and Actuators B: Chemical* 232 (2016) 165-174.
- [109] X. Zhao, B. Xiao, A. Fletcher, K. Thomas, Hydrogen adsorption on functionalized nanoporous activated carbons, *The Journal of Physical Chemistry B* 109(18) (2005) 8880-8888.
- [110] J.S. Im, S.-J. Park, Y.-S. Lee, The metal-carbon-fluorine system for improving hydrogen storage by using metal and fluorine with different levels of electronegativity, *International Journal of Hydrogen Energy* 34(3) (2009) 1423-1428.
- [111] A. Ariharan, B. Viswanathan, V. Nandhakumar, Nitrogen-incorporated carbon nanotube derived from polystyrene and polypyrrole as hydrogen storage material, *international journal of hydrogen energy* 43(10) (2018) 5077-5088.
- [112] B. Adeniran, R. Mokaya, Low temperature synthesized carbon nanotube superstructures with superior CO<sub>2</sub> and hydrogen storage capacity, *Journal of Materials Chemistry A* 3(9) (2015) 5148-5161.



- [113] E. Masika, R. Mokaya, Exceptional gravimetric and volumetric hydrogen storage for densified zeolite templated carbons with high mechanical stability, *Energy & Environmental Science* 7(1) (2014) 427-434.
- [114] E. Masika, R. Mokaya, Preparation of ultrahigh surface area porous carbons templated using zeolite 13X for enhanced hydrogen storage, *Progress in Natural Science: Materials International* 23(3) (2013) 308-316.
- [115] Y.S. Lee, Y.H. Kim, J.S. Hong, J.K. Suh, G.J. Cho, The adsorption properties of surface modified activated carbon fibers for hydrogen storages, *Catalysis today* 120(3-4) (2007) 420-425.
- [116] J.S. Im, M.J. Jung, Y.-S. Lee, Effects of fluorination modification on pore size controlled electrospun activated carbon fibers for high capacity methane storage, *Journal of colloid and interface science* 339(1) (2009) 31-35.
- [117] H. Rezvani, S. Fatemi, J. Tamnanloo, Activated carbon surface modification by catalytic chemical vapor deposition of natural gas for enhancing adsorption of greenhouse gases, *Journal of Environmental Chemical Engineering* 7(3) (2019) 103085.
- [118] Y. Li, R. Xu, B. Wang, J. Wei, L. Wang, M. Shen, J. Yang, Enhanced N-doped porous carbon derived from KOH-activated waste wool: A promising material for selective adsorption of CO<sub>2</sub>/CH<sub>4</sub> and CH<sub>4</sub>/N<sub>2</sub>, *Nanomaterials* 9(2) (2019) 266.
- [119] T. Kopac, Y. Kirca, Effect of ammonia and boron modifications on the surface and hydrogen sorption characteristics of activated carbons from coal, *International Journal of Hydrogen Energy* 45(17) (2020) 10494-10506.
- [120] Z. Han, H. Yu, C. Li, S. Zhou, Mulch-assisted ambient-air synthesis of oxygen-rich activated carbon for hydrogen storage: A combined experimental and theoretical case study, *Applied Surface Science* 544 (2021) 148963.

- [121] C. Falco, J.P. Marco-Lozar, D. Salinas-Torres, E. Morallon, D. Cazorla-Amorós, M.-M. Titirici, D. Lozano-Castelló, Tailoring the porosity of chemically activated hydrothermal carbons: Influence of the precursor and hydrothermal carbonization temperature, *Carbon* 62 (2013) 346-355.
- [122] B. Yuan, J. Wang, Y. Chen, X. Wu, H. Luo, S. Deng, Unprecedented performance of N-doped activated hydrothermal carbon towards C<sub>2</sub>H<sub>6</sub>/CH<sub>4</sub>, CO<sub>2</sub>/CH<sub>4</sub>, and CO<sub>2</sub>/H<sub>2</sub> separation, *Journal of Materials Chemistry A* 4(6) (2016) 2263-2276.
- [123] A. Jain, R. Balasubramanian, M. Srinivasan, Hydrothermal conversion of biomass waste to activated carbon with high porosity: A review, *Chemical Engineering Journal* 283 (2016) 789-805.
- [124] C.O. Ania, E. Raymundo-Piñero, Nanoporous Carbons with Tuned Porosity, *Nanoporous Materials for Gas Storage*, Springer 2019, pp. 91-135.
- [125] T.S. Blankenship, R. Mokaya, Cigarette butt-derived carbons have ultra-high surface area and unprecedented hydrogen storage capacity, *Energy & Environmental Science* 10(12) (2017) 2552-2562.
- [126] S. Schaefer, V. Fierro, M. Izquierdo, A. Celzard, Assessment of hydrogen storage in activated carbons produced from hydrothermally treated organic materials, *international journal of hydrogen energy* 41(28) (2016) 12146-12156.
- [127] M. Sevilla, W. Sangchoom, N. Balahmar, A.B. Fuertes, R. Mokaya, Highly porous renewable carbons for enhanced storage of energy-related gases (H<sub>2</sub> and CO<sub>2</sub>) at high pressures, *ACS Sustainable Chemistry & Engineering* 4(9) (2016) 4710-4716.
- [128] N. Balahmar, R. Mokaya, Pre-mixed precursors for modulating the porosity of carbons for enhanced hydrogen storage: towards predicting the activation behaviour of carbonaceous matter, *Journal of Materials Chemistry A* 7(29) (2019) 17466-17479.

- [129] W. Sangchoom, R. Mokaya, Valorization of lignin waste: carbons from hydrothermal carbonization of renewable lignin as superior sorbents for CO<sub>2</sub> and hydrogen storage, *ACS Sustainable Chemistry & Engineering* 3(7) (2015) 1658-1667.
- [130] S. Savic, K. Vojisavljevic, M. Počuča-Nešić, K. Zivojevic, M. Mladenovic, N. Knezevic, Hard Template Synthesis of Nanomaterials Based on Mesoporous Silica, *Metallurgical and Materials Engineering* 24(4) (2018).
- [131] L. Xie, Z. Jin, Z. Dai, Y. Chang, X. Jiang, H. Wang, Porous carbons synthesized by templating approach from fluid precursors and their applications in environment and energy storage: A review, *Carbon* (2020).
- [132] W. Libbrecht, A. Verberckmoes, J.W. Thybaut, P. Van Der Voort, J. De Clercq, Soft templated mesoporous carbons: Tuning the porosity for the adsorption of large organic pollutants, *Carbon* 116 (2017) 528-546.
- [133] N.P. Stadie, M. Murialdo, C.C. Ahn, B. Fultz, Anomalous isosteric enthalpy of adsorption of methane on zeolite-templated carbon, *Journal of the American Chemical Society* 135(3) (2013) 990-993.
- [134] J. Zhou, X. Wang, W. Xing, Carbon-based CO<sub>2</sub> Adsorbents, (2018).
- [135] N.P. Stadie, J.J. Vajo, R.W. Cumberland, A.A. Wilson, C.C. Ahn, B. Fultz, Zeolite-templated carbon materials for high-pressure hydrogen storage, *Langmuir* 28(26) (2012) 10057-10063.
- [136] S. Choi, M.A. Alkhabbaz, Y. Wang, R.M. Othman, M. Choi, Unique thermal contraction of zeolite-templated carbons enabling micropore size tailoring and its effects on methane storage, *Carbon* 141 (2019) 143-153.

- [137] D. Saha, Z. Wei, S.H. Valluri, S. Deng, Hydrogen adsorption in ordered mesoporous carbon synthesized by a soft-template approach, *Journal of Porous Media* 13(1) (2010).
- [138] C. Yong Liang Guana, A. Elkamel, K. Wang, Energy gas storage in template-synthesized carbons with different porous structures, *The Canadian Journal of Chemical Engineering* 93(3) (2015) 527-531.
- [139] M.K. Antoniou, E.K. Diamanti, A. Enotiadis, A. Policicchio, K. Dimos, F. Ciuchi, E. Maccallini, D. Gournis, R.G. Agostino, Methane storage in zeolite-like carbon materials, *Microporous and Mesoporous Materials* 188 (2014) 16-22.
- [140] H.-C. Kim, Y.-K. Hwang, S.J. Seo, S. Huh, Gas sorption and supercapacitive properties of hierarchical porous graphitic carbons prepared from the hard-templating of mesoporous ZnO/Zn(OH)<sub>2</sub> composite spheres, *Journal of Colloid and Interface Science* 564 (2020) 193-203.
- [141] W.A. Mohun, Mineral active carbon and process for producing same, Google Patents, 1962.
- [142] C. Vakifahmetoglu, V. Presser, S.-H. Yeon, P. Colombo, Y. Gogotsi, Enhanced hydrogen and methane gas storage of silicon oxycarbide derived carbon, *Microporous and mesoporous materials* 144(1-3) (2011) 105-112.
- [143] M. Sevilla, R. Mokaya, Activation of carbide-derived carbons: a route to materials with enhanced gas and energy storage properties, *Journal of Materials Chemistry* 21(13) (2011) 4727-4732.
- [144] Y. Zhu, A. Zhou, J. Jia, J. Wang, J. Liu, B. Xing, C. Zhang, Synthesis and Gas Adsorption Properties of Carbide-Derived Carbons from Titanium Tin Carbide, *Nano* 11(04) (2016) 1650040.
- [145] S. Osswald, C. Portet, Y. Gogotsi, G. Laudisio, J. Singer, J. Fischer, V. Sokolov, J. Kukushkina, A. Kravchik, Porosity control in nanoporous carbide-derived carbon by oxidation in air and carbon dioxide, *Journal of Solid State Chemistry* 182(7) (2009) 1733-1741.

- [146] S.-H. Yeon, S. Osswald, Y. Gogotsi, J.P. Singer, J.M. Simmons, J.E. Fischer, M.A. Lillo-Ródenas, Á. Linares-Solano, Enhanced methane storage of chemically and physically activated carbide-derived carbon, *Journal of Power Sources* 191(2) (2009) 560-567.
- [147] Y. Gogotsi, C. Portet, S. Osswald, J.M. Simmons, T. Yildirim, G. Laudisio, J.E. Fischer, Importance of pore size in high-pressure hydrogen storage by porous carbons, *International Journal of Hydrogen Energy* 34(15) (2009) 6314-6319.
- [148] F. Rezaei, P. Webley, Structured adsorbents in gas separation processes, *Separation and Purification Technology* 70(3) (2010) 243-256.
- [149] F. Rezaei, Optimization of structured adsorbents for gas separation processes, Luleå tekniska universitet, 2011.
- [150] S. Chen, H. Gong, B. Dindoruk, J. He, Z. Bao, Dense Carbon Nanoflower Pellets for Methane Storage, *ACS Applied Nano Materials* 3(8) (2020) 8278-8285.
- [151] H. Liu, S. Wu, N. Tian, F. Yan, C. You, Y. Yang, Carbon foams: 3D porous carbon materials holding immense potential, *Journal of Materials Chemistry A* 8(45) (2020) 23699-23723.
- [152] J. Ye, M. Zhou, Y. Le, B. Cheng, J. Yu, Three-dimensional carbon foam supported MnO<sub>2</sub>/Pt for rapid capture and catalytic oxidation of formaldehyde at room temperature, *Applied Catalysis B: Environmental* 267 (2020) 118689.
- [153] S.A. Song, Y. Lee, Y.S. Kim, S.S. Kim, Mechanical and thermal properties of carbon foam derived from phenolic foam reinforced with composite particles, *Composite Structures* 173 (2017) 1-8.
- [154] J.-H. Kim, Y.-S. Lee, Characteristics of a high compressive strength graphite foam prepared from pitches using a PVA–AAc solution, *Journal of Industrial and Engineering Chemistry* 30 (2015) 127-133.

- [155] F. Canencia, M. Darder, P. Aranda, F.M. Fernandes, R.F. Gouveia, E. Ruiz-Hitzky, Conducting macroporous carbon foams derived from microwave-generated caramel/silica gel intermediates, *Journal of Materials Science* 52(19) (2017) 11269-11281.
- [156] A. Arami-Niya, T.E. Rufford, Z. Zhu, Nitrogen-doped carbon foams synthesized from banana peel and zinc complex template for adsorption of CO<sub>2</sub>, CH<sub>4</sub>, and N<sub>2</sub>, *Energy & Fuels* 30(9) (2016) 7298-7309.
- [157] H.-M. Lee, L.-K. Kwac, K.-H. An, S.-J. Park, B.-J. Kim, Electrochemical behavior of pitch-based activated carbon fibers for electrochemical capacitors, *Energy Conversion and Management* 125 (2016) 347-352.
- [158] M.F. Hassan, M.A. Sabri, H. Fazal, A. Hafeez, N. Shezad, M. Hussain, Recent trends in activated carbon fibers production from various precursors and applications—A comparative review, *Journal of Analytical and Applied Pyrolysis* 145 (2020) 104715.
- [159] V. Jimenez, P. Sánchez, A. Romero, Materials for activated carbon fiber synthesis, *Activated Carbon Fiber and Textiles*, Elsevier 2017, pp. 21-38.
- [160] G. Conte, S. Stelitano, A. Policicchio, F.D. Minuto, V. Lazzaroli, F. Galiano, R.G. Agostino, Assessment of activated carbon fibers from commercial Kevlar® as nanostructured material for gas storage: Effect of activation procedure and adsorption of CO<sub>2</sub> and CH<sub>4</sub>, *Journal of Analytical and Applied Pyrolysis* 152 (2020) 104974.
- [161] T. Lee, C.-H. Ooi, R. Othman, F.-Y. Yeoh, Activated carbon fiber-the hybrid of carbon fiber and activated carbon, *Rev. Adv. Mater. Sci* 36(2) (2014) 118-136.
- [162] N. Díez, P. Álvarez, M. Granda, C. Blanco, R. Santamaría, R. Menéndez, A novel approach for the production of chemically activated carbon fibers, *Chemical Engineering Journal* 260 (2015) 463-468.

- [163] D. Edie, The effect of processing on the structure and properties of carbon fibers, *Carbon* 36(4) (1998) 345-362.
- [164] Q. Wang, W. Ma, E. Yin, S. Yu, S. Wang, H. Xiang, D. Li, M. Zhu, Melt spinning of low-cost activated carbon fiber with a tunable pore structure for high-performance flexible supercapacitors, *ACS Applied Energy Materials* 3(9) (2020) 9360-9368.
- [165] J.Y. Chen, *Activated carbon fiber and textiles*, Woodhead Publishing 2016.
- [166] A.A. Ogale, M. Zhang, J. Jin, Recent advances in carbon fibers derived from biobased precursors, *Journal of Applied Polymer Science* 133(45) (2016).
- [167] J. Alcañiz-Monge, D. Cazorla-Amorós, A. Linares-Solano, A. Oya, A. Sakamoto, K. Hosm, Preparation of general purpose carbon fibers from coal tar pitches with low softening point, *Carbon* 35(8) (1997) 1079-1087.
- [168] S.-H. Hwang, Y.K. Kim, H.-J. Seo, S.M. Jeong, J. Kim, S.K. Lim, The enhanced hydrogen storage capacity of carbon fibers: The effect of hollow porous structure and surface modification, *Nanomaterials* 11(7) (2021) 1830.
- [169] V. Georgakilas, J.A. Perman, J. Tucek, R. Zboril, Broad family of carbon nanoallotropes: classification, chemistry, and applications of fullerenes, carbon dots, nanotubes, graphene, nanodiamonds, and combined superstructures, *Chemical reviews* 115(11) (2015) 4744-4822.
- [170] Z. Zhang, Z.P. Cano, D. Luo, H. Dou, A. Yu, Z. Chen, Rational design of tailored porous carbon-based materials for CO<sub>2</sub> capture, *Journal of Materials Chemistry A* 7(37) (2019) 20985-21003.
- [171] H.W. Kroto, J.R. Heath, S.C. O'Brien, R.F. Curl, R.E. Smalley, C<sub>60</sub>: buckminsterfullerene, *nature* 318(6042) (1985) 162-163.

- [172] W. Krätschmer, L.D. Lamb, K. Fostiropoulos, D.R. Huffman, Solid C 60: a new form of carbon, *Nature* 347(6291) (1990) 354-358.
- [173] M. Darvish Ganji, F. Bonyasi, S. Tanreh, M. Rezvani, M. Hekmati, Encapsulation of Methane Molecules into C60 Fullerene Nanocage: DFT and DTFB-MD Simulations, *Journal of Nanoanalysis* 4(2) (2017) 159-168.
- [174] R.J. Whitby, S. Bloodworth, G. Bacanu, M. Light, J. Herniman, G. Sitinova, S. Alom, S. Vidal, S.J. Elliott, G.J. Langley, First Synthesis and Characterisation of CH<sub>4</sub>@ C60, (2019).
- [175] R. Mohajeri, M. Jahanshahi, M.G. Ahangari, Methane storage capacity of carbon fullerenes and their mechanical and electronic properties: Experimental and theoretical study, *Materials Chemistry and Physics* 211 (2018) 192-199.
- [176] D.S. Sabirov, A.A. Tukhbatullina, R.G. Bulgakov, Compression of methane endofullerene CH<sub>4</sub>@C60 as a potential route to endohedral covalent fullerene derivatives: a DFT study, *Fullerenes, Nanotubes and Carbon Nanostructures* 23(10) (2015) 835-842.
- [177] J.P. Hare, H.W. Kroto, R. Taylor, Preparation and UV/visible spectra of fullerenes C60 and C70, *Chemical physics letters* 177(4-5) (1991) 394-398.
- [178] W.A. Scrivens, J.M. Tour, Synthesis of gram quantities of C60 by plasma discharge in a modified round-bottomed flask. Key parameters for yield optimization and purification, *The Journal of Organic Chemistry* 57(25) (1992) 6932-6936.
- [179] N. Arora, N. Sharma, Arc discharge synthesis of carbon nanotubes: Comprehensive review, *Diamond and related materials* 50 (2014) 135-150.
- [180] H. Kroto, Space, stars, C60, and soot, *Science* 242(4882) (1988) 1139-1145.
- [181] M. Wilson, K. Kannangara, G. Smith, M. Simmons, B. Raguse, *Nanotechnology: basic science and emerging technologies*, CRC press 2002.



- [182] R. Taylor, G.J. Langley, H.W. Kroto, D.R. Walton, Formation of C<sub>60</sub> by pyrolysis of naphthalene, *Nature* 366(6457) (1993) 728-731.
- [183] J.B. Howard, J.T. McKinnon, Y. Makarovsky, A.L. Lafleur, M.E. Johnson, Fullerenes C<sub>60</sub> and C<sub>70</sub> in flames, *Nature* 352(6331) (1991) 139-141.
- [184] K.H. Homann, Fullerenes and soot formation—new pathways to large particles in flames, *Angewandte Chemie International Edition* 37(18) (1998) 2434-2451.
- [185] R. Trasca, M.W. Cole, T. Coffey, J. Krim, Gas adsorption on a C<sub>60</sub> monolayer, *Physical Review E* 77(4) (2008) 041603.
- [186] A. Kaiser, S. Zöttl, P. Bartl, C. Leidlmair, A. Mauracher, M. Probst, S. Denifl, O. Echt, P. Scheier, Methane adsorption on aggregates of fullerenes: site-selective storage capacities and adsorption energies, *ChemSusChem* 6(7) (2013) 1235.
- [187] A.W. Thornton, K.M. Nairn, J.M. Hill, A.J. Hill, M.R. Hill, Metal-organic frameworks impregnated with magnesium-decorated fullerenes for methane and hydrogen storage, *Journal of the American Chemical Society* 131(30) (2009) 10662-10669.
- [188] O.O. Adisa, B.J. Cox, J.M. Hill, Methane storage in spherical fullerenes, *Journal of Nanotechnology in Engineering and Medicine* 3(4) (2012).
- [189] Y. Gao, X. Wu, X.C. Zeng, Designs of fullerene-based frameworks for hydrogen storage, *Journal of Materials Chemistry A* 2(16) (2014) 5910-5914.
- [190] A. Kaiser, C. Leidlmair, P. Bartl, S. Zöttl, S. Denifl, A. Mauracher, M. Probst, P. Scheier, O. Echt, Adsorption of hydrogen on neutral and charged fullerene: Experiment and theory, *The Journal of chemical physics* 138(7) (2013) 074311.
- [191] D. Saha, S. Deng, Hydrogen adsorption on partially truncated and open cage C<sub>60</sub> fullerene, *Carbon* 48(12) (2010) 3471-3476.

- [192] S. Zöttl, A. Kaiser, P. Bartl, C. Leidlmair, A. Mauracher, M. Probst, S. Denifl, O. Echt, P. Scheier, Methane adsorption on graphitic nanostructures: every molecule counts, *The journal of physical chemistry letters* 3(18) (2012) 2598-2603.
- [193] Y. Rubin, T. Jarrosson, G.W. Wang, M.D. Bartberger, K. Houk, G. Schick, M. Saunders, R.J. Cross, Insertion of helium and molecular hydrogen through the orifice of an open fullerene, *Angewandte Chemie International Edition* 40(8) (2001) 1543-1546.
- [194] K. Komatsu, M. Murata, Y. Murata, Encapsulation of molecular hydrogen in fullerene C<sub>60</sub> by organic synthesis, *Science* 307(5707) (2005) 238-240.
- [195] A.A. Popov, S. Yang, L. Dunsch, Endohedral fullerenes, *Chemical reviews* 113(8) (2013) 5989-6113.
- [196] S. Iijima, T. Ichihashi, Single-shell carbon nanotubes of 1-nm diameter, *nature* 363(6430) (1993) 603-605.
- [197] Zhu. Shuyun, G. Xu. Single-walled carbon nanohorns and their applications. *Nanoscale* 2, no. 12 (2010): 2538-2549.
- [198] T. Ohba, K. Kaneko, M. Yudasaka, S. Iijima, A. Takase, H. Kanoh, Cooperative adsorption of supercritical CH<sub>4</sub> in single-walled carbon nanohorns for compensation of nanopore potential, *The Journal of Physical Chemistry C* 116(41) (2012) 21870-21873.
- [199] X. Peng, J. Zhou, W. Wang, D. Cao, Computer simulation for storage of methane and capture of carbon dioxide in carbon nanoscrolls by expansion of interlayer spacing, *Carbon* 48(13) (2010) 3760-3768.
- [200] J. Prasek, J. Drbohlavova, J. Chomoucka, J. Hubalek, O. Jasek, V. Adam, R. Kizek, Methods for carbon nanotubes synthesis, *Journal of Materials Chemistry* 21(40) (2011) 15872-15884.

- [201] E. Bekyarova, K. Murata, M. Yudasaka, D. Kasuya, S. Iijima, H. Tanaka, H. Kahoh, K. Kaneko, Single-wall nanostructured carbon for methane storage, *The Journal of Physical Chemistry B* 107(20) (2003) 4681-4684.
- [202] M. Delavar, A. Ghoreyshi, M. Jahanshahi, N. Nabian, Comparative experimental study of methane adsorption on multi-walled carbon nanotubes and granular activated carbons, *Journal of Experimental Nanoscience* 9(3) (2014) 310-328.
- [203] E. Molyanyan, S. Aghamiri, M. Talaie, N. Iraj, Experimental study of pure and mixtures of CO<sub>2</sub> and CH<sub>4</sub> adsorption on modified carbon nanotubes, *International journal of environmental science and technology* 13(8) (2016) 2001-2010.
- [204] C.-M. Yang, D. Kasuya, M. Yudasaka, S. Iijima, K. Kaneko, Microporosity development of single-wall carbon nanohorn with chemically induced coalescence of the assembly structure, *The Journal of Physical Chemistry B* 108(46) (2004) 17775-17782.
- [205] K. Shen, H. Xu, Y. Jiang, T. Pietraß, The role of carbon nanotube structure in purification and hydrogen adsorption, *Carbon* 42(11) (2004) 2315-2322.
- [206] S. Orimo, G. Majer, T. Fukunaga, A. Züttel, L. Schlapbach, H. Fujii, Hydrogen in the mechanically prepared nanostructured graphite, *Applied physics letters* 75(20) (1999) 3093-3095.
- [207] F. Liu, X. Zhang, J. Cheng, J. Tu, F. Kong, W. Huang, C. Chen, Preparation of short carbon nanotubes by mechanical ball milling and their hydrogen adsorption behavior, *Carbon* 41(13) (2003) 2527-2532.
- [208] C.-H. Chen, C.-C. Huang, Enhancement of hydrogen spillover onto carbon nanotubes with defect feature, *Microporous and Mesoporous Materials* 109(1-3) (2008) 549-559.
- [209] S. Vela, F. Huarte-Larrañaga, A molecular dynamics simulation of methane adsorption in single walled carbon nanotube bundles, *Carbon* 49(13) (2011) 4544-4553.

- [210] G. Mpourmpakis, E. Tylianakis, G.E. Froudakis, Carbon nanoscrolls: a promising material for hydrogen storage, *Nano letters* 7(7) (2007) 1893-1897.
- [211] D. Cao, X. Zhang, J. Chen, W. Wang, J. Yun, Optimization of single-walled carbon nanotube arrays for methane storage at room temperature, *The Journal of Physical Chemistry B* 107(48) (2003) 13286-13292.
- [212] S.J. Mahdizadeh, S.F. Tayyari, Influence of temperature, pressure, nanotube's diameter and intertube distance on methane adsorption in homogeneous armchair open-ended SWCNT triangular arrays, *Theoretical Chemistry Accounts* 128(2) (2011) 231-240.
- [213] X. Zhang, W. Wang, Methane adsorption in single-walled carbon nanotubes arrays by molecular simulation and density functional theory, *Fluid phase equilibria* 194 (2002) 289-295.
- [214] K.V. Kumar, K. Preuss, M.-M. Titirici, F. Rodríguez-Reinoso, Nanoporous materials for the onboard storage of natural gas, *Chemical reviews* 117(3) (2017) 1796-1825.
- [215] K.V. Kumar, E.A. Müller, F. Rodriguez-Reinoso, Effect of pore morphology on the adsorption of methane/hydrogen mixtures on carbon micropores, *The Journal of Physical Chemistry C* 116(21) (2012) 11820-11829.
- [216] H. Boehm, A. Clauss, G. Fischer, U. Hofmann, Dünnte kohlenstoff-folien, *Zeitschrift Für Naturforschung B* 17(3) (1962) 150-153.
- [217] P.R. Wallace, The band theory of graphite, *Physical review* 71(9) (1947) 622.
- [218] K.S. Novoselov, A.K. Geim, S.V. Morozov, D. Jiang, Y. Zhang, S.V. Dubonos, I.V. Grigorieva, A.A. Firsov, Electric field effect in atomically thin carbon films, *science* 306(5696) (2004) 666-669.
- [219] X. Huang, X. Qi, F. Boey, H. Zhang, Graphene-based composites, *Chemical Society Reviews* 41(2) (2012) 666-686.

- [220] X. Huang, Z. Yin, S. Wu, X. Qi, Q. He, Q. Zhang, Q. Yan, F. Boey, H. Zhang, Graphene-based materials: synthesis, characterization, properties, and applications, *small* 7(14) (2011) 1876-1902.
- [221] S. Gadipelli, Z.X. Guo, Graphene-based materials: Synthesis and gas sorption, storage and separation, *Progress in Materials Science* 69 (2015) 1-60.
- [222] L.-P. Ma, Z.-S. Wu, J. Li, E.-D. Wu, W.-C. Ren, H.-M. Cheng, Hydrogen adsorption behavior of graphene above critical temperature, *international journal of hydrogen energy* 34(5) (2009) 2329-2332.
- [223] Y. Lin, X. Han, C.J. Campbell, J.W. Kim, B. Zhao, W. Luo, J. Dai, L. Hu, J.W. Connell, Holey graphene nanomanufacturing: structure, composition, and electrochemical properties, *Advanced Functional Materials* 25(19) (2015) 2920-2927.
- [224] Z.-Y. Sui, Q.-H. Meng, J.-T. Li, J.-H. Zhu, Y. Cui, B.-H. Han, High surface area porous carbons produced by steam activation of graphene aerogels, *Journal of Materials Chemistry A* 2(25) (2014) 9891-9898.
- [225] S. Yun, S.-O. Kang, S. Park, H.S. Park, CO<sub>2</sub>-activated, hierarchical trimodal porous graphene frameworks for ultrahigh and ultrafast capacitive behavior, *Nanoscale* 6(10) (2014) 5296-5302.
- [226] Z. Huang, K. Xia, L. Zheng, B. Han, Q. Gao, H. Wang, Z. Li, C. Zhou, Facile and scalable synthesis of hierarchically porous graphene architecture for hydrogen storage and high-rate supercapacitors, *Journal of Materials Science: Materials in Electronics* 28(23) (2017) 17675-17681.

- [227] A. Klechikov, G. Mercier, T. Sharifi, I.A. Baburin, G. Seifert, A.V. Talyzin, Hydrogen storage in high surface area graphene scaffolds, *Chemical Communications* 51(83) (2015) 15280-15283.
- [228] G. Srinivas, J. Burrell, T. Yildirim, Graphene oxide derived carbons (GODCs): synthesis and gas adsorption properties, *Energy & Environmental Science* 5(4) (2012) 6453-6459.
- [229] J.-J. Chen, W.-W. Li, X.-L. Li, H.-Q. Yu, Improving biogas separation and methane storage with multilayer graphene nanostructure via layer spacing optimization and lithium doping: a molecular simulation investigation, *Environmental science & technology* 46(18) (2012) 10341-10348.
- [230] A. Peigney, C. Laurent, E. Flahaut, R. Bacsa, A. Rousset, Specific surface area of carbon nanotubes and bundles of carbon nanotubes, *Carbon* 39(4) (2001) 507-514.
- [231] L. Jiang, Z. Fan, Design of advanced porous graphene materials: from graphene nanomesh to 3D architectures, *Nanoscale* 6(4) (2014) 1922-1945.
- [232] B. Szcześniak, J. Choma, M. Jaroniec, Gas adsorption properties of graphene-based materials, *Advances in colloid and interface science* 243 (2017) 46-59.
- [233] A. Pedrielli, S. Taioli, G. Garberoglio, N.M. Pugno, Gas adsorption and dynamics in pillared graphene frameworks, *Microporous and Mesoporous Materials* 257 (2018) 222-231.
- [234] M. Razmkhah, F. Moosavi, M.T.H. Mosavian, A. Ahmadpour, Tunable gas adsorption in graphene oxide framework, *Applied Surface Science* 443 (2018) 198-208.
- [235] F. Yavari, Z. Chen, A.V. Thomas, W. Ren, H.-M. Cheng, N. Koratkar, High sensitivity gas detection using a macroscopic three-dimensional graphene foam network, *Scientific reports* 1(1) (2011) 1-5.

- [236] P. Xu, F. Rahmani, Y.C. Chiew, Adsorption and diffusion of methane and light gases in 3D nano-porous graphene sponge, *Molecular Simulation* (2021) 1-9.
- [237] C. Li, G. Shi, Three-dimensional graphene architectures, *Nanoscale* 4(18) (2012) 5549-5563.
- [238] J. Wang, Z. Shi, J. Fan, Y. Ge, J. Yin, G. Hu, Self-assembly of graphene into three-dimensional structures promoted by natural phenolic acids, *Journal of Materials Chemistry* 22(42) (2012) 22459-22466.
- [239] T. Wu, M. Chen, L. Zhang, X. Xu, Y. Liu, J. Yan, W. Wang, J. Gao, Three-dimensional graphene-based aerogels prepared by a self-assembly process and its excellent catalytic and absorbing performance, *Journal of Materials Chemistry A* 1(26) (2013) 7612-7621.
- [240] S. Gilje, S. Dubin, A. Badakhshan, J. Farrar, S.A. Danczyk, R.B. Kaner, Photothermal deoxygenation of graphene oxide for patterning and distributed ignition applications, *Advanced Materials* 22(3) (2010) 419-423.
- [241] V. Abdelsayed, S. Moussa, H.M. Hassan, H.S. Aluri, M.M. Collinson, M.S. El-Shall, Photothermal deoxygenation of graphite oxide with laser excitation in solution and graphene-aided increase in water temperature, *The Journal of Physical Chemistry Letters* 1(19) (2010) 2804-2809.
- [242] K. Fu, Y. Wang, C. Yan, Y. Yao, Y. Chen, J. Dai, S. Lacey, Y. Wang, J. Wan, T. Li, Graphene oxide-based electrode inks for 3D-printed lithium-ion batteries, *Advanced Materials* 28(13) (2016) 2587-2594.
- [243] E. García-Tuñón, S. Barg, J. Franco, R. Bell, S. Eslava, E. D'Elia, R.C. Maher, F. Guitian, E. Saiz, Printing in three dimensions with graphene, *Advanced materials* 27(10) (2015) 1688-1693.
- [244] L. Jiang, T. Yang, F. Liu, J. Dong, Z. Yao, C. Shen, S. Deng, N. Xu, Y. Liu, H.J. Gao, Controlled synthesis of large-scale, uniform, vertically standing graphene for high-performance field emitters, *Advanced materials* 25(2) (2013) 250-255.

- [245] Y. Li, Z. Li, P.K. Shen, Simultaneous formation of ultrahigh surface area and three-dimensional hierarchical porous graphene-like networks for fast and highly stable supercapacitors, *Advanced Materials* 25(17) (2013) 2474-2480.
- [246] X. Wang, Y. Zhang, C. Zhi, X. Wang, D. Tang, Y. Xu, Q. Weng, X. Jiang, M. Mitome, D. Golberg, Three-dimensional strutted graphene grown by substrate-free sugar blowing for high-power-density supercapacitors, *Nature communications* 4(1) (2013) 1-8.
- [247] A. Hassani, M.T. Hamed Mosavian, A. Ahmadpour, N. Farhadian, Hybrid molecular simulation of methane storage inside pillared graphene, *The Journal of chemical physics* 142(23) (2015) 234704.
- [248] A. Sharma, R. Babarao, N.V. Medhekar, A. Malani, Computational design of multilayer frameworks to achieve DOE target for on-board methane delivery, *Carbon* 152 (2019) 206-217.
- [249] L. Mahmoudian, A. Rashidi, H. Dehghani, R. Rahighi, Single-step scalable synthesis of three-dimensional highly porous graphene with favorable methane adsorption, *Chemical Engineering Journal* 304 (2016) 784-792.
- [250] R. Kumar, V.M. Suresh, T.K. Maji, C. Rao, Porous graphene frameworks pillared by organic linkers with tunable surface area and gas storage properties, *Chemical communications* 50(16) (2014) 2015-2017.
- [251] S.M. Lyth, H. Shao, J. Liu, K. Sasaki, E. Akiba, Hydrogen adsorption on graphene foam synthesized by combustion of sodium ethoxide, *International journal of hydrogen energy* 39(1) (2014) 376-380.
- [252] N. Kostoglou, G. Constantinides, G. Charalambopoulou, T. Steriotis, K. Polychronopoulou, Y. Li, K. Liao, V. Ryzhkov, C. Mitterer, C. Rebholz, Nanoporous spongy graphene: Potential



applications for hydrogen adsorption and selective gas separation, *Thin Solid Films* 596 (2015) 242-249.